Universidade de Aveiro
2015

Departamento de Ciências Médicas

Soraia Alexandra Araújo Martins

Proteínas interactoras da CD81

CD81 interacting proteins

Universidade de Aveiro
2015

Departamento de Ciências Médicas

Soraia Alexandra Araújo Martins

Proteínas interactoras da CD81

CD81 interacting proteins

Tese apresentada à Universidade de Aveiro para cumprimento dos requisitos necessários à obtenção do grau de Mestre em Biomedicina Molecular, realizada sob a orientação científica da Professora Doutora Sandra Vieira, Professora Auxiliar convidada do Departamento de Ciências Médicas da Universidade de Aveiro

Este trabalho contou com o apoio do grupo de Neurociências e Sinalização - iBiMED, Departamento de Ciências da Sáude da Universidade de Aveiro, e foi financiando pelo fundo PTCD/BEX-BCM/0493/2012.

o júri

presidente

Professora Doutora Ana Gabriela da Silva Cavaleiro Henriques
Professora Auxiliar Convidada, Universidade de Aveiro

Professora Doutora Sandra Isabel Moreira Pinto Vieira
Professora Auxiliar Convidada, Universidade de Aveiro

Professora Doutora Ana Cristina de Fraga Esteves
Professora Auxiliar Convidada, Universidade de Aveiro

agradecimentos

À minha orientadora, Professora Doutora Sandra Vieira, agradeço por toda a disponibilidade, amizade, apoio, dedicação e ensinamentos transmitidos. O meu mais sincero e profundo agradecimento por todo o tempo perdido e pela paciência prestada durante o decorrer deste trabalho.

À Professora Doutora Odete da Cruz e Silva pela oportunidade de participar neste projecto, assim como pelo encorajamento e motivação transmitida.

Ao Professor Doutor João Ramalho-Santos pela colaboração neste projecto.

A todos os meus colegas do Laboratório de Neurociências, por todos os conselhos, pela amizade, pelo apoio e por todos os sábios ensimentos que partilharam comigo ao longo desta minha etapa. Um agradecimento especial ao Roberto, à Pipa, à Rocha e à Oli sobretudo pela paciência que tiveram, por nunca terem rejeitado um pedido de ajuda, por todas as gargalhadas partilhadas e por me mostrarem o verdadeiro significado de “ciência”.

À Renata, por toda a ajuda incansável e conhecimento que me me transmitiu sobre o mundo dos espermatozóides.

A todos os meus colegas de mestrado, em especial ao Hélder, Catarina, Hugo e Daniela, pelo companheirismo e apoio demostrado ao londo desta minha estadia em Aveiro.

Um especial agradecimento à Joana, por ter partilhado esta aventura comigo, pela ajuda sempre disponibilizada, por todos os conselhos, apoio e espiríto critico demostrado. Por todas as gargalhadas que animaram os nossos serões, pelas narrativas ouvidas, mas sobretudo pela paciência e boa disposição que sempre me transmitiu.

À Guida e à Rafa, com quem tive o prazer de partilhar esta nova estapa em Aveiro. Por terem sido o meu apoio, pela preocupação mostrada e por todos os bons momentos vividos.

À Cátia, por me ter mostrado o verdadeiro significado de amizade e por ter estado sempre presente, apesar da distância.

Aos meus pais e à minha irmã, por toda a força, ternura, coragem e confiança que me transmitiram. Obrigada por todo o apoio e por estarem sempre presentes em todos os momentos da minha vida, por me ensirarem a contornar os obstáculos, e acima se tudo, a ser feliz. Porque tudo o que tenho é a vocês que o devo. Muito obrigada.

palavras-chave

Proteína CD81; interacção proteína-proteína; Proteína Percursora de Amilóide (PPA); espermatozóides; células SH-SY5Y; fecundação; remodelação do citoesqueleto

resumo

A fecundação é um processo complexo e faseado que culmina na fusão celular das membranas dos gametas, do citoplasma e do genoma. A CD81 é uma proteína tetraspanina que participa na interacção espermatozóide-oócito, estando presente na superfície do oócito. A CD81 também tem sido associada a outros processos biológicos, contudo a sua função específica e os seus mecanismos de acção não estão elucidados. A ligação entre a CD81 e as suas proteínas interactoras fundamenta o envolvimento da CD81 numa variedade de processos celulares e funções específicas. O desenvolvimento de um sistema de Dois Híbrido em Leveduras, anteriormente realizado no nosso laboratório, mostrou que a CD81 potencialmente interage com a Proteína Percursora de Amilóide (PPA).

No presente trabalho, foi realizada a análise bioinformática das proteínas interactoras da CD81. A informação obtida permitiu a construção de uma rede de interações proteína-proteína, bem como a análise de enrequecimento de Ontologia de Genes. Adicionalmente, a expressão da CD81 foi avaliada nas linhas celulares CHO, GC-1 e SH-SY5Y e em espermatozóides humanos. A sua localização subcelular foi também analisada em espermatozóides humanos e na linha de neuroblastoma SH-SY5Y. Foram ainda realizados ensaios de co-imunoprecipitacão nas linhas celulares CHO e SH-SY5Y, com a tentativa de provar a intercação física entre a CD81 e a PPA. A interação funcional entre estas duas proteínas foi estudada através da análise do efeito da sobreexpressão da CD81 nos níveis de PPA. Foram também realizados estudos de colocalização entre a CD81 e algumas proteínas interactoras, nos espermatozóides humanos e na linha celular SH-SY5Y. Os interatores analisados, PPA, AKT1 e proteínas relacionadas com o citoesqueleto, foram obtidos da análise bioinformática previamente realizada. O efeito da CD81 na remodelação do citoesqueleto foi avaliado através da monitorização dos efeitos da sobre-expressão da CD81 nos níveis de actina e tubulina, bem como através da análise da colocalização entre a CD81 sobre-expressa e a F-actina.

Os nossos resultados mostram que a CD81 está expressa em todas as linhas celulares testadas, providenciando a primeira evidência da presença da CD81 em espermatozóides humanos. A marcação da CD81 foi predominantemente detectada na cabeça do espermatozóde e na peça intermédia, onde colocaliza com a PPA, bem como na região pós-acrossómica. Em adição, a CD81 colocaliza com a PPA na membrana plasmática e nas projecções celulares das células SH-SY5Y, onde a sobre-expressão da CD81 influencia os níveis de PPA, efeito também observado nas células CHO. A análise de proteínas interactoras da CD81, como a AKT1 e proteínas relacionadas com o citoesqueleto, evidenciou que a CD81 está envolvida na remodelação do citoesqueleto, nomeadamente na motilidade dos espermatozóides, na migração celular e na neuritogénese. Estes resultados permitiram aprofundar o conhecimento das funções da CD81 e de alguns dos seus interactores, em espermatozóides e em células neuronais.

keywords

CD81 protein; protein-protein interaction; Amyloid precursor protein (APP); sperm cells; SH-SY5Y cells; fertilization; cytoskeleton remodeling

abstract

Fertilization is a multistep and complex process culminating in the merge of gamete membranes, cytoplasmic unity and fusion of genome. CD81 is a tetraspanin protein that participates in sperm-oocyte interaction, being present at the oocyte surface. CD81 has also been implicated in other biological processes, however its specific function and molecular mechanisms of action remain to be elucidated. The interaction between CD81 and its binding partner proteins may underlie the CD81 involvement in a variety of cellular processes and modulate CD81/interactors specific functions. Interestingly, in a Yeast two Hybrid system previously performed in our lab, CD81 has emerged as a putative interactor of the Amyloid Precursor Protein (APP).

In the work here described, bioinformatics analyses of CD81 interacting proteins were performed and the retrieved information used to construct a protein-protein interaction network, as well as to perform Gene Ontology enrichment analyses. CD81 expression was further evaluated in CHO, GC-1 and SH-SY5Y cell lines, and in human sperm cells. Additionally, its subcellular localization was analyzed in sperm cells and in the neuronal-like SH-SY5Y cell line. Subsequently, co-immunoprecipitation assays were performed in CHO and SH-SY5Y cells to attempt to prove the physical interaction between CD81 and APP. A functional interaction between these two proteins was accessed thought the analyses of the effects of CD81 overexpression on APP levels. A co-localization analysis of CD81 and some interactors proteins retrieved from the bioinformatics analyses, such as APP, AKT1 and cytoskeleton-related proteins, was also performed in sperm cells and in SH-SY5Y cells. The effects of CD81 in cytoskeleton remodeling was evaluated in SH-SY5Y cells through monitoring the effects of CD81 overexpression in actin and tubulin levels, and analyzing the co-localization between overexpressed CD81 and F-actin.

Our results showed that CD81 is expressed in all cell lines tested, and also provided the first evidence of the presence of CD81 in human sperm cells. CD81 immunoreactivity was predominantly detected in the sperm head, including the acrosome membrane, and in the midpiece, where it co-localized with APP, as well as in the post-acrosomal region. Furthermore, CD81 co-localizes with APP in the plasma membrane and in cellular projections in SH-SY5Y cells, where CD81 overexpression has an influence on APP levels, also visible in CHO cells. The analysis of CD81 interacting proteins such as AKT1 and cytoskeleton-related proteins showed that CD81 is involved in a variety of pathways that may underlie cytoskeleton remodeling events, related to processes such as sperm motility, cell migration and neuritogenesis. These results deepen our understanding on the functions of CD81 and some of its interactors in sperm and neuronal cells.

List of contents

Abbreviations v

1. Introduction 1

1.1 Sperm cells and fertilization 1

1.1.1 Sperm Capacitation 3

1.1.2 Acrosome reaction 4

1.1.3 Proteins involved in sperm-oocyte interaction 5

1.2 CD81: a member of the protein tetraspanin superfamily 10

1.2.1 CD81 structural features 10

1.2.2 The tetraspanin web: a dynamic network of molecular interactions 12

1.2.3 CD81 physiological role 13

1.3 Amyloid Precursor Protein (APP) 16

1.3.1 APP superfamily and isoforms 16

1.3.2 APP Proteolytic Processing 18

1.3.3 APP functions 20

1.3.4 Putative APP-CD81 interactaction in human testis 22

2. Aims of the Thesis 23

3. Materials and Methods 25

3.1 Bioinformatics analyses 25

3.1.1 Collection of literature-curated CD81 interacting proteins and constructing a protein-protein network 25

3.1.2 Gene ontology and pathways 25

3.2 Preparation of CD81 cDNAs 25

3.3 Mammalian cell assays 26

3.3.1 Culture and maintenance of the cell lines 27

3.3.2 Human sperm samples 27

3.3.3 CHO cells growth curve 27
3.3.4 Cells transient transfection using the TurboFect™ reagent 28
3.3. Antibodies 29
3.4 Proteomic assays 31
3.4.1 Cell collection and quantification of protein content 31
3.4.2 Co-immunoprecipitation (Co-IP) assay 31
3.4.3 RFP-Trap and GFP-Trap 32
3.4.4 Western-blot (WB)/Immunoblotting (IB) assays 33
3.4.5 Ponceau Red staining 34
3.4.6 Immunodetection 34
3.5 Immunocytochemistry (ICC) assays 34
3.5.1 ICC on cell lines 35
3.5.2 ICC on sperm cells 36
3.6 Data Analysis 36
3.7 Micropotographs analysis 36
4. Results 39
4.1 Bioinformatics analyses of CD81 interacting proteins 39
4.1.1 CD81 protein-protein interaction network 39
4.1.2 Gene enrichment analysis 41
4.1.3 Pathway analysis 43
4.2 Optimization of cellular and molecular tools 46
4.2.1 CHO Growth Curve 46
4.2.2 Optimization of CHO and SH-SY-5Y cells transient transfection 49
4.2.3 Optimization of anti-CD81 antibodies 53
4.3 Study of CD81 expression and subcellular localization in different cells 55
4.4 Unravel the association between CD81 and APP 58

4.4.1 Study of APP/CD81 physical interaction 58

4.4.2 Influence of CD81 overexpression in APP levels 60

4.4.3 APP/CD81 subcellular co-localization 62

4.5 CD81 and other interacting proteins 66

4.5.1 CD81 and AKT1 66

4.5.2 CD81 and cytoskeleton-related proteins 68

5. Discussion and conclusion 71

6. References 79

Appendix 1 91

Appendix 2 99

Abbreviations

AD	Alzheimer´s disease
AICD	APP intracellular domain
AKT	RAC-alpha serine/threonine-protein kinase
APLP	APP-like protein
APP	Amyloid precursor protein
AR	Acrosome reaction
Aβ	Amyloid beta-peptide
ATP	Adenosine Triphosphate
BCA	Bicinchoninic acid
BSA	Bovine Serum Albumine
cAMP	Cyclic adenosine monophosphate
cDNA	Complementary Deoxyribonucleic acid
CHO	Chinese ovary hamster
CTF	C-terminal fragment
DAPI	4',6-diamidino-2-phenylindole
DNA	Deoxyribonucleic acid
ER	Endoplasmic reticulum
GFP	Green Fluorescent Protein
GO	Gene Ontology
HRP	Horseradish peroxidase
ICC	Immunocytochemistry
IP	Immunoprecipitation
KPI	Kunitz-type protease inhibitor
LB Medium	Luria Bertani growth medium
LB	Loading buffer
LEL	Large extracellular loop
mAb	Monoclonal antibody
mRNA	Messenger ribonucleic acid
OD	Optical density
ON	Overnight

PBS	Phosphate buffered saline
PFA	Paraformaldehyde
PKA	Protein Kinase A
PLC	Phospholipase C
PM	Plasma membrane
PPI	Protein-protein interaction
PSA-FITC	*Pisum sativum agglutinin* coupled with fluorescein isothiocynate
RFP	Red Fluorescent Protein
RNA	Ribonucleic Acid
rpm	Rotation per minute
RT	Room temperature
sAPP	Secreted APP
SDS-PAGE	Sodium dodecylsulfate – Polyacrilamide gel electrophoresis
SEL	Small extracellular loop
TB	Trypan blue
TBS	Tris-buffered saline solution
TBS-T	TBS supplemented with Tween detergent
TEM	Tetraspanin-enriched microdomains
TGN	Trans-Golgi-network
TM	Transmembrane
WB	Western Blot
WHO	World Health Organization
Wt	Wild type
YTH	Yeast Two Hybrid
ZP	ZonaPellucida

1. Introduction

1.1 Sperm cells and fertilization

Fertilization is a multistep and complex process culminating in the merge of gamete membranes, cytoplasmic unity and fusion of genome, initiating the development of a new individual. This merge is achieved through gamete interactions, specifically cell adhesion and subsequent fusion of the gametes' plasma membranes (PM). Although a key event in this process, there is still very little information about the mechanism or the molecules involved in membrane fusion[1,2]. Fertilization begins when free-swimming sperm approach oocyte within the oviduct. Mammalian sperm cannot fertilize the oocyte immediately when ejaculated and must first undergo a physiological change called capacitation (in the reproductive tract) and a subsequent morphological alteration known as the acrosome reaction when they contact with the zona pellucida (ZP) of the oocyte. After completion of the acrosome reaction, sperm penetrates the ZP, finally adhering and fusing with the plasma membrane of the oocyte. Gamete fusion results in egg activation, pronuclear formation and syngamy[3,4] (Figure 1).

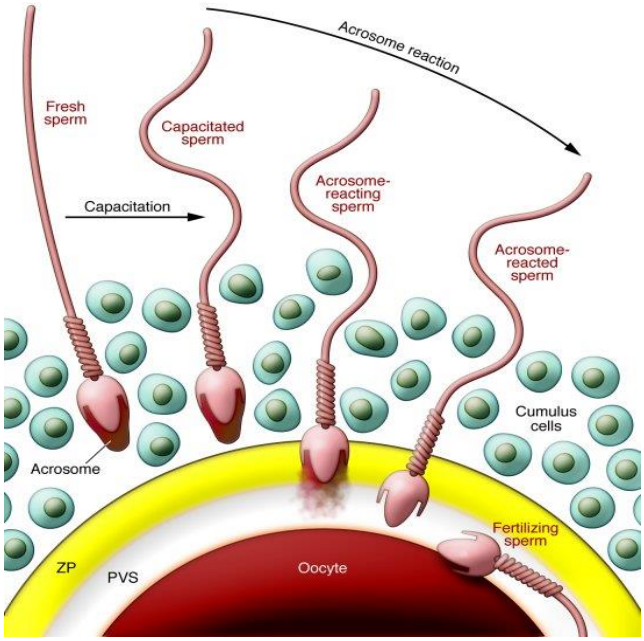

Figure 1. Fertilization process: mechanism of sperm-oocyte interactions. PVS: Perivetelline space; ZP, Zona Pellucida Reproduced from[24].

Sperm are remarkable and atypical cells with a peculiar functionality: they are produced in the testis of one organism, and upon release they invade the female tract and deliver their genetic material to an oocyte (fertilization). During spermatogenesis, spermatozoa became terminally differentiated. These highly specialized cells are composed of three main regions: the head, the midpiece, and the tail (Figure 2). The head comprises the condensed nucleus (in which DNA condensing histones are removed and replaced by protamines, resulting in a super condensed DNA), redundant nuclear envelope, and the acrosome vesicle. The acrosome is a large secretory vesicle holding hydrolytic enzymes that assist the sperm penetration though the ZP at fertilization. The sperm tail consists of a flagellum, a motile cilium that comprises an axoneme that consists of an array of microtubules in a typical 9+2 arrangement (two central microtubules surrounded by a ring of nine microtubules pairs). Other proteins structures are arranged around the axoneme, such as the outer dense fibres and fibrous sheath, adding strength and resistance to the tail. This fibrous sheath functions as a scaffold for proteins in signalling pathways that regulate sperm maturation, motility, capacitation and acrosome reaction. The sperm midpiece connects the head and the tail and is composed by a large number of mitochondria (where ATP production occurs through oxidative phosphorylation) that are spiral wrapped around the central flagellum[5–11]. During spermatogenesis most of the cytosol and redundant organelles such as the Golgi apparatus, endoplasmic reticulum (ER), lysosomes, peroxisomes and ribosomes are removed. The sperm cells are transcriptionally silent and it is generally accepted that they are translationally silent too. There are some findings indicating that mammalian spermatozoa contains nuclear-encoded mRNAs in addition to their ability to synthesize mitochondrial-encoded RNA and proteins. According to Gur *et al*. (2005)[12], the ability of sperm cells to synthesize proteins is critical for the maturation step leading to successful fertilization. The sperm PM, tightly attached to the underlying cellular structures along the whole sperm body to provide rigidity, is highly polarized and dynamically reorganizes itself during capacitation and other fertilization processes, such as sperm-oocyte adhesion and fusion processes[7,8,13] .

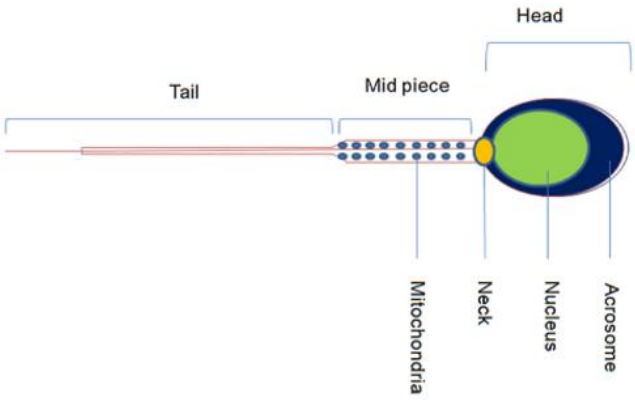

Figure 2. Sperm geometry: a mature sperm cell consists of head, midpiece and tail. The head is essentially divided into condensed DNA and acrosome. The miedpiece contains the mitochondrial sheath. The tail or flagellum is composed by microtubules that allow sperm motility. Reproduced from[14].

1.1.1 Sperm Capacitation

As soon as sperm cells are deposited in the female reproductive tract and pass the cervical mucus, they undergo many biochemical and physiological changes in a process called capacitation; this includes a change in the pattern of sperm motility known as hyperactivation, and the sperm becomes competent to fertilize an oocyte[15,16]. The biochemical changes that occur in this process include an efflux of cholesterol from the PM leading to an increase in membrane fluidity and permeability to bicarbonate and calcium ions. This results in increased bicarbonate (HCO_3^-) concentration, intracellular pH, and increased Ca^{2+} and cyclic adenosine monophosphate (cAMP) levels[4,17]. The process of capacitation can be divided into two signalling events: a) fast events such as the initiation of sperm motility, occurring as soon as the spermatozoa is released from the epididymis, and b) slow events such as changes in the motility pattern and the acquisition of the sperm capacity to undergo agonist-stimulated acrosome reaction (Figure 3)[17,18].

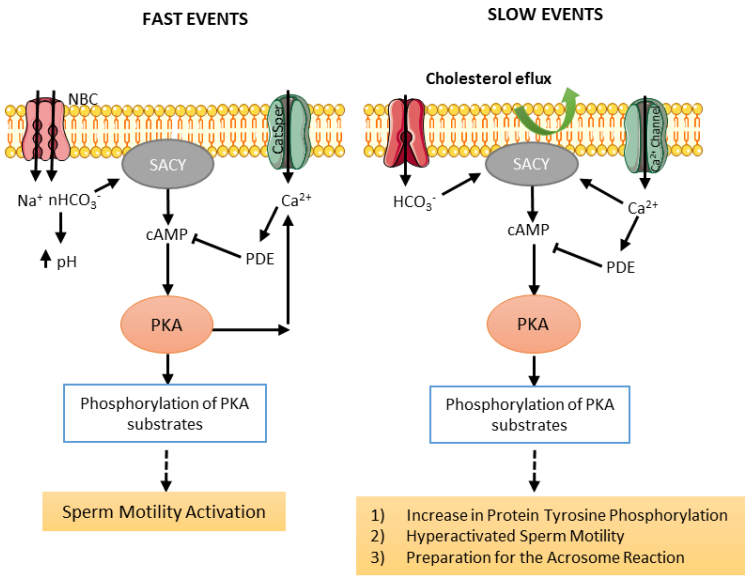

Figure 3. Molecular basis of fast (a) and slow (b) events associated with sperm capacitation. Adapted from[19].

Capacitation is regulated by two parallel pathways, one requiring activation of PKA and another involving activation of Ser/Thr protein phosphatases, such as PP2A. Taken together, sperm capacitation results in the induction of glycolysis in the sperm tail required for the hyperativated motility. In the sperm head it causes the redistribution of surface molecules, aggregation of lipid rafts and formation of a functional ZP binding protein complex[20].

Once capacitated, sperm cells demonstrate a vigorous swimming pattern considered to give sperm the strong thrusting power that allows them to penetrate the ZP[4,21] .

1.1.2 Acrosome reaction

After capacitation sperm undergo a morphological change called acrosome reaction, initiating the process of fertilization. The sperm acrosome is a Golgi-derived organelle localized in the apical region of sperm head. The acrosome exocytosis is a multipoint membrane fusion event since the outer acrosome membrane and the PM fuse at multiples sites, and as a consequence, only the inner acrosome membrane becomes a new plasma membrane[20,22]. During the process of acrosome reaction this vesicle undergoes exocytosis and releases its contents including hydrolytic enzymes such as hyaluronidase (PH-20), which are required for the penetration of cumulus cell layers and the ZP for completing the sperm-oocyte fusion[4,23]. The sperm surface binds to at least three of the four human ZP proteins (ZP1, ZP3 and ZP4) by multiple proteins, most likely organized into 'zona binding protein complexes'[20,24]. Binding of a capacitated sperm to the zona matrix activates two prominent signalling pathways (Figure 4). One is the pertussis toxin-sensitive G_i protein-coupled receptor linked to PLCβ1. The other is a putative tyrosine kinase receptor coupled to PLCγ, which leads to activation of components involved in fusion of the outer acrosomal membrane with the sperm plasma membrane, resulting in the acrosome reaction[23,24].

The acrosome exocytosis enables the sperm to reach the perivitelline space and exposes the inner acrosomal membrane and the equatorial segment of the head, which is required for the sperm to fuse with the oocyte membrane[20].

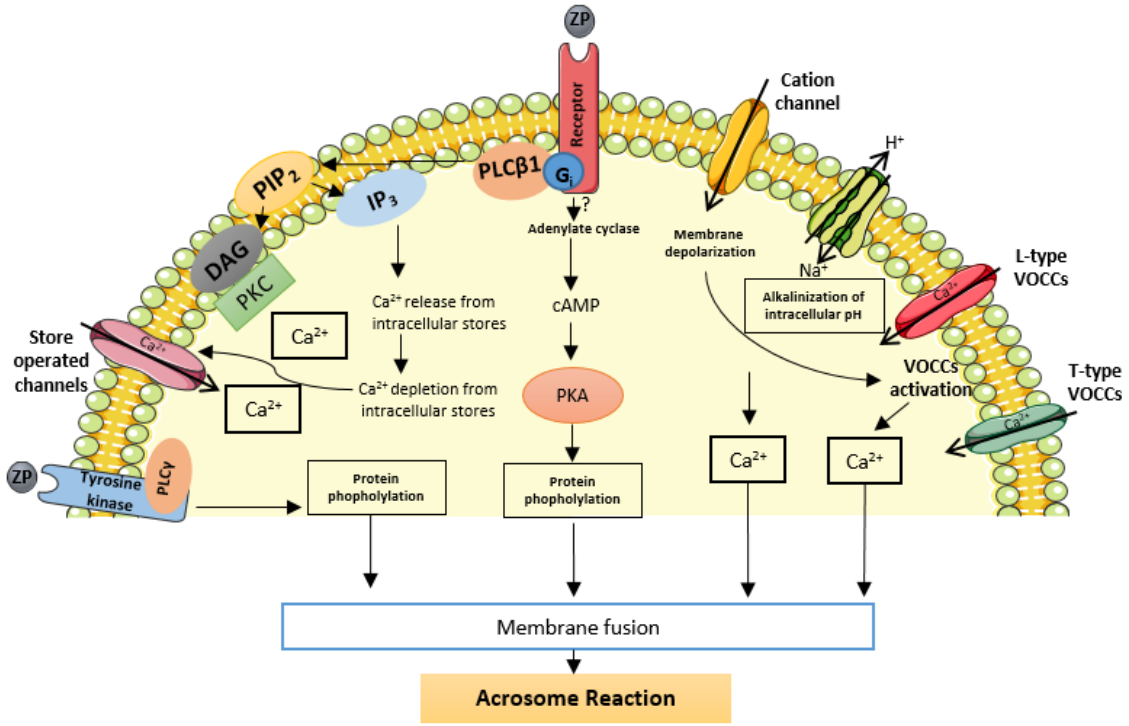

Figure 4. Schematic representation of various pathways involved in ZP-mediated acrosomal exocytosis; cAMP, cyclic adenosine monophosphate; DAG, 1,2-diacylglycerol; PKA, protein kinase A; IP3, 1,4,5-inositol triphosphate; PIP2, phosphatidylinositol 4,5-bisphosphate; PLC, phospholipase C; SOC, store-operated channel; VOCC, voltage-operated calcium channel; ZP, zona pellucida. Adapted from[23].

1.1.3 Proteins involved in sperm-oocyte interaction

Although fascinating, the interaction between sperm and oocyte is yet poorly understood[25]. Currently, the term sperm-oocyte interaction includes two cellular events: sperm-oocyte adhesion and sperm-oocyte fusion (Figure 5). For cell-cell fusion, cell adhesion is a precursor step, mediated by adhesion molecules on the sperm and oocyte surfaces, which brings the membranes in close apposition. Ultimately, this membrane interaction leads to the actual fusion event, with mixing of the lipid bilayers, formation of the fusion pores, and establishment of cytoplasmic continuity between the two cells[2].

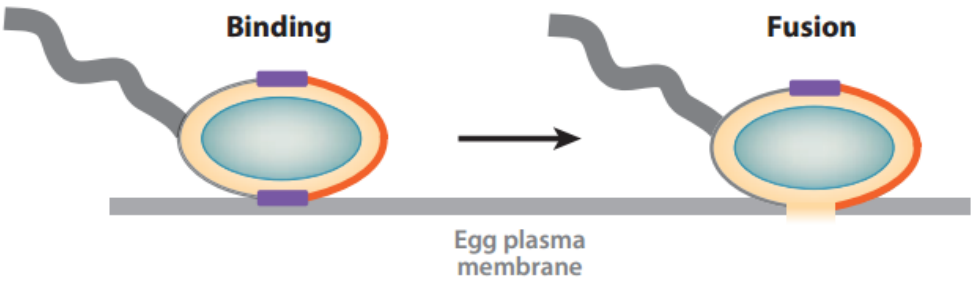

Figure 5. Schematic diagram illustrating the distinct steps of sperm binding and fusion with the oocyte plasma membrane. Purple, equatorial segment; orange, inner acrosomal membrane. Reproduced from[2].

During recent years, efforts have been made towards the identification of the molecular players in sperm-oocyte interactions and their function. Several molecules on the oocyte or the sperm side were classified essential, highly relevant, or associated with essential molecules. Although the concept of multiprotein complexes on both membranes has been accepted in recent years, the first known molecules directly implicated in mammalian fertilization have been only recently discovered[1]. The proteins involved in sperm-oocyte interactions are summarized in Table 1 (sperm proteins) and Table 2 (oocyte proteins).

Table 1. Sperm proteins involved in sperm-oocyte interaction[1,2,20,25–29].

Protein		Summary of Data	Role in fertilization	Binding partner
Izumo 1		Belongs to an immunoglobulin superfamily of type I membrane proteins; Izumo1 relocates during acrosome reaction from the anterior part of the sperm head to the sites where the fusion would take place.	*Izumo1*$^{-/-}$ mice are completely infertile; essential for fertilization	Juno
ADAMs (A desintegrin and metalloprotease)	**Fertilin (ADAM 1 and ADAM2)**	Fertilin is composed of two glycosylated transmembrane subunits (ADAM1B and ADAM2) that make a heterodimer. It is distributed on the plasma membrane over the entire sperm head.	*Adam*$^{-/-}$ knockout has serious defects in gamete membrane interaction	ADAMs are binding partners for several members of integrin family expressed in oocyte (α9β1 integrin)
	ADAM3	ADAM3 may have a role in regulating aspects of sperm function. ADAM3 has been proposed to be a sperm protein that mediates sperm-ZP3 interaction	*Adam3*-null sperm bind poorly to the ZP. ADAM3 is not essential for fusion	ADAM3 binds a ZP component(s) directly
SPESP 1 (Sperm equatorial segment protein)		Belong to the SPESP1 family. Localized in the equatorial region before acrosome reaction and a part of the SPESP1 fragment may remain in the equatorial segment after the acrosome reaction.	*Spesp1*$^{-/-}$ males have sperm with reduced ability to undergo sperm-oocyte fusion.	Unknown

Protein	Summary of Data	Role in fertilization	Binding partner
SLLP1 (Sperm Lyzozyme-Like Acrosomal Protein)	Belong to the glycosyl hydrolase 22 family; SLLP1 relocates into the equatorial segment after the acrosome reaction.	Specific antibody against SLLP1 blocked both fertilization and binding.	SAS1B

Table 2. Oocyte proteins involved in sperm-oocyte interaction[1,2,20,25–28] .

Protein		Summary of data	Role in fertilization	Binding partner
Juno (Folate receptor 4)		GPI-anchored extracellular protein on the oocyte surface. The exact molecule structure has not been fully examined.	*Juno*$^{-/-}$ female mice are absolute infertile.	IZUMO1 This interaction seems to represent a necessary and essential adhesion step rather that the exact fusogenic action.
Tetraspanins	**CD9**	Members of the tetraspanin family. Through interactions with other proteins in *cis,* tetraspanins create tetraspanin-enriched microdomains, which are a distinct type of membrane microdomain.	*Cd9*$^{-/-}$ oocytes failed to fuse with sperm. Recent observations suggest that the CD9 molecule is secreted from the oocytes in vesicle, translocating to the sperm surface and promoting in this way the fusion process. CD9 is likely to function in conjunction with CD81.	There is no evidence for an exact binding partner, as the interaction with IZUMO1, however tempting, has not been proved.
	CD81		*Cd81*$^{-/-}$ mouse shows defects in female fertility and sperm-egg interaction. *Cd9*$^{-/-}$/ *Cd81*$^{-/-}$ female mice are completely infertile	CD9

Protein	Summary of data	Role in fertilization	Binding partner
Integrins	Integrins are heterodimeric membrane proteins, made up of an α and a β subunit.	Oocytes deficient in β1 integrin show defects in sperm-oocyte binding and oocytes with reduced amounts of α9 support sperm binding and fusion less well than the control oocytes.	α9β1 integrin interact with several ADAMs.
GPI-anchored proteins	GPI-anchored proteins possess a covalently linked glycosylated phosphatidylinositol moiety which serves to attach the protein portion of the molecule to the cell surface lipid bilayer.	The absence of all the oocyte GPI-anchored proteins may alter the normal lipid domain composition and may change the repertoire of protein-protein interaction in lipid domains.	Because tetraspanins localize in raft-like microdomains, it is possible that exists an association between these molecules.
SAS1B (Sperm Acrosomal SLLP1 Binding)	SAS1B is an oolemal metalloprotease that is concentrated in a dome corresponding to the microvilli region and in the perivetelline space.	$Sas1b^{-/-}$ mice showed a significantly lowered fertilization rate	SLLP1 is believed to be one of the binding factors in the attachment-fusion machinery on the oocyte surface.

Gamete's proteins that participate in sperm-oocyte interactions not only may act as a binding partner for a molecule on the opposite gamete or as a fusogen, but they also may interact in cis with other membrane proteins and regulate those proteins function, organization or overall membrane order. Figure 6 shows a schematic diagram illustrating the molecules implicated in gamete membrane binding and fusion.

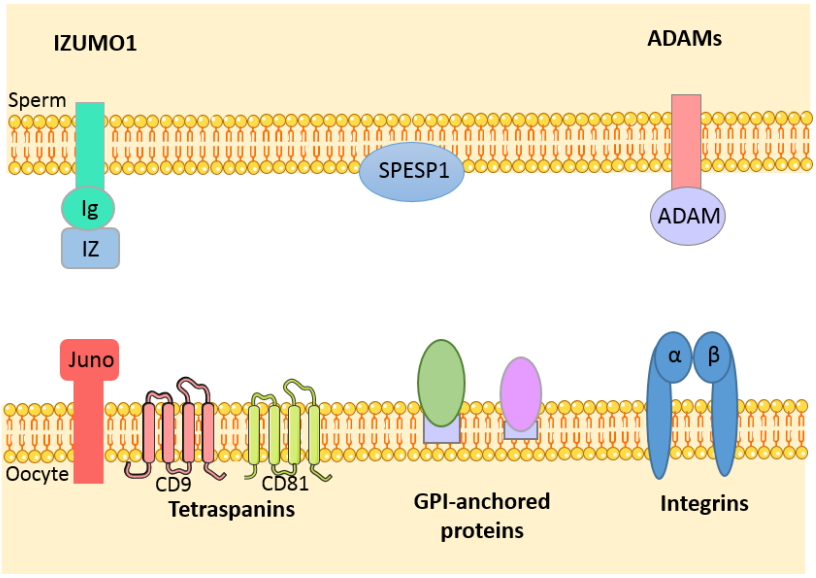

Figure 6. Sperm and oocyte molecules implicated in gamete membrane interactions. Adapted from[2]

Upon fusion, sperm activates the egg by inducing calcium oscillations and leading to the completion of the second meiotic cell division. This activation leads to exocytosis from peripherally located cortical granules, such as ovastacin-containing granules, which results in cleavage of ZP2 and by its turn in a decrease of the affinity to sperm. This phenomenon is called the 'zona reaction' and prevents polyspermy[4].

1.2 CD81: a member of the protein tetraspanin superfamily

One of the oocyte proteins involved in sperm-oocyte interactions is CD81 (also known as a target of antiproliferative antibody 1, TAPA-1). CD81 is a 26 kDa integral membrane protein member of the tetraspanin family, an evolutionarily conserved family of membrane proteins, with at least 32 distinct family members in mammals[30]. Tetraspanins are defined by four transmembrane (TM) domains delimiting two extracytoplasmic regions of unequal size, a small extracellular loop (EC1) and a large extracellular loop (EC2), and by the presence of several conserved amino acids, including an absolutely conserved CCG motif and two other cysteine residues in the EC2 [30]. This family of proteins have been implicated in a multitude of biological processes, including fertilization of oocytes, susceptibility to infection, metastasis of cancer, and cell-cell interactions in the central nervous and immune systems. These activities are due to the association of different tetraspanins with each other and with other tissue type-specific proteins in the cell membrane. These associations take the form of tetraspanin-enriched microdomains (TEM) that form a dynamic membrane network known as the 'tetraspanin web'[31].

CD81 was originally discovered in 1990 as a target of an antiproliferative antibody on human B cells, and subsequent studies have shown that it is involved in a surprising range of physiological responses[32]. This molecule is highly conserved in mammals and is expressed on most human tissues with notable exceptions of red blood cells and platelets[33]. CD81 is abundant on various types of endocytic membranes and has been widely used as an exosomal marker. The *CD81* gene has been mapped to chromosome 11p15.5 in human and in the syntenic region of chromosome 7 in mouse. Several other tetraspanin genes are located on chromosome 11 and 12 and the genomic structure is shared by each of the tetraspanin genes, indicating that they derive from a common ancestral gene[34].

1.2.1 CD81 structural features

The molecular model of the complete CD81 structure was proposed in 2006 by Seigneuret[35]. These studies on the protein topology demonstrated that the two long hydrophilic domains of the molecule are extracellular (Figure 7). The EC1 domain, also referred to as the small cellular loop (SEL), is located between TM1 and TM2, and EC2 or LEL (large extracellular domain) is located between TM3 and TM4. The SEL is thought not to be involved in protein binding. The LEL domain is the most variable between the tetraspanin family members. The sequence variability within LEL is clustered in one hypervariable region that is coded by exon 6. This exon also codes for

the short CCG motif, conserved in all tetraspanins. The LEL region is folded into a mushroom-like structure as a result of two disulphide bridges. The crystal CD81 structure shows helical regions (a, b and e) that are conserved among the tetraspanins and form a tetraspanin-homodimerization interface. The mushroom-like patch is formed by helices c and d, and mediates specific lateral protein-protein interactions and ligand binding[32,33,36].

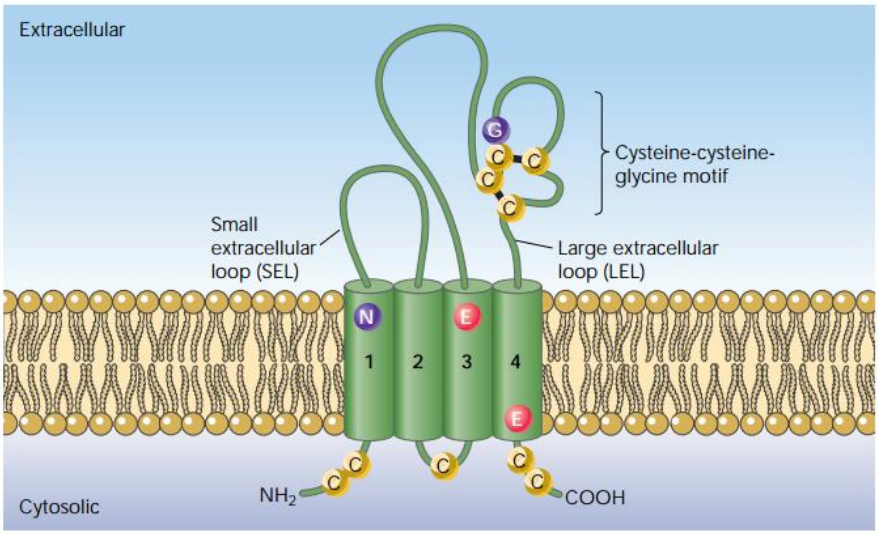

Figure 7. Structural features of tetraspanins. Reproduced from[37] .

CD81 consists of four TM domains: TM1 and TM2 flank the SEL, whereas TM3 and TM4 flank the LEL. Each TM domain contains conserved polar and non-polar aminoacid residues. These conserved residues in TM 1, 3 and 4 are responsible for a proper tetraspanin biosynthesis and maturation via intramolecular interactions, and contribute to the formation of the tetraspanin web through hydrophobic interactions between tetraspanins. Despite their short length, the cytoplasmic regions of tetraspanins (the cytoplasmic tails and short inner loop), can participate in various functions. These domains contain highly conserved cysteine residues that provide sites for palmitoylation, which contributes to the clustering of tetraspanin microdomains. The N-terminal intracellular CD81 contains two palmitoylatable cysteines, and the cytoplasmic C-terminal domain is involved in the sorting and targeting of CD81 to a determined intracellular region, and can mediate interactions with cytoskeletal or signalling proteins[33,36,38].

CD81 is a nonglycosylated protein, differing from other tetraspanin proteins that are glycosylated in either one of two extracellular domains. The CD81 protein undergoes posttranslational modifications by acylation with a fatty acid, not necessarily myristic acid[33].

1.2.2 The tetraspanin web: a dynamic network of molecular interactions

As mentioned above, one of the most striking features of tetraspanins is their ability to form lateral associations with multiple partner proteins, including each other, in a dynamic assembly described as the 'tetraspanin web'. The composition of the web is cell type-specific, where partnerships are formed with cell surface receptors, adhesion molecules, and transmembrane signalling proteins (Figure 8). The tetraspanin web mediates the cross talk between cell surface stimuli and intracellular signaling pathways, allowing cells to respond to a constantly changing environment in a specific and highly regulated manner[31].

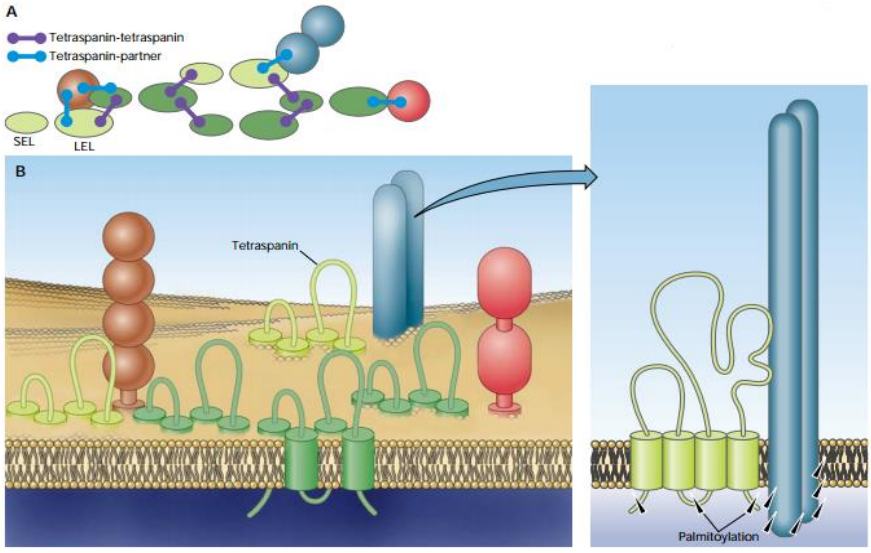

Figure 8. Membrane clustering of tetraspanin-enriched microdomains. A. Aerial view of tetraspanin-partner and tetraspanin-tetraspanin interactions. B. Side view of lateral associations of tetraspanin with partner molecules. Clustering is facilitated by palmitoylation. Tetraspanins are shown in shades of green; partners of the immunoglobulin superfamily are shown in red and brown; and partners of the integrin are in blue. Reproduced from[39].

Through the use of different detergents in tetraspanin co-immunoprecipitations, three levels of interactions in the tetraspanin web have been proposed: primary, secondary and tertiary. Primary interactions have been referred to direct associations within the tetraspanin web with their non-tetraspanin partner molecules. Some associations with partners are highly stoichiometric, are highly avid and retained after lysis in harsh detergents such as 1% NP-40 or 1% Triton X-100. The most common primary partners of tetraspanins are specific members of the integrin and of the immunoglobulin superfamilies and these partnership can be formed with the extracellular domains of the interacting molecules. The secondary interactions have been referred to the 'tetraspanin-tetraspanin associations' and are the weaker interactions between direct complexes. These interactions are not disrupted by mild detergents (as 1% Brij 96 or 1% Brij 97), and are not

stoichiometric. Recent studies have demonstrated that palmitoylation is necessary for the maintenance of these secondary tetraspanin-tetraspanin interactions. The tertiary interactions refer to the indirect associations of tetraspanins with additional proteins. These interactions are not disrupted in mild detergents, such as 1% CHAPS or 1% Brij 98. Functionally, these interactions cluster with cholesterol in tetraspanin-enriched microdomains, enabling lateral dynamic organization in the membrane and cross-talk with intracellular signalling and cytoskeletal structures[39,40].

The tetraspanin-partner associations occur during the biosynthesis of tetraspanins. The web assembly may occur in multiple steps in conjunction with trafficking within the different cellular compartments in which web subunits are formed. Early in biosynthesis, tetraspanins can form specific interactions with their associated partner proteins in the ER, serving as building blocks for the assembly of the tetraspanin web. Tetraspanin-tetraspanin interactions are likely to form in the Golgi upon palmitoylation, serving as building blocks for the assembly of large multicomponent cell-surface complexes[39].

1.2.3 CD81 physiological role

A major difficulty in the study of tetraspanins is to identify functions that are specific for a given tetraspanin, and to determine how this function relates to specific tetraspanin-associated proteins. CD81 has been implicated in immune cell functions and can directly associate with EWI-2 and EWI-F, a pair of cell surface proteins of the immunoglobulin superfamily. CD81 supports maturation and surface expression of EWI-2, which modulates integrin-dependent cell motility and spreading. Antibody crosslinking of CD81 can co-stimulate T cells, suggesting positive effector roles. On B cells CD81 is required for molecular organization and efficient collaborations between the B cell receptors and its partners (CD21, CD19 and various signalling enzymes). Also, CD81 associates with and facilitates the biosynthesis of CD19, a molecule that plays a role in the B-cell receptor signalling. CD81 also closely associates with the α4β1 integrin, regulating α4β1 adhesion under shear flow conditions. CD81 plays a specific role in various human infection diseases: it is essential for the entry of malaria parasite into hepatocytes; its expression in immune cells is associated with HCV-induced pathogenesis; CD81 has been identified as a cell-surface receptor for hepatitis C virus (HCV)[30,40].

CD81 modulates cell signalling events, affecting processes such as cell proliferation, apoptosis and tumour metastasis. CD81 interacts with different cytoplasmic molecules, facilitating

the activation of signalling cascades. The association of CD81 with type II phosphatylinositol 4-kinase (PI4K) may play a role in cell migration, bacterial infection and tumour cell proliferation. Recent studies strongly suggest that CD81 control cell migration due to its interaction with the small GTPase Rac. Further CD81 and CD9 positively modulate the activation of the extracellular signal-regulated kinase 1/2 (ERK1/2)/MAPK pathway to induce proliferation. CD81 and CD9 are closely related tetraspanins that have been linked to several processes, including apoptosis, and cell-cell fusion processes, such as like sperm-oocyte fusion. Few recent studies have started to implicate CD81 in nervous system physiology[30,40].

1.2.3.1 CD81 in fertility

From the membrane molecular players involved in mouse fertilization, only three so far have been shown to be essential: Izumo1 on the sperm surface, its oocyte-based receptor Juno, and the tetraspanin CD9 on the oocyte surface. These molecules are also present on human oocyte and sperm cells. CD9 is not the only tetraspanin expressed by human and mouse oocytes, which also express CD81, shown to associate with tetraspanin-enriched membrane structures on the surface of oocytes[27,41].

The lack of CD81 in the mouse female induces fertility defects, and the use of an anti-CD81 mAb partially inhibited sperm-oocyte binding and fusion[42]. The role of CD81 in sperm-oocyte fusion was demonstrated by in vitro insemination using *Cd81* $^{-/-}$ knockout mice. Deletion of the *Cd81* gene in mice results in a 40% reduction of female fertility. *Cd9*$^{-/-}$ *Cd81*$^{-/-}$ double knockout mice were completely infertile[41].

Tanigawa *et al.* (2008) demonstrated that CD81 is continuously expressed in the oocyte and in cumulus cells surrounding ovulated oocytes. These results indicate that the sperm may encounter CD81 on the somatic cells surrounding oocytes before sperm and oocyte directly interact. When *Cd81*$^{-/-}$ oocytes are incubated with sperm, some of the sperm that penetrated into the *Cd81*$^{-/-}$ oocytes perivitelline space fail to undergo the acrosome reaction. The impaired fusibility of CD81$^{-/-}$ oocytes may thus be partially caused by failure of the acrosome reaction[43]. A recent study performed by Ohnami *et al*. (2012) shows that oocyte CD81 was mainly localized at the inner portion of ZP, and may be involved in any step of fusion-related events prior to membrane fusion (Figure 9). Before the sperm-oocyte fusion, CD9 inside the PVS is transferred to the sperm membrane[44]. The CD9-containing membrane fragments are transferred from the oocyte to sperm via “exosome-like” vesicles. This interaction between membranes could be involved in the activation of sperm molecular complexes involved in binding and/or fusion with the oocyte

membrane[45]. Ohnami *et al*. (2012) suggest that CD81 may help to transfer CD9 of the oocyte into the sperm membrane through the formation of a complex between them[44].

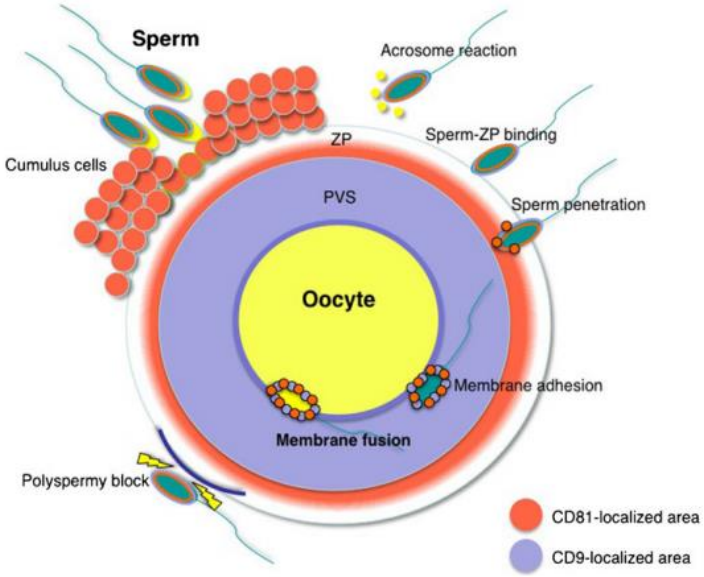

Figura 9. Schematic representation of the distribution of the CD81 tetraspanin in oocytes and sperm upon fertilization. Before fertilization, CD81 localizes in the inner region of the ZP. When the sperm penetrates the PVS, CD81 and CD9 appears to adhere to the sperm surface via exosomes. Orange area, CD81-localized area; light blue area, CD9-localized area; ZP, zona pellucida; PVS, perivitelline space. Reproduced from[44].

Interestingly, CD81 was one of the most abundant interactors that appeared in a Yeast Two-Hybrid screen of human testis cDNA library previously performed[46]. The protein used as bait, and whose interactors we were studying, was the Amyloid Precursor Protein, APP.

1.3 Amyloid Precursor Protein (APP)

Since the molecular cloning of the *APP* gene in 1987, the functions of APP and its cleavage products have been subject of intense investigation. *APP,* located in chromosome 21, is the most well studied member of APP family due its role in Alzheimer´s disease(AD)[47–50]. AD is the most prevalent neurodegenerative disorder and it is characterized by the presence of neurofibrillary tangles and amyloid plaques in the brain. Neurofibrillary tangles consist largely of hyperphosphorylated twisted filaments of the microtubule-associated protein tau. Extracellular amyloid plaques are deposits of differently sized small peptides, ranging in size from 38 to 44 aminoacids and called β-amyloid (Aβ), derived from sequential proteolytic cleavages of its APP precursor[51].

1.3.1 APP superfamily and isoforms

APP is a member of an evolutionary conserved gene family that also includes the mammalian APP-like protein-1 and -2 (APLP1 and APLP2). These proteins are highly homologous, sharing ~38-51% amino acid sequence identity[52,53]. The nearest APP-relative is APLP2 in which a segment of the deduced polypeptide (position 694-763) has 70.6% homology with the transmembrane cytoplasmic domain of the APP[54,55]. This family is conserved across a variety of species, and members can be found in invertebrates, including *C. elegans* (APP-like, APL-1) and *D. melanogaster* (APP-like, APPL)[56,57].

All APP family members are type 1 integral membrane proteins with a single membrane-spanning domain, a large ectoplasmic N-terminal regions and a shorter cytoplasmic C-terminal region. The APP sequence can be divided into multiple distinct domains, as demonstrated in Figure 10. The ectoplasmatic region of APP, which constitutes the major part of the protein, can be divided into E1 and E2 domains. The E1 domain can be further subdivided into a heparin-binding/growth factor-like domain (HFBD/GFLD) and a metal binding domain (cooper-binding domain and zinc-binding domain). The E1 domain is followed by an acidic region (Ac) and a Kunitz-type protease inhibitor (KPI) domain (that is subject to alternative splicing in both APP and APLP2). The E2 region consists of another HFBD/GFLD and a RERMS motif. The cytoplasmic region of APP contains a protein interaction motif, namely the YENPTY sequence, which is conserved in all APP homologues and participated in APP/APLPs endocytosis. The Aβ domain derived from the region of the protein encoded by parts of exons 16 and 17 is unique to the APP protein (Figure 10)[58,59].

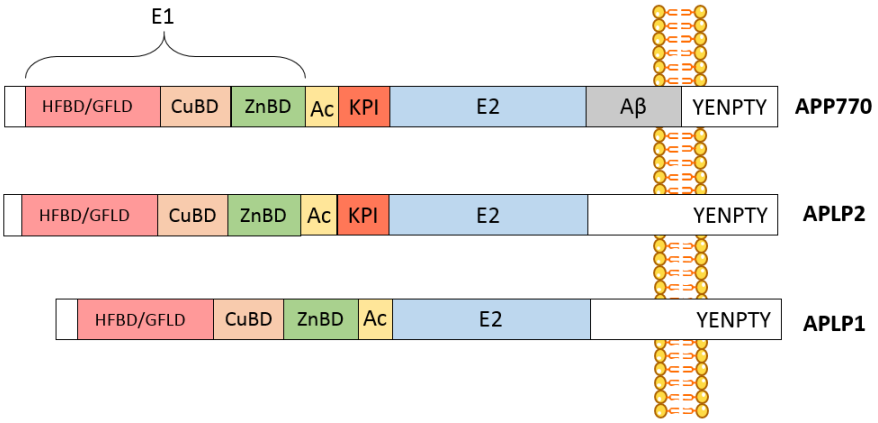

Figure 10. Schematic illustration of the domain organization of the members of APP protein family. All members share conserved E1 and E2 extracellular domains, an acid domain (Ac) and the internalization YENPTY motif in the carboxyl terminus. Note that Aβ is unique for APP. HFBD/GFLD, Heparin-binding/growth factor-like domain; CuBD, Copper binding domain; ZnBD, Zinc binding domain; KPI, Kunitz-type protease inhibitor domain. Adapted from[58,59].

The mammalian *APP* gene contains 18 exons (exons 1-13, 13a, and 14-18), of which exons 7, 8 and 15 can be alternatively spliced and generate multiple isoforms that are named according to their length in amino acids: L-APP 677, APP695, L-APP696, APP714, L-APP733, APP751, L-APP752, APP770[60–62] (Figure 11). APP is ubiquitously expressed, but the relative abundance of each isoform varies according to the cell type. The predominant transcripts are APP695, APP751 and APP770, in which APP695 isoform is mainly found in neuronal tissue, whereas APP751 is the predominant variant elsewhere[62]. The APP transcripts excluding exon 15 were first discovered in peripheral leukocytes and immunocompetent cells of the brain and where named leukocyte-derived APP (L-APP); these are ubiquitously expressed with the exception of neurons[63].

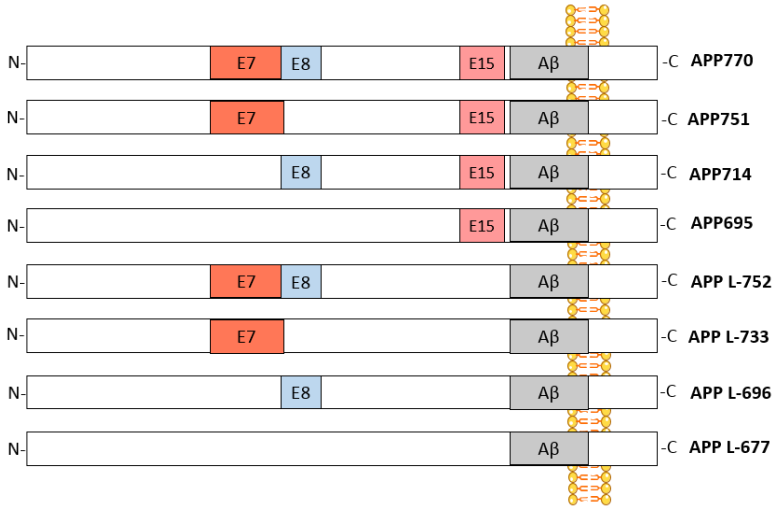

Figure 11. Exon structure of APP isoforms. The alternatively spliced exons are indicated in colours (E7, E8 and E7, exon 7 (KPI domains); E8, exon 8; E15, exon 15; Aβ, beta-amyloid.

Like *APP*, *APLP2* contains three exons that can be alternatively spliced. Four APLP2 isoforms are denoted as L-APLP2 isoforms in analogy to alternative splicing of *APP* exon 15. *APLP1* gene does not give rise to alternatively spliced exons, producing a single transcript[60]. APLP2, similarly to APP, is ubiquitous, whereas APLP1 is found primarily in cells of the nervous system[64].

1.3.2 APP Proteolytic Processing

APP is produced in large quantities in neurons and is very rapidly metabolized. Initially targeted to the secretory pathway, it is proteolytic processed into various fragments during its intracellular trafficking[65] (Figure 12).

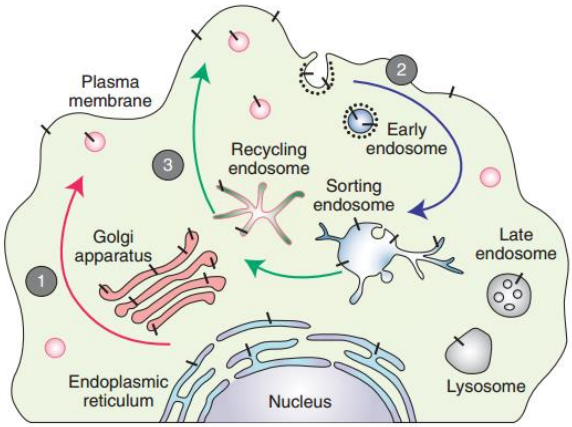

Figure 12. Intracellular trafficking of APP. Reproduced from[66].

APP is synthetized in the endoplasmic reticulum (ER) and then transported though the Golgi apparatus to the trans-Golgi-network (TGN). From the TGN, APP can be transported in TGN-derived secretory vesicles to the PM (Figure 12, step 1). During the transport from the ER to the PM, APP can undergo post-translational modifications by N- and O-linked glycosylation, ectodomain and cytoplasmic phosphorylation, and tyrosine sulphation. Only a small fraction of APP remains in the plasma membrane, whereas the majority of APP localizes in the TGN. On PM, APP undergoes proteolytic processing or is internalized due to the presence of its YENPTY internalization motif (Figure 12, step 2). Following endocytosis, APP is delivered to endosomes, and a fraction of the endocytosed molecules is recycled to the cell surface. Significant amounts of internalized APP also undergo degradation in lysosomes (Figure 12, step 3)[66–68].

The proteolytic processing of APP can be divided into two different pathways: the amyloidogenic pathway, which leads to generation of Aβ, and the nonamyloidogenic pathway (Figure 13). Both pathways are mediated by at least three cleavage events. In the non-

amyloidogenic pathway APP is cleaved approximately in the middle of the Aβ region by α-secretase, which generates a soluble N-terminal ectodomain termed sAPPα, that is release from the cell surface, and a truncated APP C-terminal fragment (CTF) (αCTF or C83). This fragment is subsequently cleaved by γ-secretase, leading to the secretion of a small non-pathogenic peptide p3 and a free APP intracellular domain (AICD) which is released into the cytosol. In the amyloidogenic pathway, the β-secretase activity initiates Aβ generation by shedding a large part of the ectodomain of APP (sAPPβ) and generating an APP CTF (βCTF or C99). This fragment is then cleaved by γ-secretase, generating Aβ and AICD. This final cleavage is not precise and under physiological conditions can occur at least between aminoacids 37 and 43 of the Aβ domain, generating Aβ1-40, Aβ1-42, carboxyl-terminal-truncated and amino-terminal-truncated Aβ peptides[59,65,66,69,70].

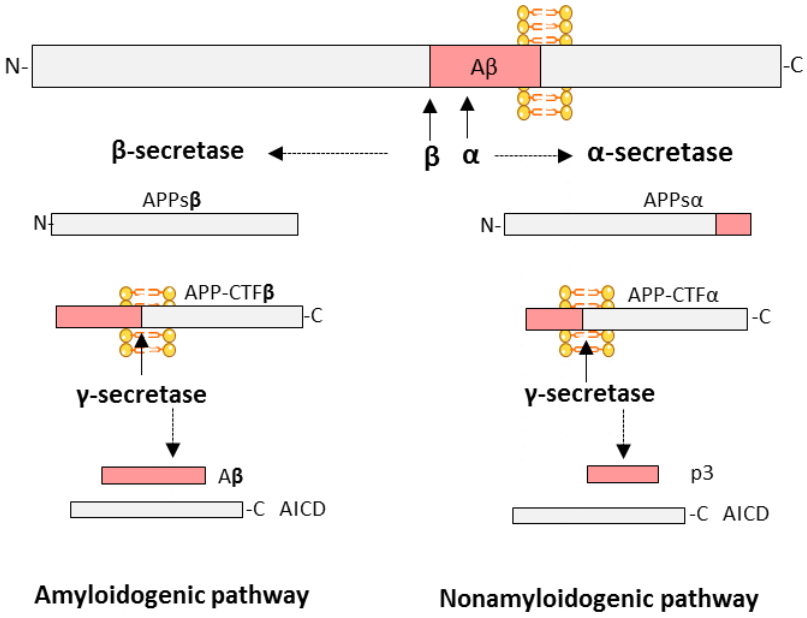

Figure 13. APP processing involves proteolytic cleavage by several secretases. The amyloidogenic pathway releases Aβ peptides through cleavage by β- and γ-secretases. The non-amyloidogenic pathway is initiated by α-secretase cleavage, which occurs in the middle of the Aβ domain, and results in the release of several soluble APP fragments. Aβ, β-amyloid; APP-CTF, APP C-terminal fragment; AICD, APP intracellular domain. Adapted from[70].

Although APP processing has been widely studied, the location of the secretase activities within the cell, and the identification of the enzymes involved have not yet been fully elucidated. α-secretase is a zinc metalloproteinase and is a member of the ADAM (A Desintegrin and Metalloprotease) family. Three of this family members have been suggested to be α-secretase:

ADAM9, ADAM10, and ADAM17. α-cleavage occurs at the PM and in intracellular post-Golgi compartments. Beta-site amyloid precursor protein cleaving enzymes 1 and 2 (BACE1 and BACE2) were identified as the major β-secretases. BACE is a membrane-bound aspartyl proteases with a characteristic type I transmembrane domain. The optimal pH of BACE activity agrees with the β-site cleavage of APP taking place in more acidic cellular compartments, such as the endosomes. BACE cleavage has also been suggested to occur in the PM lipid rafts. γ-secretase is an aspartyl protease with low sequence specificity that cleaves the substrate within its transmembrane domain. This enzyme is a protein complex that consists of anterior pharynx defective 1 (APH-1), nicastrin, presenilin 1 or 2 (PS1 or PS2), and presenilin enhancer-2 (PEN-2). The existing *in vivo* and *in vitro* data on presenilin point it as the responsible for the aspartyl γ-secretase activity. Noteworthy, there is some evidence that Aβ1-40 and Aβ1-42 are generated in different cellular compartments[59,65,66,69]. Of note, although the sequences where the various secretases cleave are very different in the two mammalian homologous, both APLP1 And APLP2 are believed to be proteolytically processed in a similar way as APP[59].

1.3.3 APP functions

Although APP and its homologues have been the subject of several studies, the physiological functions remains largely unknown. Several *in vitro* and *in vivo* studies have yielded strong evidence for the roles of APP, APLP1 and APLP2 in the developing and adult nervous system, in cell adhesion, neuronal survival, neurite outgrowth, synaptogenesis, vesicular transport, neuronal migration, modulation of synaptic plasticity, calcium metabolism, and insulin and glucose homeostasis. APP-derived proteolytic fragments mediate various and sometimes antagonist functions. Therefore, the net effect of full-length APP in cellular activity may be a combination of its metabolites´ functions. The N-terminal fragment, sAPPα, is neuroprotective, promotes neurite outgrowth and synaptogenesis, acts as a growth factor, and regulates cell adhesion. On the other hand, sAPPβ fragment can stimulate axonal pruning and neuronal cell death. The Aβ peptide has neurotoxic effects resulting in a neurodegenerative cascade leading to synaptic dysfunction and formation of intraneuronal fibrillary tangles. Although excessive Aβ causes neurotoxicity, low levels can positively modulate synaptic plasticity, revealing a novel physiological function for Aβ. The AICD fragment has been shown to possess transactivation activity and can regulate transcription of multiple genes, induce apoptosis, and may play a role in sensitizing neurons to toxic stimuli. Full length APP has been suggested to function as a cell surface receptor contributing to cell adhesion

and cell-cell interactions via its extracellular domain and possibly though trans-dimerization (reviewed in[59,65,71]).

1.3.3.1 APP and fertility

Although APP has been extensively investigated in association with AD pathology of the brain, APP biological functions are not restricted to the nervous system. Based on findings using the double *App* and *Aplp2* knockout mice, APP and APLP2 have been implicated in fertilization and may play a role in mammalian fertility. Knockout (KO) mice, homozygotes to either *App* (-/-) or *Aplp2* (-/-) were healthy and fertile. Contrary to this data, 80% double KO mice to *App* (-/-) and *Aplp2* (-/-) die within the first week and the surviving mice are infertile (9 of 10 females and all males). This findings suggests that APP and APLP2 can substitute each other functionally and are required for early postnatal development, normal growth, strength/balance, and fertility[72].

In 1990, Shoji and Kawarabayashi[73] demonstrated that native APP is present in acrosomes and in growing flagella, suggesting that APP appears in particular phases of spermatogenesis, especially the head and tail formation phase in spermatids.

A human sperm membrane protein termed YWK-II (latter shown to be homologous with APLP2) was immunolocated in male and female gametes. YWK-II/APLP2 is expressed in the mouse PM that envelops the acrosome, suggesting its participation in sperm-egg interactions. YWK-II/APLP2 may be a Gαo-coupled receptor and was shown to interact with Müllerian-inhibiting substance (MIS), which is well known to be required for sex determination. These interactions suggest that YWK-II/APLP2 may participate on germ cell differentiation and sperm metabolism[74–76]. Given the high degree of homology between APP and APLP2, and taking into account the Shoji and Kawarabayashi (1990) findings, da Cruz e Silva group performed a study in order to characterize the subcellular distribution of the APP superfamily members in human sperm. This study was carry out using a battery of antibodies that either recognize APP-specific epitopes or epitopes shared with other APP family members[77]. The results of this study show that in human sperm, the tail mainly expresses full-length KPI-positive APP, the mid-piece mainly expresses KPI-positive APLP2 variants, the equatorial region mainly contain KPI-containing ALPL2 variants, and the surface of the entire spermatozoa contains APP and/or APLPs, with particular abundance on the head (Figure 14). These results prove the presence of APP itself in human sperm. According to the authors the presence of APP family members along the entire length of the tail may be related to signalling events involved in sperm motility, whereas their presence on the surface, especially in the equatorial region,

suggests their involvement in sperm-oocyte interactions[77]. However, no binding partner has been described for APP in sperm-oocyte interactors or many other sperm functions.

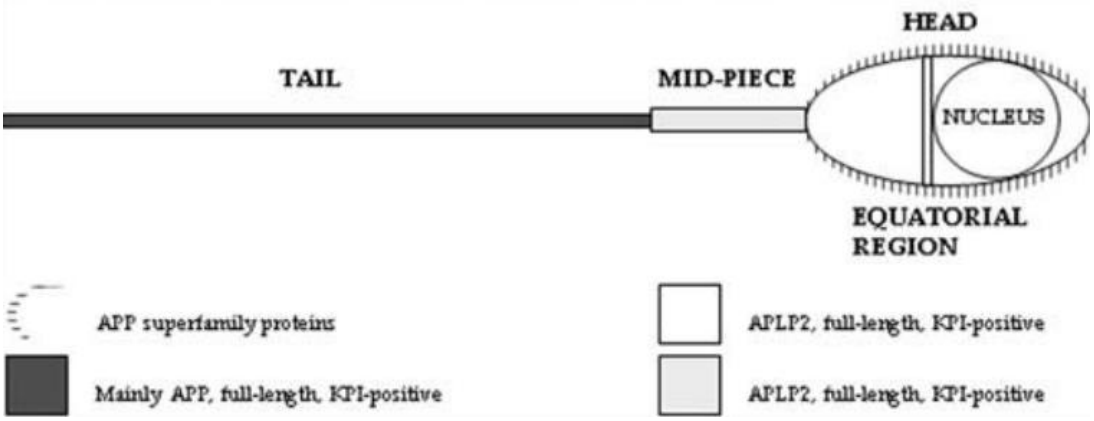

Figure 14. Schematic representation of the APP superfamily distribution in human sperm. Taken from[77].

1.3.4 Putative APP-CD81 interaction in human testis

The identification of the protein networks interacting with APP can be very useful to approach APP functions. To date, most proteins interacting with APP have been identified in the brain, but less is known about the pathways involved in testis and sperm functions.

In order to identify tissue-specific interacting proteins to approach APP functions in sperm and testis, our lab performed a Yeast Two-Hybrid (YTH) screen of a human testis cDNA library, using full-length human APP as bait, followed by a comprehensive bioinformatics analysis. From the total of the clones screened, 147 were positive and encoded 37 known proteins. Only one protein had previously been identified as an APP interacting protein (RANBP9)[46]. The analysis of the YTH screen revealed that one of the most abundant interactions was with CD81 (5 out of the 147 positive clones). The study included a network structure and bioinformatics analyses to determine the biologically relevant APP protein-protein interactions and revealed prominent topological properties for CD81[46].

2. Aims of the Thesis

CD81 is involved in reproduction, namely in sperm-oocyte interaction, but few is known about the molecular mechanisms involved in this CD81 function. APP and APLPs are expressed in the plasma membrane of the sperm head, a region involved in sperm-oocyte interaction, and APP has revealed to be a putative CD81 interacting protein. Taking these data into account, and the facts that APP is a very important protein of the nervous system and the CD81 biological functions in neuronal cells are also still far from clear, CD81 has emerged as a very interesting target of study for us.

The main general aim of this thesis was to expand the knowledge of CD81 in sperm cells and in a neuronal cell line, though the study of some of its interactions with proteins such as APP. The specific objectives set to attain this goal were to:

- Perform a bioinformatics analysis of CD81 interacting proteins;
- Characterize the expression of CD81 in sperm cells and in different cell lines, including a neuronal-like cell line;
- Determine and characterize the CD81-APP physical and functional interaction;
- Evaluate the co-localization of CD81 with some of its interacting proteins, in sperm-cells and in a neuronal cell line.

3. Materials and Methods

3.1 Bioinformatics analyses

3.1.1 Collection of literature-curated CD81 interacting proteins and constructing a protein-protein network

The identification of proteins that interact with human CD81 was carried out using the public database 'Biological General Repository for Interaction Dataset' (BioGrid)[78]. Only the interactions that were curated in *Homo sapiens* have been included. In addition, a literature survey was conducted to complement data on other interactions of CD81 absent from BioGrid by searching these in PubMed. The proteins involved in this study were collected with their own ID: gene symbol (www.genecards.org/) and UniProtKB (www.uniprot.org/uniprot/?query=&sort=score).The gene symbol of all collected proteins were loaded into the GeneMANIA[79] tool to generate a protein-protein interaction network. The network was generated using only data on physical interactions and using the "Biological process based" as the network weighting method.

3.1.2 Gene ontology and pathways

The Gene Ontology (GO)-term enrichment analysis was carried out using PANTHER - Protein Analysis Through Evolutionary Relationships[80] according to GO annotation ('biological processes', 'molecular functions' and 'cellular component'). The gene symbol of all collected proteins were loaded into PANTHER and the enrichment of specific GO-terms was tested using the "statistical overrepresentation test", followed by the Bonferroni multiple testing correction to control for the false discovery rate.

Similar to the GO-term enrichment analysis, cell-signalling pathways were also analysed using the "statistical overrepresentation test" implemented in PANTHER.

3.2 Preparation of CD81 cDNAs

The mApple-CD81 (Plasmid #54875) and pCDM8 hCD81 (Plasmid #11588) plasmids were purchased from Addgene (Cambridge, UK). Both plasmids encoded CD81, but mApple-CD81 has an orange-fluorescing tag (mApple) on N-terminal. The mApple-CD81 plasmid has bacterial resistance to kanamycin and pCDM8 hCD81 to ampicillin.

The plasmids were acquired as transformed bacteria in stab culture format. After being received, the bacteria were streaked from the stab onto a Luria Broth (LB) agar plate to isolate single colonies, further used to amplify and purified the plasmidic DNA by "Midiprep" using NucleoBond® Xtra Midi (Macherey-Nagel, Germany). One isolated colony of streaked LB agar plate was used to inoclute 3 ml of LB medium containing the appropriate antibiotic, and incubated for 16-18 h at 37°C with shaking (200 rpm). An aliquot of 150 µl was used to inoculate 150 ml of LB medium, also with the appropriate antibiotic, and the culture incubated overnight (ON) at 37°C with shaking (200 rpm). Cells were centrifuged at 6000 *g,* for 10 min at 4°C, the supernatant discarded, and 8 ml of resuspension Buffer RES added. After resuspension, 8 ml of lysis Buffer LYS was added, gently mixed by inverted the tube 5 times and incubated at RT for 5 min. Once the solution became clear and viscous, 8 ml of neutralization Buffer NEU was added to the lysate cells and then centrifuged at 12000 *g* for 10 min. Following, a NucleoBond® Xtra column filter was equilibrated with 12 ml of equilibration buffer EQU, placed into a 50 ml disposable plastic tube and the supernatant was poured into the column. The column filter was washed with 5 ml of equilibration buffer EQU and then discarded. The column was then washed with 8 ml of washing buffer WASH. To elute the DNA, the column was transferred to a new 15 ml plastic tube and 5 ml of elution buffer EDU was added. The precipitation of eluted DNA was carried out by adding 3.5 ml RT isopropanol and the DNA recovered by centrifugation (15000 *g,* 30 min at 4°C). The supernatant was discarded, and the pellets rinsed with 2 ml of 70% ethanol RT. The solutions were centrifuged at (15000 *g*, 5 min) the supernatant again removed, and the pellet allowed to dry. After all traces of ethanol have disappeared, the DNA was resuspended in Milli Q water and stored at -20°C. DNA concentration and its 260/280 nm purity ratio were calculated upon spectrophotometer measurement.

3.3 Mammalian cell assays

In the impossibility of performing sperm-oocyte interaction assays in our lab, immortalized cell lines were used to study the putative CD81 and APP interaction. The Chinese hamster ovary (CHO) cell line, of ovary nature, and the CG-1 spg cell line, derived from postnatal day 10 mouse testis and described as an intermediate spermatogenic cell type between type B spermatogonia and primary spermatocytes, were used. SH-SY5Y cell line was also used, due to its neuronal nature and its good expression of endogenous APP. The SH-SY5Y human neuroblastoma cells are originally derived from the cell line SK-N-SH, established from a bone marrow biopsy of a neuroblastoma patient.

3.3.1 Culture and maintenance of the cell lines

CHO cells were maintained in Ham's F-12 nutrient mixture (F-12; Sigma-Aldrich) containing 2 mM L-glutamine, 10% heat inactivated Foetal Bovine Serum (FBS; Gibco) and 1% antibiotic/antimycotic (AA) mix (Gibco). GC-1 cells were maintained in Dulbeco's Minimum Essential Media (DMEM; Gibco) supplemented with 10% FBS (Gibco) and 1% AAs mix (Gibco). SH-SY5Y were maintained in 10%FBS/1% AA mix-supplemented Minimum Essential Media (MEM):F12 (1:1). All cell lines were maintained in a 5% CO2 humidified incubator at 37°C, and subcultured when a 70-80% confluence was reached.

3.3.2 Human sperm samples

Fresh sperm samples were obtained from patients undergoing routine semen analysis or fertility treatments in the Human Reproduction Service at University Hospitals of Coimbra. Patients signed informed consent forms and the samples were used in accordance with the appropriate Ethical and Internal Review Board of the participating institution. Sperm samples were obtained by masturbation after 3-5 days of sexual abstinence and routine seminal samples analysis was performed according to the World Health Organization (WHO) guidelines[81]. All the samples used in this study had no detectable leukocytes (or any other round cells). After liquefaction, sperm cells were prepared by direct swim-up and allowed to capacitate in a supplemented Earl's balance salt solution (sEBSS) for at least 3 h at 37°C under 5% CO_2/95% air before starting the experiments.

3.3.3 CHO cells growth curve

Since the CHO line was a recent cell line used in our laboratory, we first characterize its growth. A CHO cells growth curve was determined by using two different methods of cell viability analysis, the Trypan blue (TB) exclusion dye method and the Resazurin metabolic colorimetric assay.

CHO cells suspended in growth medium were seeded ($1x10^4$ cells/well) of 6-well plate (Corning) and incubated at 37°C in a humidified 5% CO2. At a daily basis, media was substituted with fresh medium supplemented 10% of a resazurin solution [0.1 mg/ml resazurin salt solution (Sigma- Aldrich) in phosphate buffer solution (PBS; Pierce, Thermo Scientific)] with an end-volume of 1 ml per well. The cultures were incubated for 4h at 37°C in 5% CO2. Following this incubation period, the resazurin-containing growth medium was collected, the cells washed with PBS, suspended in PBS (volume depending on the average cell number), an aliquot mixed 9:1 with Trypan Blue solution (Sigma-Aldrich) was loaded in a hemocytometer, and cells were scored. In parallel, the rate of resazurin conversion to resofurin by metabolically active cells was evaluated via

spectrophotometric analysis at 570 and 600 nm (Infinite M200 microplate reader; Tecan Männedorf, Switzerland) of the resazurin-containing medium. A final optical density (O.D.f) was determined for each sample, as follows: (O.D. 570/O.D.600)-(O.D.570c/O.D. c 600), where 'OD.c' are the O.D.s of control samples (fresh medium supplemented with resazurin, never in contact with cells). This procedure was carried out during 10 days, at the same hour, in triplicate.

3.3.4 Cells transient transfection using the TurboFect™ reagent

In order to study the physical and functional interactions between APP and CD81, transient transfections of their cDNAs were performed in CHO and SH-SY5Y cells. Cells were plated and growth on plastic culture dishes (6-well or 100 mm) (Corning), 24 h before transfection, to be at ~70-80% confluence at the time of transfection. The growth medium was changed immediately prior to the transfection procedure. Cells were transient transfected with CD81 cDNAs (mApple-CD81 and untagged pCDM8 hCD81), alone or together with APP cDNAs (Wt APP-GFP and untagged pRC/CMV APP).The empty vectors (mApple, pCDM8, pEGFP-N1 and pRC/CMV) were single- or co-transfected as experimental controls.

All the transfection procedures were performed using the TurboFect™ reagent (Fermentas Life Science), a cationic polymer that forms a positively charged complex with DNA that is easily endocytosed by eukaryotic cells. For each well of 6-well plate, a certain amount of different cDNA was diluted in 100 µl of serum-free growth medium. After gently vortexing, a ratio of 1:2 µl TurboFect™ reagent was added to the DNA, mixed and incubated during 20 min at RT. This solution was added to each well and mixed by gently agitating the plate. The cells were incubated at 37^{o}C in a 5% CO_2 incubator, the cell medium changed after 6 h of transfection and cells and conditioned media (in some experiments) were collected after 24h of total transfection time. Table 3 presents details on the transient transfections performed in each assay.

Table 3. Cell transient transfection conditions adopted for each procedure.

Assay/cell line	Transfected cDNAs	Quantity (µg)/plate (mm)
CD81 expression CHO and SH-SY5Y cells	mApple-CD81 pCDM8 hCD81	0,5; 1.0; 1,5; 2.0 / 32 mm plated
GFP-Trap and RFP-Trap CHO cells	GFP/mApple APP-GFP/mApple APP-GFP/mApple-CD81 GFP/mApple-CD81	1.0 µg +1.0 µg (co-transfection) / 32 mm
Co-Immunoprecipitation of CD81 CHO cells	mApple-CD81	12 µg/ 100 mm plates
Co-Immunoprecipitation of APP and CD81 SH-SY5Y cells	APP pRC/CMV pCDM8 hCD81 APP pRC/CMV/ pCDM8 hCD81 pRC/CMV /pCDM8	12 µg (single transfection) 6 µg +6 µg (co-transfection) / 100 mm

3.3. Antibodies

Several primary antibodies were used in this study. Since it was the first time that in our group that we work with CD81 protein, we performed an optimization of the primary antibodies used against this protein (see section 4.2.3).

The primary antibodies used for immunoblotting assays were the rabbit monoclonal antibody EPR4244 (Abcam) against CD81 aa 150-250, which enables to detect the endogenous and exogenous CD81; the rabbit polyclonal antibody ab28664 (Abcam) against Red Fluorescent Protein (RFP), for detecting mApple-CD81; and mouse monoclonal anti-APP 22C11 (Chemicon) against the APP N-terminus aa 60-100, which enabled the evaluation of endogenous and exogenous APP and to measure the levels of total sAPP (α and β) in the conditioned medium. To analyse the effects of CD81 overexpression in cytoskeleton-related proteins, mouse monoclonal anti-Acetylated Tubulin (Sigma-Aldrich) and anti-β-actin (Novus Biologicals) antibodies were used. All the secondary antibodies, either recognizing mouse or rabbit antibodies were goat antibodies labelled with horseradish peroxidase (HRP), purchased from GE Healthcare.

For co-immunoprecipitation assays, the mouse monoclonal antibody 1D6 (Abcam) was used to immunoprecipitate the CD81 protein, and the anti-APP 22C11 was used to imunoprecipitate the APP protein.

In the immunocytochemistry assays, the following antibodies were used: the monoclonal antibody M38 (Abcam) against CD81, to analyse the location of CD81 in cells; the rabbit polyclonal anti-APP CT695 (Invitrogen), direct against APP C-terminus (last 50 aa); the rabbit monoclonal anti-AKT1 (Cell Signalling). Of note, Alexa Fluor 568 Phalloidin (Life Technologies), a drug that specifically targets filamentous actin (F-actin) was also used in the co-localization studies. Regarding the ICC in sperm cells, the rabbit anti-phosphotyrosine (Invitrogene) was used to evaluate the sperm capacitation, and *Pisum sativum agglutinin*- an acrosome content marker- coupled with fluorescein isothiocynate (PSA-FICT, Sigma) was used to access acrosomal integrity. The secondary antibodies used in ICC assays were Alexa Fluor 594 goat anti-mouse and anti-rabbit, and Alexa Fluor 488 goat anti-mouse and anti-rabbit (Life Technologies). Table 4 summarized the different antibodies and their dilutions used in all this work.

Table 4. Summary of the primary and secondary antibodies, and their specific dilutions, used to probe the target proteins in the different assays.

Target protein	Primary antibodies	Secondary antibodies
	Assay/Dilution	**Assay/Dilution**
CD81	**M38** ICC dilution: 1:100	Alexa Fluor 594 goat anti-mouse IgG ICC: 1:300
	1D6 IP: 8 µg	N/A
	EPR4244 WB: 1:1000	HRP conjugated anti-rabbit IgG WB: 1:2500
APP	**22C11** IB: 1:250 WB: 25 µl	HRP conjugated anti-mouse IgG WB: 1:5000
	CT695 ICC: 1:100	Alexa Fluor 488 goat anti-rabbit IgG ICC: 1:300
RFP	**ab28664** WB: 1:1000	HRP conjugated anti-rabbit IgG WB: 1:5000
Phosphotyrosine	ICC: 1:10	Alexa Fluor 488 goat anti-rabbit IgG ICC: 1:300
Acetylated Tubulin clone 6-11B-1	WB: 1:2000	HRP conjugated anti-mouse IgG WB: 1:5000
β- actin	WB: 1:10000	HRP conjugated anti-mouse IgG WB: 1:5000
AKT	ICC: 1:200	Alexa Fluor 488 goat anti-rabbit IgG Alexa Fluor 594 goat anti-rabbit IgG ICC: 1:300

Abbreviations: APP, Amyloid precursor protein; AKT, RAC-alpha serine/threonine-protein kinase; ICC, immunocytochemistry; IP, immunoprecipitation; RFP, Red Fluorescent Protein; WB, Western blot

3.4 Proteomic assays

3.4.1 Cell collection and quantification of protein content

Cell´s conditioned media were collected with 1/10 v/v 10% SDS, and cells washed with PBS and harvested in 250 µl (6-well) , 750 µl (100 mm) or 500 µl ($42x10^6$ sperm cells) of 1% SDS for WB. Cells and media lysates were boiled at 90ºC for 10 min and cell lysates sonicated for 10 sec; both were stored at -20 ºC. The cell collection procedure for the pull-down assays is slightly different and is described further ahead.

Total protein content of cell lysates was carried out using the Pierce's bicinchoninic acid (BCA) protein assay kit (Thermo Scientific), following the manufacturer's instruction. This method combines the reduction of Cu^{2+} to Cu^{+} by protein in an alkaline environment with the highly sensitive and selective colorimetric detection of the cuprous cation (Cu^{+}) by bicinchoninic acid. The result of this two reactions is the formation of an intense purple-coloured reaction product, a water-soluble complex with a strong absorbance at 562 nm with increasing protein concentrations over a working range of 20-2000 µg/ml[82]. Total protein concentration of each sample was determined by comparision to standard samples that were prepared using increasing known amounts of bovine serum albumin (BSA).

An aliquot of cell lysates samples (5 µl) was diluted with 20 µl of 1% SDS in a 96 well plate, and these aliquots incubated at 37ºC for 30 min with 200 µl of working reagent (compound of 50 parts of reagent A to 1 part of reagent B), alongside with BSA protein standards (both in duplicate). Following, the absorbance at 562 nm was measured with the Infinite M200 microplate reader. A standard curve was obtained by plotting BSA vs BSA concentration, and used to determine the total protein concentration of each sample.

3.4.2 Co-immunoprecipitation (Co-IP) assay

In order to determine if APP and CD81 physically interact, we performed co-immunoprecipitation (Co-IP) assays. These are an extension of immunoprecipitation (IP) that is based on the potential of IP reactions to capture and purify the primary target protein as well as other proteins that are bound to the primary target by native interactions. In our experimental procedure, the Co-IP was carried out using Protein G Dynabeads® (Invitrogen). The procedure is based on the ability of Protein G Dynabeads® to bind to the Fc region of primary antibodies. The immune complex is then precipitated on a beaded support to which an antibody-binding protein is

immobilized. The tube is placed on a magnet, where the beads migrate to the side of the tube facing the magnet and allow for easy removal of the supernatant. Proteins not precipitated on the beads are hence washed away[83].

The co-IP assays of CD81 were performed in CHO and SH-SY5Y grown in 100 mm culture dishes (section 3.3.1). Following 24 h of transient transfection with the CD81 and/or APP cDNAs (section 3.2.2), media were removed and cells washed with cold PBS 1x and then gently scrapped off the culture plate with 750 µl of non-denaturing lysis buffer. CHO cells were collected in NP-40 lysis buffer [10 mM Tris-HCl pH 7.5; 150 mM NaCl, 0.5 mM EDTA, 1%NP-40, 1mM PMSF and protease inhibitor cocktail (0.1%, Sigma-Aldrich)]. SH-SY5Y cells were collected in CHAPS lysis buffer [50 mM Tris-HCl pH 8.0, 120 nM NaCl, 4% CHAPS, 1mM PMSF and protease inhibitor cocktail]. Lysates were mass-normalized using the BCA assay (section 3.4.1) and 1000 µg of each lysate precleared with 15 µl Dynabeads for 1 hour at 4°C with agitation. In a separate microtube, 40 µL of Dynabeads were added to 200 µl of Washing solution (3% BSA in PBS) containing the primary antibody (APP or CD81 at respective dilutions, depicted in Table 4) for 1 hour at 4°C with agitation. Prior to use, Dynabeads were washed thrice with Washing Solution and stored at 4°C.

After 1 h, each sample was transferred to the antibody/Dynabeads-containing microtube, previously washed with 200 µl of washing solution, and incubated overnight at 4°C with agitation. Following, the supernatant was removed and the beads washed thrice with 500 µl of PBS 1x for 10 min at 4°C with agitation. After the last wash, the supernatant was fully discarded and the beads resuspended in 100 µl of 1x Loading Buffer (LB) and boiled for 10 min at 90°C for disruption of the Dynabead-proteins complex. Dynabeads were magnetically removed, and lysates and immunoprecipitates further resolved in a 5-20% gradient SDS-PAGE followed by immunoblotting, as described in section 3.4.4. Co-IP controls were performed by incubating cell extracts with Dynabeads linked to Normal Mouse IgGs (Santa Cruz Biotechnologies).

3.4.3 RFP-Trap and GFP-Trap

Another approach used to study the interaction between APP and CD81 was to pull-down these proteins when fused to GFP and mApple (RFP derivated) proteins.RFP and GFP-fusion proteins and their binding partners can be fast and efficiently isolated via pull-down of the RFP with RFP-Trap® (Chromotek) and GFP with GFP-Trap® (Chromotek). After CHO cells transient transfection for 24 h with APP-GFP and mApple-CD81 cDNAs (as in section 3.2.2), cells were washed with 1x PBS and subsequently collected with a scrapper in 1 ml of cold PBS with 1x PMSF solution.

Samples were then centrifuged for 5 min at 3000 *g* (4°C), the supernatant removed and 500 µl of freshly prepared Triton-X lysis buffer (10 mM Tris-HCl pH 7.5; 150 mM NaCl, 0.5 mM EDTA, 1% Triton-X, 1mM PMSF and 0,1% protease inhibitor cocktail were added to the pellet. Samples were maintained on ice for 30 min and mixed twice, with 10 min intervals. Meanwhile, the RFP-Trap or GFP-Trap beads were washed 4 times in freshly prepared wash buffer, isolated by a magnet and kept at 4°C. After lysis, the samples were centrifuged for 5 min at 10000 *g* (4°C), and the supernatant transferred to a new microtube. Mass normalized (150 µg/sample) were adjusted to 300 µl with freshly prepared dilution buffer, and 10 µl of the RFP-Trap or GFP-Trap beads added to each sample and incubated for 4 h with orbital shaking at 4°C. Following the incubation period, the supernatant was removed and the beads washed thrice with 300 µl of wash buffer. After the last wash, the supernatant was fully discarded and the beads resuspended in 100 µL of 1x Loading Buffer and boiled for 10 min at 90°C for disruption of the trap beads proteins complexes. Trap beads were removed, and lysates and immunoprecipitates were then resolved in a 5-20% gradient SDS-PAGE followed by immunoblotting as described in section 3.4.4.

3.4.4 Western-blot (WB)/Immunoblotting (IB) assays

Western-blot (WB) or immunoblot (IB) is a rapid and sensitive assay used in cellular and molecular biology for the identification and quantification of specific proteins from a complex mixture of proteins. The technique uses three elements: 1) separation by size; 2) transfer to a solid support and 3) probing a target protein with a proper primary and secondary antibody, linked to an enzyme or fluorophore to visualize[84].

In the present work, mass-normalized samples were resolved by electrophoresis on a 5-20% gradient sodium dodecyl sulphate (SDS) polyacrylamide gel electrophoresis (SDS-PAGE), a denaturing gel that allows for the separation of proteins solely on the basis of their molecular weight. It consists of two gels: a resolving (bottom) gel, with higher concentration of polyacrylamide to separate proteins, and a stacking (top) gel, with lower concentration of polyacrylamide and high concentration of SDS, which confers negative charge for the proteins to migrate to the anode.

Prior to loading, the samples were prepared by the addition of ¼ volume of loading buffer (4x), which consists of glycerol, SDS, a reducing agent (β-mercaptoethanol) and a dye (bromophenol blue). Electrical current is then applied to the gel (90 mA) enabling the separation of proteins. Precision plus Protein ™ Dual Colour Standards (Bio Rad) was used as a molecular weight marker.

After separation, the proteins were electrotransferred at 200 mA onto a nitrocellulose membrane (0.2 µm pore size; Whatman®).

3.4.5 Ponceau Red staining

Ponceau Red staining is normally applied to assess successful electrotransfer of proteins to the membrane, but it can be also used as a loading control as an alternative to actin or β-tubulin when the levels of these proteins may change with the conditions under test. This type of staining has been described as a fast, inexpensive, and nontoxic method, and it is fully reversible in a few minutes[85]. The nitrocellulose membrane were incubated in Ponceau S Solution (Sigma Aldrich) for 10 min, followed by a wash with deionized water for making the protein bands clearly visible. Membranes were then scanned in a GS-800 calibrated imaging densitometer (Bio-Rad), after which membranes were washed with 1x TBS-T for complete removal of the staining.

3.4.6 Immunodetection

Concerning the immunological detection, briefly, the nitrocellulose membranes were first hydrated in 1x TBS for 10 min and then blocked with 5% BSA in Tris Buffered Saline Tween (TBS-T) 1x for 4 h. Membranes were then washed in TBS-T 1x for 10 min, incubated with a specific primary antibody (depicted in Table 4) overnight, washed thrice with TBS-T 1x for 10 min each, incubated with the appropriate HRP-conjugated secondary antibody for 2 h and washed thrice with TBS-T 1x for 10 min. Following, membranes were incubated with enhanced chemiluminescence (ECL) detection kit for 1 min, with Luminata™ Crescendo Western HRP Substrate (Millipore) or with ECL™ Select WB detection reagent (GE Healthcare) for 5 min, in a dark room. After exposure of the membranes to X-ray films (GE Healthcare), these were developed and fixed with the appropriate solutions (Kodak). Films were then scanned in the GS-800 calibrated imaging densitometer (Bio-Rad) and the results analysed.

3.5 Immunocytochemistry (ICC) assays

To determine if APP and CD81 co-localize in mammalian cells and their sub cellular localization, immunocytochemistry (ICC) assays were performed in CHO, GC-1 and SH-SY5Y cell lines, as well as in sperm cells.

ICC is a technique that permits the visualization of the localization of a specific protein, thought protein-antibody interactions, in fixed cells[86].

Initially, samples are prepared by fixing with a fixation agent such as paraformaldehyde (PFA), which helps to stabilize and preserve cells as close to life-like as possible. This occurs by binding of the agent to reactive groups on cellular proteins and lipids, what holds them in the same position as if they were in living cells. Fixed cells are then permeabilized, so that antibodies and other probes can penetrate inside. This is achieved by the addition of detergents, which can solubilize membranes without destroying protein-protein interactions. Following permeabilization, non-specific binding sites in cells are blocked, incubated with the proper specific antibody primary and fluorescent secondary antibodies, and mounted on a microscope slide in a media with anti-fading and anti-photobleaching properties. The preparation can be further visualized through a fluorescent microscope[86]. The excitation and emission wavelengths peaks of the secondary antibodies, fluorescent tags and PSA-TRICT are presented in table 5.

Table 5. Summary of the excitation and emission wavelengths of the secondary antibodies, fluorescent tags and PSA-TRICT.

Fluorophores	Excitation maximum (nm)	Emission maximum (nm)	Observed colour
Alexa Fluor 488	495	519	Green
Alexa Fluor 594	590	617	Red
mApple Tag	568	592	Red
GFP Tag	488	507	Green
PSA-FITC	495	515	Green
Alexa Fluor 568 Phalloidin	578	600	Red

3.5.1 ICC on cell lines

In the present work, the cell culture was performed as described in section 3.2.1 in 6-well plates containing glass coverslips. Cells were washed (PBS 1x) and 1 ml of 4% PFA was added for 20 min. Following fixation, cells were washed trice with PBS 1x, and 300 µl of 0.2% Triton-X was added for 10 min. After another 3 washes with 1x PBS, cells were covered with 1x PBS/3% BSA blockage solution for 30 min, followed by 2 h incubation with the specific antibodies diluted in 1x PBS/3%BSA, washed with 1x PBS, and further incubated for 1 h with a fluorescent secondary antibody (Table 4).

Samples were then mounted on a microscope slide with DAPI-containing VECTASHIELD® Mounting Media (Vector Laboratories) and visualized using a LSM510-Meta confocal microscope (Zeiss) with the 63x/1.4 or 100x/1.4 oil immersion objectives. The 405 nm argon diode laser, the argon laser line 488 nm, and the 561 nm DPSS laser were used.

3.5.2 ICC on sperm cells

Capacitated and acrosome reacted sperm cells were fixed with 2% formaldehyde in PBS for 40 min, washed with PBS, and permeabilized with 1% Triton X-100 in PBS for 20 min. After washing with PBS, sperm cells were blocked with 1% BSA and 100 mmol/L glycine in PBS for 30 min. After blocking, 100 µl of sperm cells were incubated for 2 h at 37°C with the respective primary antibody (Table 4). Sperm cells were subsequently washed with 300 µl of washing solution (0,1% Triton X-100 in PBS) for 30 min. Sperm cells were then incubated 1 h at 37°C with the respective secondary antibody and acrosome reacted sperms were also incubated with PSA-FITC (1:200). Sperm cells were washed with 300 µl of washing solution for 15 min. Among washing steps, sperm cells were centrifuged at 1800 rpm/ 5 min. Samples were mounted on a microscope slide with DAPI-containing VECTASHIELD® Mounting Media and visualized using the LSM510-Meta confocal microscope under a 100x/1.4 oil immersion objective, and using the lasers above identified. Sperm cells stained in the entire tail were considered capacitated; those with a negative staining for PSA-FITC were considered acrosome-reacted.

3.6 Data Analysis

The protein bands resultant from the WB procedures were quantified using Image Lab Software (Bio-Rad) and data presented as mean ± SEM (standard error of the mean) of at least three different experiments.

3.7 Micropotographs analysis

Image analysis was performed using the ImageJ Fiji software[87]. The co-localization analysis was conducted using the JACoP (‘Just another colocalization Plugin’). This plugin uses several pixel intensity spatial correlation methods to determine co-localization between two different colour channels, such as the Manders, the Costes, the Pearson or the Li methods. In the work here

described, results were obtained using the Manders' method, since it is normally the most used method when comparing two objects of different amounts (in this case two proteins which most probably have different expression levels)[88]. Co-localization of APP and CD81 was analyzed using ~20 images with an average of 10 cells per image. The results are presented as the percentage of co-localization of one protein with the other.

4. Results

4.1 Bioinformatics analyses of CD81 interacting proteins

A major difficulty in the study of tetraspanins is to determine functions that are specific to a given tetraspanin; however, specific tetraspanin-associated proteins may help to clarify this issue. The spatial organization of membrane proteins in the plasma membrane is critical for signal transduction, cell communication and membrane trafficking. As mentioned earlier, tetraspanins are organized functionally in protein complexes called TEM via interactions with partner proteins and other tetraspanins. Considering the large tissue distribution of CD81, this tetraspanin protein has been implicated in a large number of biological processes. However its specific function in these processes remain to be elucidated. The interaction between CD81 and certain partner proteins may underlie the CD81 involvement in a variety of cellular processes and modulate CD81/partner proteins specific functions[40,89].

To better understand the physiological role of CD81, a search for the available CD81 interacting proteins was performed in databases and in the literature. The retrieved information was then further investigated by constructing a protein-protein interaction (PPI) network, and by performing Gene Ontology (GO) term enrichment analysis for functional interpretation of the interacting proteins, and by performing a pathway analysis though various computational tools.

4.1.1 CD81 protein-protein interaction network

Identification of literature curated interactions

In order to identify the interactors of CD81, human PPIs were collected from the public database Biological General Repository for Interaction Dataset (BioGrid)[78]. During the literature research performed for this current work, many CD81 interacting proteins were identified. Since some of these interactions were not included in the BioGrid database, the interactions that were elsewhere identified, namely in articles retrieved from PubMed, were manually included.

A total of 222 proteins were identified as CD81 interacting proteins, among which 196 proteins were retrieved from BioGrid and 26 were identified in the literature. Only interactions that were curated have been used. A full list of the CD81 interacting proteins is presented in Table 1 (Appendix 1).

Construction of CD81 protein interaction network

All collected proteins were loaded into GeneMANIA[79] to construct a CD81 protein interaction network. The network was generated using physical interactions and "Biological process based" as the network weighting method. From the total of 222 genes used as input, 219 ID were recognized. GeneMANIA introduced 20 genes, as genes that are functionally similar, or have shared properties with CD81 interactors. The extracted network (Figure 14) consists of 239 protein nodes and 2632 interactions between these proteins. The full list of proteins with the associated scores extracted from this network are presented in Table 2 (Appendix 1).

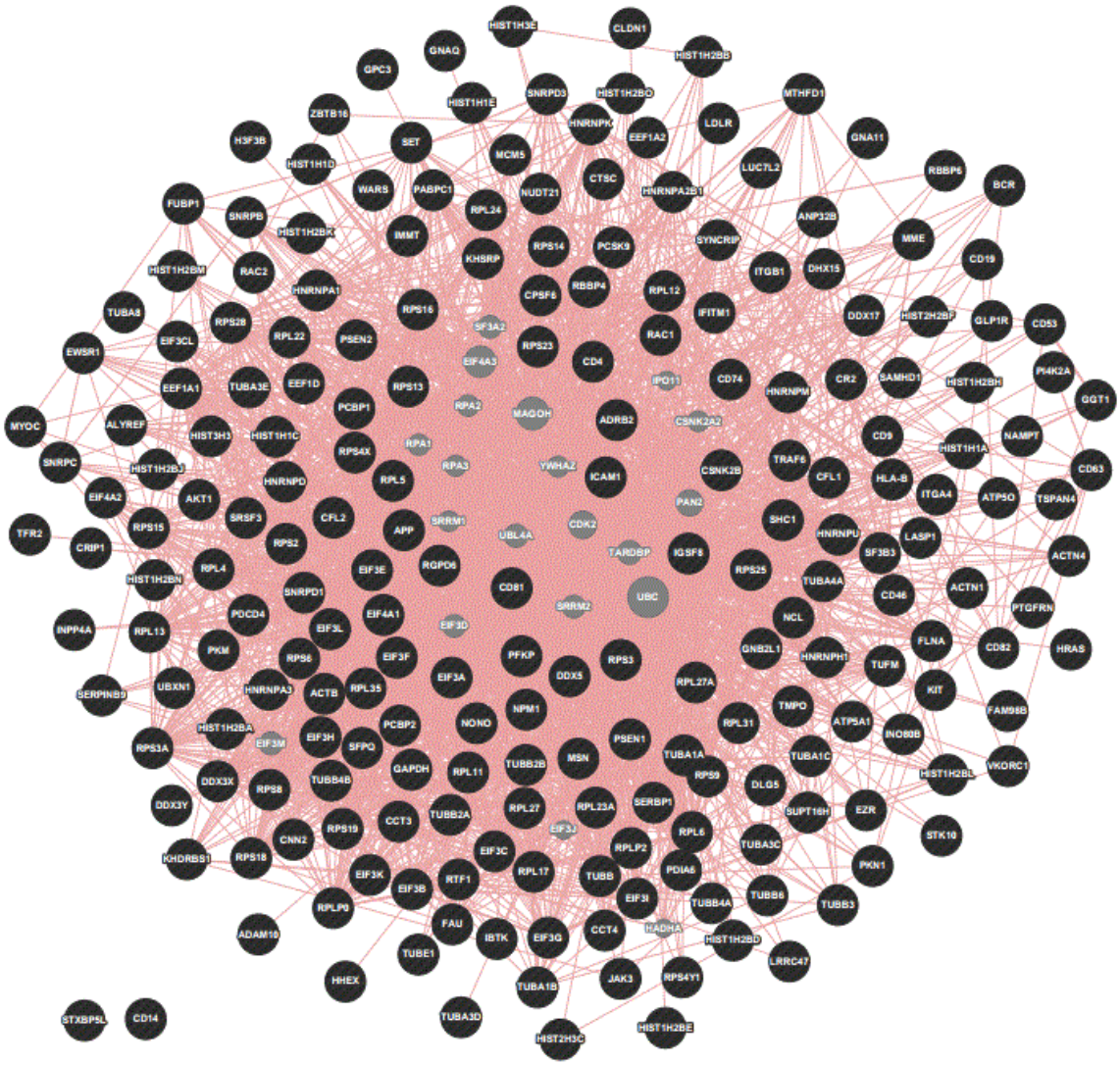

Figure 14. CD81 protein interaction network .This protein interaction network consists of 239 protein nodes and 2632 interactions Black nodes correspond to the query proteins and grey nodes corresponds to proteins that were added by GeneMANIA**.**

Compared with the affluence of cell-surface molecules that associated with tetraspanins, only a few cytoplasmic molecules have been shown to interact with tetraspanins[90]. In contrast with this data, the analysis of CD81 interacting network showed that the majority of proteins were located in the cytoplasm and nucleus.

4.1.2 Gene enrichment analysis

A GO-term enrichment analysis was used to compare the abundance of specific GO-terms in the CD81 interacting network with the natural abundance in the organism in question (*Homo sapiens*).

The proteins identified in the present study that interact with CD81 were analysed using PANTHER - Protein Analysis Through Evolutionary Relationships[80] according to GO annotation by grouping them into 3 categories: biological processes, molecular functions and cellular components. Not all the protein entries were fully annotated with the corresponding GO terms but from the total of 222 proteins entries, 214 were categorized using the "statistical overrepresentation test" analysis. The statistical method using the Bonferroni correction was applied and only GO terms with a p-value < 0.05 were considered.

Regarding the biological process (Table 6), the results revealed that the categories with the largest number of proteins were related to: metabolic processes (56%; p-value = 4.02E-09), primary metabolic processes (53%; p-value = 1.09E-12), cellular processes (41%; p-value = 4.87E-03), protein metabolic process (33%; p-value = 7.43E-15), and protein translation (22%; p-value = 7.33E-34). 25 proteins were not classified (12%; p-value = 0).

Table 6. Significantly enriched gene ontology categories by biological process of gene products interacting with CD81. p-value < 0.05. "% ID" indicates the percentage of proteins associated with each GO term relative to the total number of proteins that were categorized.

Most Significant Biological process					
GO term	**% ID**	**p-value**	**GO term**	**% ID**	**p-value**
Translation	22	7.33E-34	Chromatin organization	8	4.99E-09
Protein metabolic process	33	7.43E-15	Anatomical structure morphogenesis	11	2.84E-07
Chromatin assembly	5	1.69E-13	Intracellular protein transport	13	7.32E-05
Primary metabolic process	53	1.09E-12	Protein transport	13	1.28E-04
mRNA splicing, via spliceosome	9	2.42E-12	Organelle organization	9	2.89E-04
mRNA processing	10	3.05E-12	Nuclear transport	4	2.96E-04

Most Significant Biological process					
Cellular component organization or biogenesis	21	7.34E-12	Cellular component morphogenesis	8	4.48E-04
Regulation of translation	8	1.30E-11	DNA metabolic process	7	5.13E-04
RNA splicing, via transesterification reactions	7	3.27E-11	Nucleobase-containing compound metabolic process	26	1.26E-03
RNA splicing	7	4.57E-11	Cellular process	41	4.87E-03
Cellular component biogenesis	10	3.07E-10	Cell cycle	12	5.52E-03
Cellular component organization	18	3.32E-09	Developmental process	19	3.44E-02
Metabolic process	56	4.02E-09	Chromosome segregation	3	4.43E-02

Regarding molecular function (Table 7), results show that the majority of proteins are involved in binding processes (53%; p-value = 1.01E-12), more specifically nucleic acid binding (40%; p-value = 3.29E-18), RNA binding (19%; p-value = 5.85E-23), and structural molecular activity (27%; p-value = 5.85E-23). This category contains 49 unclassified protein (23%; p-value = 0). When proteins are categorized according to their cellular component (Table 7), most of the proteins are considered intracellular (28%; p-value = 2.58E-08), located in macromolecular complexes (23%; p-value = 3.06E-21), organelle (19%; p-value = 2.43E-04) and ribonucleoprotein complexes (8%; p-value = 7.27E-12). However, in this category a high number of proteins were not classified (66%; p-value = 0)

Table 7. Significantly enriched gene ontology categories by cellular component and molecular function of gene products interacting with CD81. p-value < 0,05. "% ID" indicates the percentage of proteins associated with each GO term relative to the total number of proteins that were categorized.

Most Significant Molecular Function			Most Significant Cellular component		
GO term	**% ID**	**p-value**	**GO term**	**% ID**	**p-value**
Structural molecule activity	27	5.85E-23	Macromolecular complex	23	3.06E-21
RNA binding	19	5.85E-23	Protein-DNA complex	5	5.37E-13
Nucleic acid binding	40	3.29E-18	Ribonucleoprotein complex	8	7.27E-12
Structural constituent of ribosome	11	5.52E-16	Nuclear chromosome	5	1.83E-09
Translation factor activity, nucleic acid binding	9	1.06E-13	Chromosome	5	2.31E-08
Binding	53	1.01E-12	Intracellular	28	2.58E-08
Translation regulator activity	7	1.17E-10	Tubulin complex	3	1.94E-07
Translation initiation factor activity	7	5.06E-10	Cell part	30	3.00E-07
mRNA binding	7	7.02E-08	Ribosome	4	3.24E-07

Most Significant Molecular Function			Most Significant Cellular component		
Structural constituent of cytoskeleton	12	5.05E-06	Cytosol	3	3.97E-05
RNA helicase activity	3	4.18E-03	Organelle	19	2.43E-04
Helicase activity	4	1.02E-02	Nucleus	6	6.38E-04
Translation elongation factor activity	2	2.17E-02	Protein complex	9	1.56E-03

The analysis of enriched GO categories showed that, regarding their biological processes, most proteins that interact with CD81 are mainly involved in the determination of DNA and RNA fate, including RNA splicing and translation, or in cell metabolism. To achieve these processes, the result of the analysis of molecular functions suggests that the majority of proteins are involved in nucleic acid/RNA/mRNA binding and binding to molecules involved in Protein Translation. Some of these are proteins with an active role in the regulation of translation once they act as initiation and elongation factors. Regarding the cellular component, as expected from their molecular functions, most proteins were located in the cytosol and nucleus, more specifically in ribosomes and chromosomes.

4.1.3 Pathway analysis

Similar to GO term enrichment analysis, an analysis of pathway abundance was performed. This analysis might be more meaningful since it moves the data interpretation away from a gene-centric view towards the identification of common functional biological processes [91].

Cell-signalling pathways were analysed using PANTHER. A PANTHER overrepresentation test analysis was performed, and from the total of 222 proteins entries, 214 were categorized. Table 8 presents the signalling pathways in which some of the CD81 interacting proteins are involved. The top 5 significant pathways were: cytoskeletal regulation by Rho GTPase (p-value = 3.48E-11); Huntington's disease (p-value = 2.11E-08); integrin signalling pathway (p-value = 2.22E-05); Gonadotropin releasing hormone receptor (p-value = 6.08E-04) and Alzheimer's disease-amyloid secretase pathway (p-value = 6.17E-04). It is important to note that 166 proteins were not classified using this approach. From the proteins that were classified, AKT1, RAC1, RAC2, and proteins of the Tubulin beta family are interesting CD81 interacting proteins that play a key role in various CD81 pathways. Further, from the 24 pathways identified, two are related to the APP proteolytic processing.

Table 8. Significant signalling pathways in which gene products interacting with CD81 are involved. p-value < 0.05.

Pathways	Gene ID	p-value
Cytoskeletal regulation by Rho GTPase	TUBB4B, TUBB3, CLF1, RPL12, TUBB6, TUBB2B, TUBB, ACTB, RAC1, CFL2, RAC2	3.48E-11
Huntington disease	TUBB4B, TUBB3, RPL12, TUBB6, TUBB2B, TUBB, TUBB2A, AKT1, GAPDH, TUBB4B, ACTB, RAC1, RAC2	2.11E-08
Integrin signalling pathway	ITB1, RAC1, ACTB, ITGA4, ACTN1, FLNA, ACTN4, HRAS, SHC1, RAC2	2.22E-05
Unclassified	166 IDs	2.55E-05
Gonadotropin releasing hormone receptor pathway	ITGB1, GNAQ, AKT1, RAC1, TUBA1B, GNA11, HRAS, TUBA1C, TUBA1A	6.08E-04
Alzheimer's disease-amyloid secretase pathway	PKN1, APP, PSEN1, PSEN2, ADAM10	6.17E-04
Inflammation mediated by chemokine and cytokine signalling pathway	ITGB1, ATP50, GNAQ, AKT1, RAC1, ACTB, ITGA4, GNA11, SHC1	1.10E-03
Ras Pathway	AKT1, RAC1, HRAS, SHC1, RAC2	1.46E-03
T cell activation	AKT1, RAC1, HRAS, CD74, RAC2	1.54E-03
PI3 kinase pathway	GNAQ, AKT1, GNA11, HRAS	1.76E-03
VEGF signalling pathway	AKT1, RAC1, HRAS, RAC2	3.42E-03
B cell activation	CD19, RAC1, HRAS, RAC2	4.81E-03
p38 MAPK pathway	TRAF6, RAC1, RAC2	7.90E-03
CCKR signalling map	ITGB1, RPS6, TRAF6, AKT1, RAC1, SHC1	8.54E-03
FGF signalling pathway	AKT1, RAC1, HRAS, SHC1, RAC2	9.31E-03
EGF receptor signalling pathway	AKT1, RAC1, HRAS, SHC1, RAC2	1.16E-02
Muscarinic acetylcholine receptor 1 and 3 signalling pathway	GNAQ, PKN1, GNA11	1.53E-02
Axon guidance mediated by semaphorins	RAC1, RAC2	2.20E-02
Glycolysis	GAPDH, PKM	2.58E-02
Axon guidance mediated by Slit/Robo	RAC1, RAC2	2.58E-02
Histamine H1 receptor mediated signalling pathway	GNAQ, GNA11	3.64E-02
Alzheimer's disease-presenilin pathway	APP, PSEN1, ACTB, PSEN2	3.82E-02
Metabotropic glutamate receptor group I pathway	GNAQ, GNA11	4.35E-02
Corticotropin releasing factor receptor signalling pathway	GNAQ, GNA11	4.59E-02
Axon guidance mediated by netrin	RAC1, RAC2	4.84E-02

Tetraspanins are linked to intracellular signalling components suggesting that they mediate the cross-talk between cell surface stimuli and intracellular signalling pathways[38]. Regarding the

pathway analysis, it seems that some of the CD81 interactors are involved in cytoskeletal regulation by Rho GTPase, a typical small GTPase that is the representative of its family that bind actin and regulated its polymerization into Filamentous actin (F-actin).

Another significant pathway regulated by CD81 is the Integrin signalling pathway, which is triggered when integrins in the cell membrane bind to extracellular matrix components[80]. Integrin proteins also bind actin, and are mainly involved in cell-cell adhesion and cell-substrate adhesion processes, being therefore key regulators of cell migration and cellular differentiation.

The analysis of pathways also revealed two pathways that are related to the proteolytic cleavage of APP. As depicted in chapter 1.3.2, APP can be processed to yield the Aβ peptide, a triggering factor in Alzheimer's disease. To produce this peptide, full-length APP is first cleaved by β-secretase, into a fragment that is further cleaved by γ-secretase. Alternatively, full-length APP can be cleaved by α-secretase, releasing a soluble fragment (sAPPα) with neuroprotective properties. CD81 can participate in both pathways since it interacts with ADAM10 (α-secretase), with Presinilins PS1 and PS2 (γ-secretase) and with APP itself[92–94]. This last interaction was proved to occur in neurons, more specifically in axonal growth cones, but its functional relevance was not clarified since the aim of that work was to study CD81 interaction with laminin[99]. CD81 physically interacts with ADAM10, and CD81 expression in MCF7 and SH-SY5Y cells promotes ADAM-10-dependent APP proteolysis[92]. On the other hand, Wakabayashi and colleagues (2013)[93] showed that the interaction between CD81 and PS1 or PS2 modulated the γ-secretase APP processing.

In synthesis, through the interaction with a large number of molecular partners, CD81 can induce intracellular signalling that is required for functional effects such as cell adhesion, migration and proliferation, and it can also influence the proteolytic cleavage of proteins such as APP.

4.2 Optimization of cellular and molecular tools

4.2.1 CHO Growth Curve

Cellular growth curves are applied in the evaluation of growth characteristics such as population doubling time, lag time, and saturation density. After re-seeding cells present a 'lag-phase" that can take from a few hours up to 48 h, a period of time required for a cell to recover from trypsinization, to rebuild its cytoskeleton, and to secret an extracellular matrix that facilitates cell-substrate adhesion and their propagation along the substrate. Subsequently, the cells enter into an exponential growth termed the 'log-phase' that lasts until the entire growth surface is occupied, or the cell concentration exceeds the capacity of the substrates in the growth medium. When the cell proliferation slows and stops, the cellular population enter in a 'stationary phase'. Finally, if the culture medium in not replaced and the cell number is not reduced, the cells lose viability and their number decreases, entering a 'decline phase'. This mean that cells in culture need to be subcultured on a regular basis before they enter in the stationary growth phase[95,96].

In order to determine the growth characteristics of the CHO cell line, a growth curve was performed, as described previously (section 3.3.3), using two different methods to measure cell viability. One involves the use of Trypan Blue (TB), which penetrates dead cell membrane and gives them a characteristic blue colour, whereas the living cells are not permeable to TB and remained uncoloured. This method has some advantages over spectrophotometric measurements because it can be very sensitive for conditions of only a few number of cells, and allows the observation of the cell morphology and the detection of culture contaminants[96]. The second method used was the resazurin metabolic assay. This assay served as an effective tool for assessing cell viability and cell proliferation because it is one-step, sensitive, safe, non-toxic for cells, and cost-effective. The resazurin is a blue indicator dye that enters inside the cell and undergoes enzymatic reduction in mitochondria due to the activity of NADH. The product of its reduction, resofurin, is excreted outside cells into the growth medium, which results in a visible medium colour change from blue to pink. The rate of reduction, and thus the colour change, reflects the number of viable cells[97]. Figure 15 shows the growth curves for CHO cells, as determined by the Trypan blue and Resazurin metabolic assays.

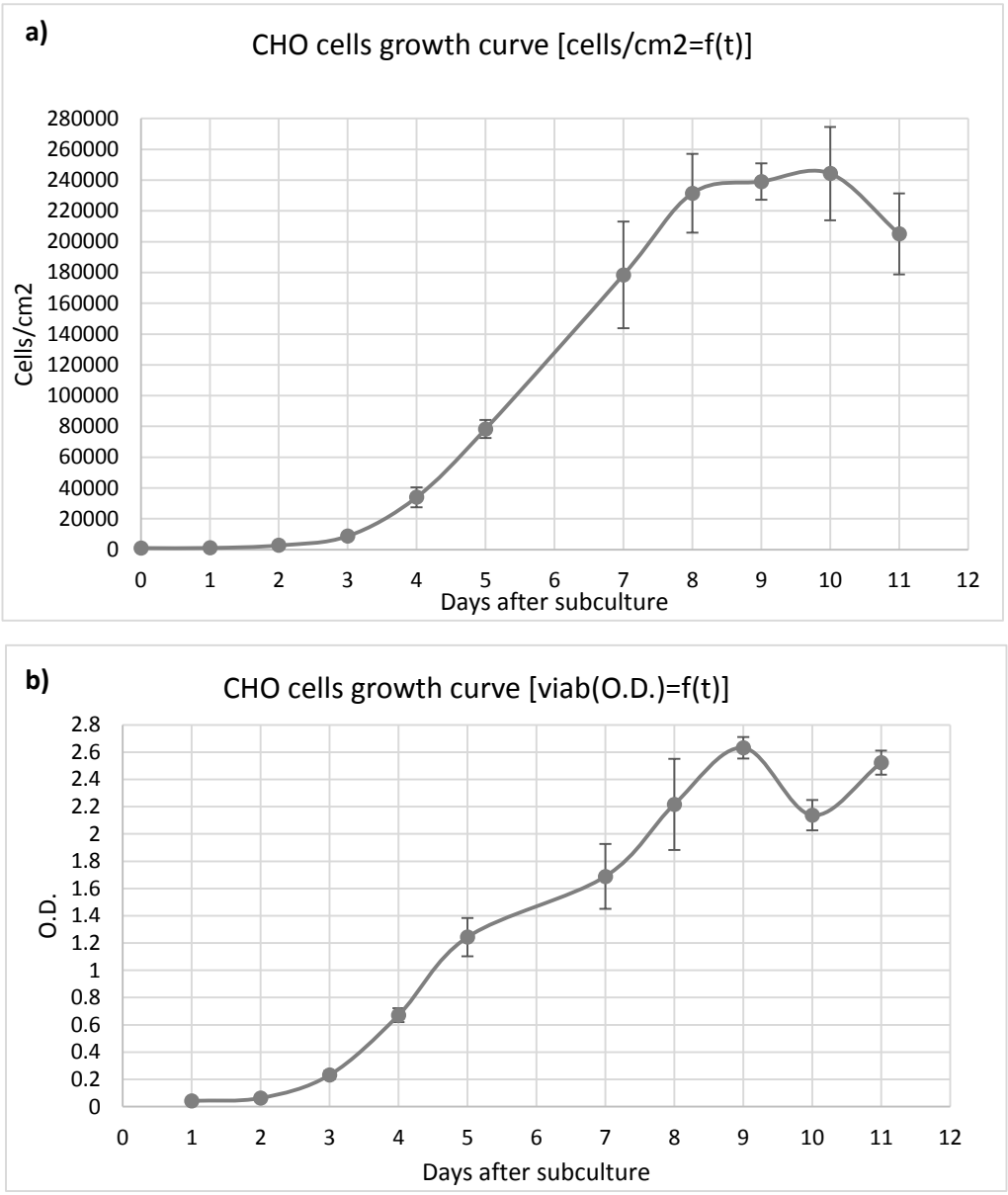

Figure 15. CHO cells growth curve determined by the **a)** Trypan blue method and **b)** the Resazurin metabolic assay.

The CHO cells manifested the expected four phases of cell growth. After 2-3 days of incubation, cells left the lag phase and the cellular growth began an exponential phase (Figure 15). Cells reached the stationary phase after 8-9 days of subculture, and entered in a decline phase where the number of cells started to decrease after 10 days of subculture. This behaviour was better observed with the Trypan blue method, as the Resazurin assay failed particularly at the end of the log phase and during the stationary and decline phase. For example, according to the growth curve determined by this method, after 8 days of subculture the number of viable cells were still increasing, which not did reflect the real number of viable cells. This method is thus preferentially

used for cells in the exponential phase, fact that can be observed in Figure 16. When CHO cells exceed the ~2.4x10^5 number, resazurin assay was no longer sensible. Hence, for a higher number of cells, the conditions (resazurin concentration and time of incubation) of this method should be optimized.

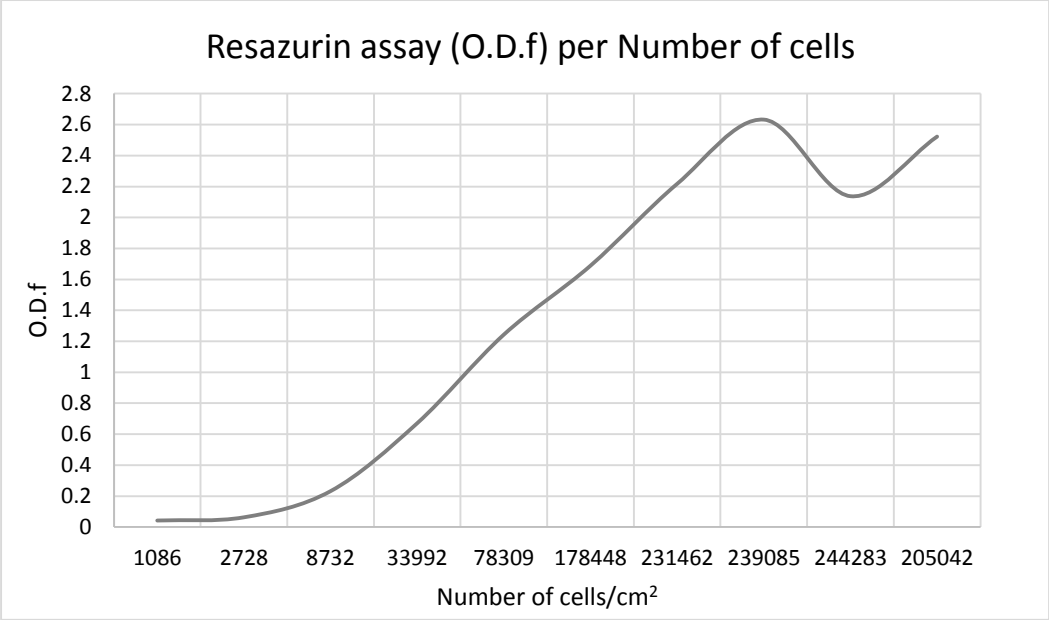

Figure 16. Relation between CHO cells Resazurin assay O.D.f per number of viable CHO cells**.**

These growth curves allow to determinate the population doubling time (DT). According to ATCC®, the population DT is the time required for a culture to double in number, and is calculated using the following formula, where T is the incubation time (any units), Xb is the cell number at the beginning of the incubation, and Xe is the cell number at the end of incubation)[98]:

$$DT = \frac{\mathrm{T}\ \ln 2}{\ln\left(\frac{\mathrm{Xe}}{\mathrm{Xb}}\right)}$$

To ensure viability, genetic stability and phenotypic stability, a cell line needs to be maintained in the exponential phase, and the DT should be calculated in this phase. The experimentally determined DT of CHO cells was of 25h32.

The determination of the growth curve of CHO cells permitted a better maintenance and handling of these cells in culture, previously and during the assays performed in this study.

4.2.2 Optimization of CHO and SH-SY-5Y cells transient transfection

Before performing a routine transfection procedure, a critical first step is to optimize conditions. This optimization is not just about getting cells to take up as much DNA as possible. It is about finding the optimal balance between maximal protein expression and minimal impact on cell viability. Different amounts of CD81 and APP cDNAs were first tested (Table 9) in order to choose the ones to use throughout the experiments. Cells were seeded in a 6-well plates before transfection and then transfected with different cDNAs for 24 h using the TurboFect™ reagent.

Transient transfection of CD81 constructs: mApple-CD81 and pCDM8 hCD81

To optimize the transient transfection of CHO cells with CD81 cDNAs, these were transfected with 0.5; 1.0; 1.5 and 2.0 µg of mApple-CD81 and pCDM8 hCD81 cDNAs. The transfection efficiency was evaluated by: 1) WB using an anti-RFP or the anti-CD81 EPR4244 antibody and 2) by ICC; since the mApple tag is fluorescent, the anti-CD81 antibodies were only used for the detection of cells transfected with pCDM8 hCD81. WB results for the transfection efficiency of CHO cells are presented in Figure 17, and ICC data in Figure 18. When mApple-CD81 was transfected, the expected band corresponding to the CD81 protein fused to mApple tag was detected at ~44 kDa (Figure 17a, arrow). pCDM8 hCD81 expression increased the pool of endogenous CD81, detected at ~24 kDa (Figure 17b)

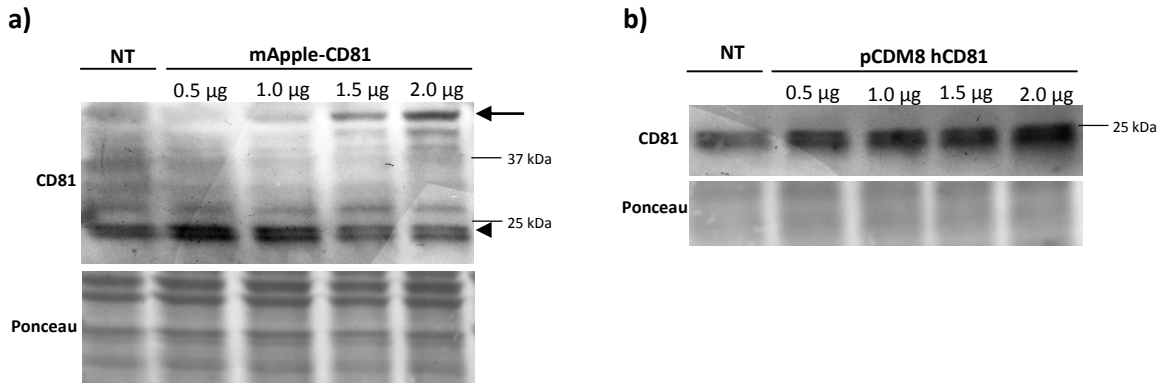

Figure 17. Efficiency of transfection of CD81 cDNA upon 24h of CHO transfection; **a)** WB analysis of CD81 expression in mApple-CD81 transfected CHO cells using the anti-CD81 EPR4244 antibody. Arrow indicates mApple-CD81 and arrowhead indicates endogenous CD81. **b)** WB analysis of CD81 expression in pCDM8 hCD81 transfected CHO cells using the anti-CD81 EPR4244 antibody

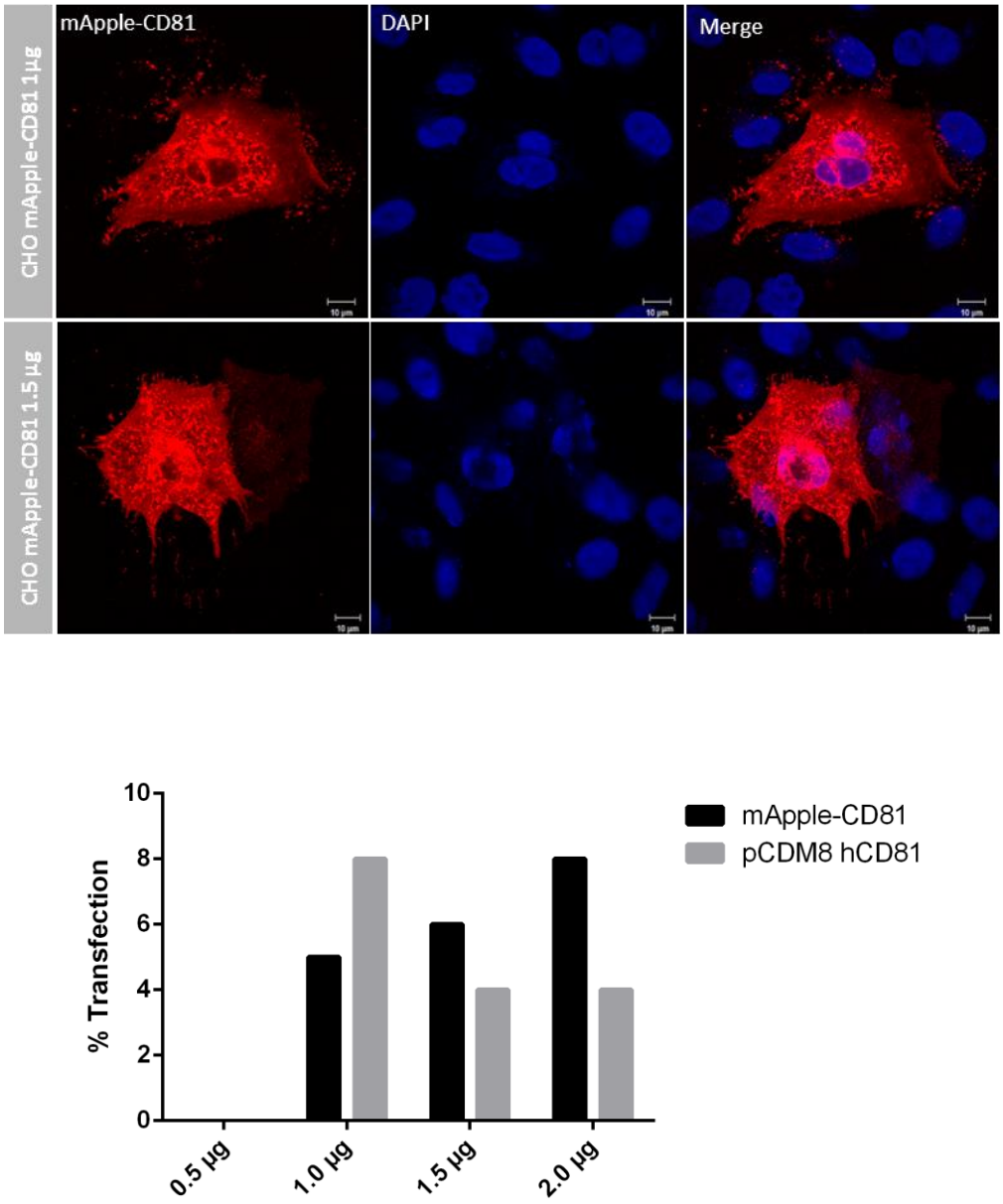

Figure 18. Efficiency of transfection of CD81 cDNAs upon 24 h of CHO transfection. a) Analysis of subcellular distribution of mApple-CD81 upon 24h of transfection with 1 and 1.5 µg of mApple-CD81. DAPI (nuclear blue staining) was used as a counterstaining. b) Percentage of CHO cells transfected with mApple-CD81 and pCDM8 hCD81 cDNAs; the number of transfected cells (red channel) and total cells (blue channel) were scored in various microphotographs, and the percentage of transfected cells calculated.

According to the WB and ICC results, transfection with 0.5 µg of mApple-CD81 and pCDM8 hCD81 cDNAs in CHO cells was not very efficient. Regarding the maximum of transfection, this occurred at 2.0 µg of cDNA for mApple-CD81 (Figure 17a and 18b) and at 1.0 µg of pCDM8 hCD81 (Figure 18b). However, despite the results achieved with 2.0 µg of mApple-CD81, at this conditions

CD81 overexpression affected the cells normal behaviour and led to an increase in cellular apoptosis, as indicated by the presence of apoptotic nucleus in the ICC (Figure 18). For this reason 1.0 µg of mApple-CD81 was chosen in subsequent experiments using CHO cells.

Optimization of the transfection of mApple-CD81 in SH-SY5Y cells was also performed and SH-SY5Y cells transfected with 0.5; 1.0; 1.5 and 2.0 µg of mApple-CD81. The transfection efficacy was evaluated by scoring the percentage of cells transfected under a fluorescence microscope (Figure 19). As we can observe from the results, the percentage of cells transfected was higher when 1.0 µg of mApple-CD81 was used (~40%), suggesting that the neuronal cell-line SH-SY5Y is more sensitive than CHO cells to high amounts of this protein.

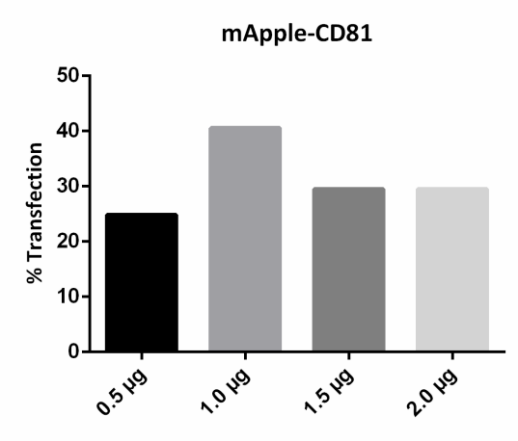

Figure 19. Percentage of SH-SY5Y cells transfected with mApple-CD81. The number of transfected cells (red channel) and total cells (phase contrast brightfield) were scored in various microscope fields, and the percentage of the transfected cells calculated for each amount of cDNA transfected.

To further analyse the pattern of transfection with mApple-CD81 in these cells, an ICC of cells transfected with 1.0 and 1.5 µg was performed (Figure 20). Results presented in Figure 20 showed that mApple-CD81 is present across the cytoplasm and at the cell membrane. When 1.0 µg of cDNA was used, cells appeared to have increased formation of cellular projections. When transfected with 1.5 µg mApple-CD81, there was a clear increase in cell volume. Further, transfection of SH-SY5Y cells with amounts of cDNA superior than 1 µg caused cellular toxicology, denoted by the presence of apoptotic nucleus and higher cell death. With these results we concluded that the optimal amount of cDNA to use in SH-SY5Y cellular transfection is 1.0 µg of mApple-CD81.

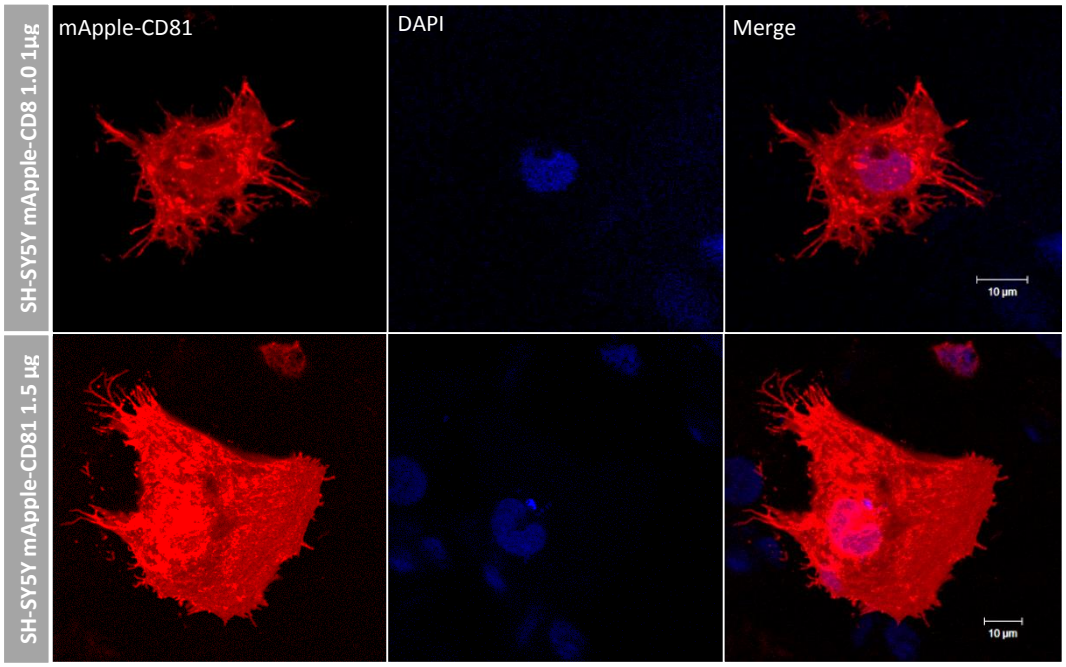

Figure 20. Analysis of subcellular distribution of mApple-CD81 in SH-SY5Y transfected 24h with 1.0 and 1.5 µg of mApple-CD81 cDNAs. DAPI (nuclear blue staining) was used as a counterstaining.

Transient transfection of APP-GFP in CHO cells

Since transient transfections of APP-GFP cDNAs in SH-SY5Y cells are already optimized in our lab (established at 1.0 µg of APP-GFP), we only performed this optimization in CHO cells. For this purpose, CHO cells were transiently transfected with 1.0 and 1.5 µg of APP-GFP cDNAs. The transfection efficiency is presented in Figure 21.

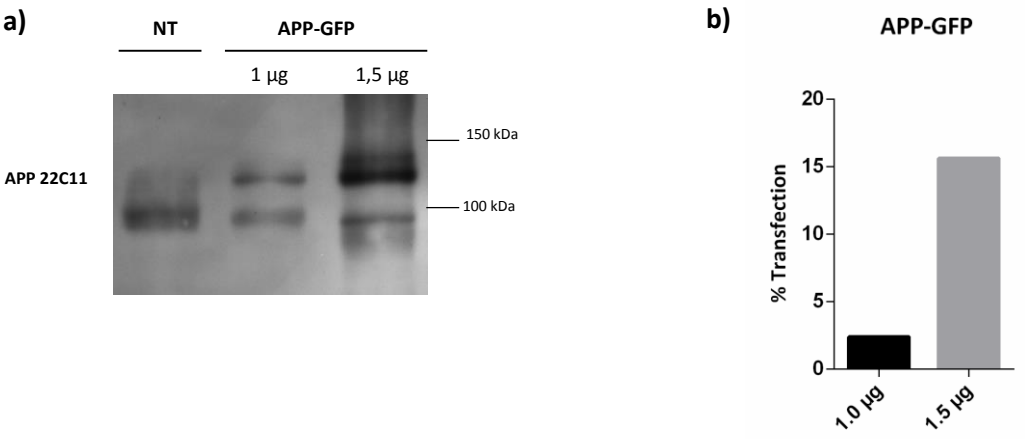

Figure 21. Efficiency of transfection of APP-GFP cDNA upon 24 h of CHO transfection; a) WB of APP expression in APP-GFP transfected CHO cells using the anti-APP 22C11 antibody. Exogenous APP-GFP correspond to the upper two bands nearer 150 kDa; **b)** Percentage of CHO cells transfected with APP-GFP. The number of transfected cells (green channel) and total cells (phase contrast brightfield) were scored in various microscope fields, and the percentage of transfected cell calculated, for each amount of cDNA transfected.

The efficiency of transfection was higher when 1.5 µg of APP-GFP was used, but again cells presented apoptotic nucleus (data not shown). Hence, for further experiments we decided to use 1.0 µg of APP-GFP.

4.2.3 Optimization of anti-CD81 antibodies

Three different antibodies against CD81 were acquired: two mouse monoclonal antibodies (clone M38 and 1D6; Abcam) and one rabbit monoclonal antibody (EPR4244, Abcam). MAb (monoclonal antibody) M38 was the first antibody acquired. It was tested in WB assays but never gave a signal at the various dilutions tested (from a 1:2000 dilution that was concentrated in up 1:500). The substitute mAb 1D6 (sent by the company) did not work either in WB, although according to the antibodies datasheets, should work in WB. The third one send by the company, the rabbit monoclonal antibody EPR4244 only works in WB. We tested this mAb in three different dilutions: 1:2000 (recommended), 1:1000 and 1:500. This mAb did not work well at any dilution, so we also concentrated the secondary antibody (to 1:2500, instead of 1:5000). The dilution that worked better was 1:1000, with a secondary goat anti-rabbit dilution at 1:2500. Although the antibody worked, the signal obtained was not very good, and hence we have also acquired an anti-RFP antibody against mApple-tag (used at recommended 1:500 dilution). The mAb M38 and 1D6 antibodies where tested in ICC assays at a 1:100 dilution, and both exhibited a pattern that was expected for CD81 (e.g. presence at the plasma membrane and co-localization with mApple-CD81 in transfected cells) (Figure 22).

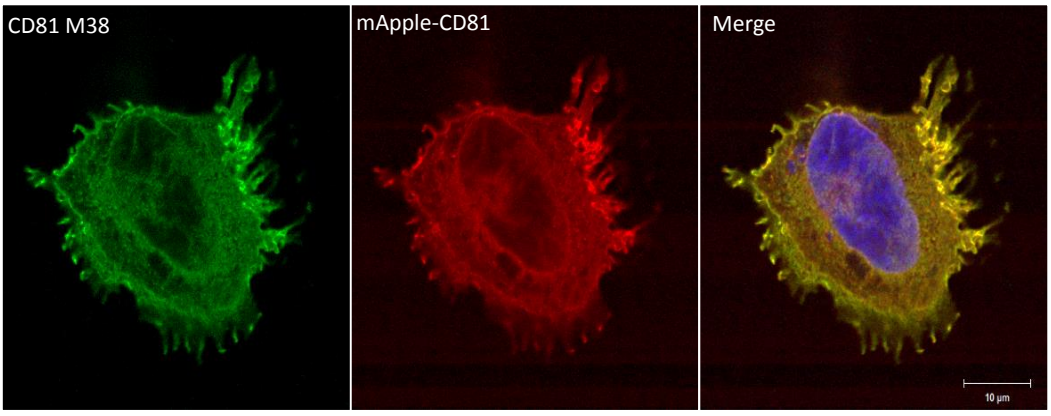

Figure 22. Immunocytochemistry of SH-SY5Y cells transfected with mApple-CD81. The anti-CD81 M38 antibody (1:100) was used, together with a secondary antibody labelled with Alexa Fluor 488 (green). As expected, the M38 antibody perfectly co-localized with mApple-CD81, showing sensitivity and specificity against the CD81 protein**.**

M38 and 1D6 probably only recognize the native form of CD81, so they were only used in ICC and IP assays, while the anti-CD81 EPR4244 and anti-RFP were used in WB assays. The full detail list of anti-CD81 antibodies, the applications that they should work for, and the tested applications are present in Table 9.

Table 9. Purchased antibodies against CD81: species reactivity, expected applications and confirmed applications and dilution upon optimization.

Antibodies against CD81	Species reactivity	Expected applications	Confirmed applications	Dilution
M38	Rabbit, Cat, Human	WB, IP, IHC-F, Functional Studies, ICC, FC	ICC	1:100
1D6	Human, Chimpanzee	WB, IP, IHC-F, Functional Studies, ICC, FC	ICC, IP	ICC:1:100 IP: 5µg
ERP4244	Mouse, Rat, Human	WB	WB	1:2000

4.3 Study of CD81 expression and subcellular localization in different cells

As previously reported, CD81 is expressed on most human tissues and its subcellular localization is well known in immune system cells and in mouse oocytes[33]. CD81 was also recently showed to be present in mouse sperm cells[99].

In the present work, the expression of CD81 was evaluated in cell lines of different species and in human sperm cells. Since CD81 is expressed in the surface of oocytes, we decided to study its expression in a Chinese hamster ovary (CHO) cell line. We also used the mouse CG-1 spg cell line to investigate the expression of this protein in a male germ cell line. To further assess the expression of CD81 in a neuronal cell line, the SH-SY5Y cell line was also used. Cells were plated on a 100 mm culture plates, collected and subjected to a WB; the expression of CD81 was also analysed in human sperm cells lysates (Figure 23).

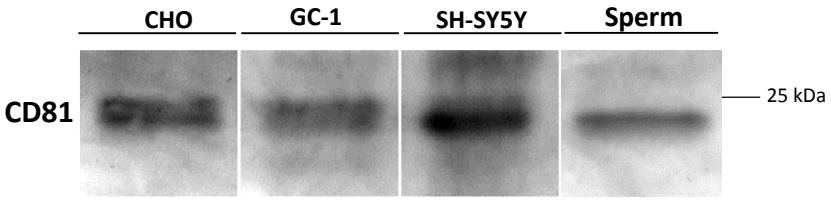

Figure 23. CD81 expression in CHO, GC-1 and SH-SY5Y cells, and in capacitated sperm cells. Immunoblot of cells lysates probed by anti-CD81 EPR4244 antibody.

Figure 23 shows that CD81 is expressed in all the cell lines tested (CHO, GC-1 and SH-SY5Y) and also in human capacitated sperm cells. A major band could be observed as the expected molecular weight of CD81, approximately 24 kDa, as described for cell lines of the immune system. A second fainter band could also be observed above, and may correspond to a post-translational modified CD81.

Since CD81 is expressed in the cells lines tested, it was important to investigate its subcellular localization. Unfortunately, our anti-CD81 antibodies that work in ICC do not react with hamster or mouse species. Taking this limitation into account, the subcellular localization of endogenous CD81 was only performed in SH-SY5Y cells. CD81 was stained with the monoclonal anti-CD81 M38 antibody, labelled with a secondary and Alexa Fluor 594-linked antibody (red fluorescence), and monitored with a confocal microscope (Figure 24).

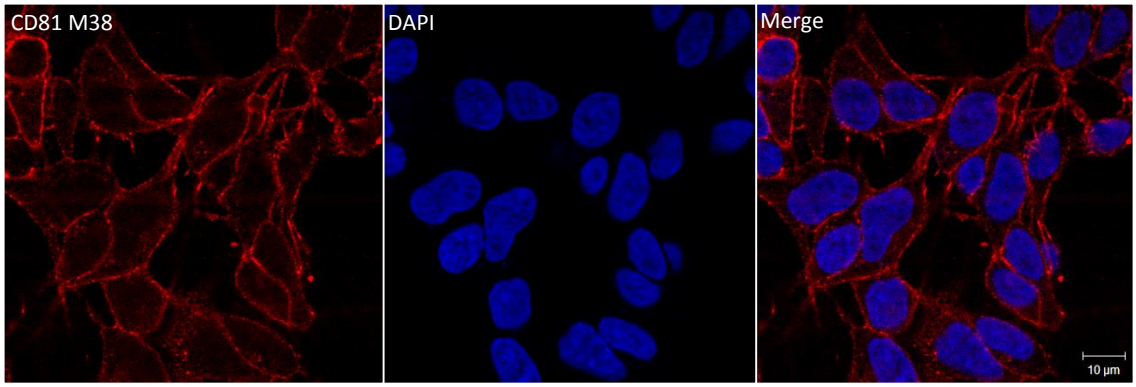

Figure 24. Subcellular localization of CD81 in SH-SY5Y cells. ICC was performed with anti-CD81 M38 monoclonal antibody, labelled with a secondary anti-mouse Alexa Fluor 594-linked antibody.

By analysing the Figure 24, it is possible to observe that CD81 is highly concentrated at the cell plasma membrane, as expected.

Given that we successfully detected the presence of CD81 in human sperm, we further analysed the subcellular localization of this protein in sperm cells, and investigated if its distribution pattern changed during capacitation. For this purpose, sperm cells were allowed to capacitate, and an ICC was performed using anti-CD81 M38 antibody (green fluorescence) and an anti-phosphotyrosine antibody (red fluorescence). This latter was used to confirm the capacitated status of sperm cells (Figure 25).

As seen in Figure 25, CD81 immunoreactivity was predominantly detected in the sperm head and in the midpiece, but could also be observed in the entire length of the tail. ICC experiments using the anti-CD81 M38 antibody showed a fainter uniform fluorescence over the entire surface, and several small strongly fluorescent spots along the entire sperm surface. The head CD81 staining pattern did not change in capacitated vs non-capacitated (arrow in Figure 25) sperm cells, but CD81 appears to be more intense in the tails of non-capacitated sperm cells. Of note, the CD81 staining was specific, since no fluorescence was observed in the negative controls (absence of primary antibody; data not shown).

Since CD81 is located in the sperm head, we further confirmed if this protein has an acrosomal localization. For this purpose, human capacitated sperm cells were stained with the anti-CD81 M38 antibody (Alexa Fluor 594, red) and with PSA-FITC (green), an acrosome marker (Figure 26).

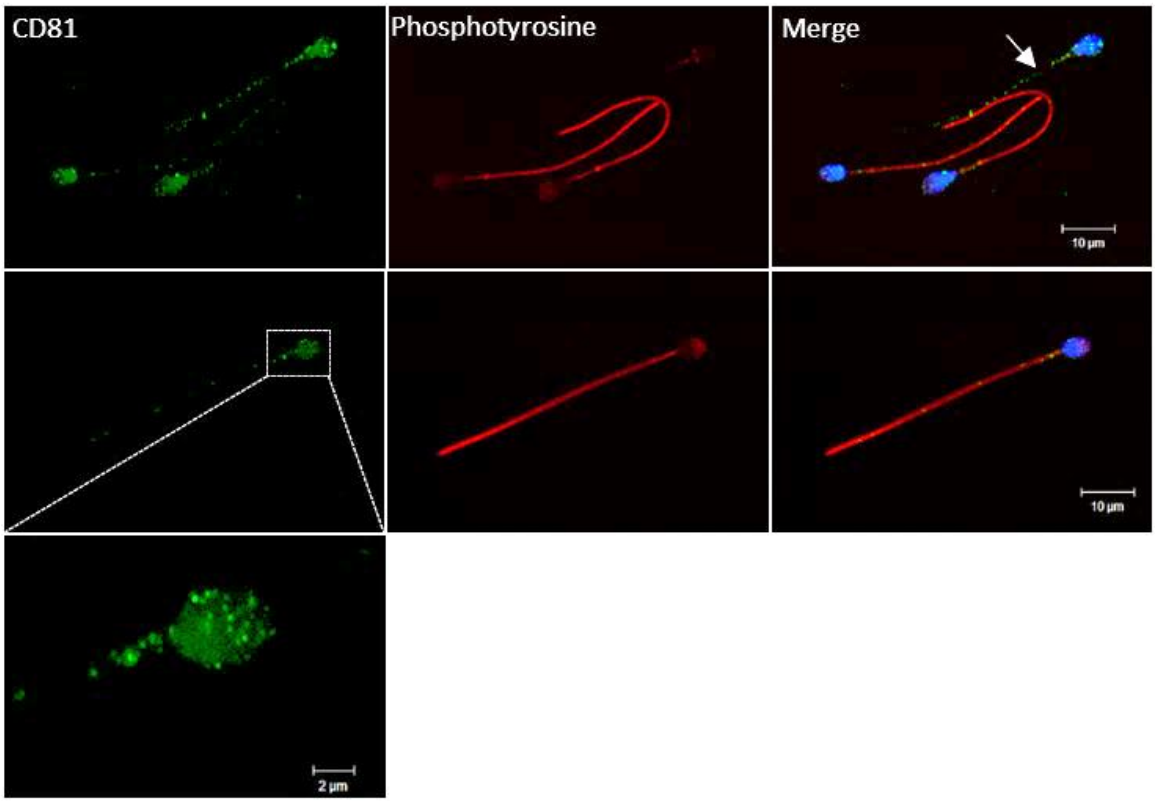

Figure 25. Subcellular localization of CD81 in human non-capacitated and capacitated sperm cells. Sperm cells were stained with anti-CD81 M38 antibody (green) and anti-phosphotyrosine (red) after induced capacitation. Arrow indicates non-capacitated sperm cell. Front view.

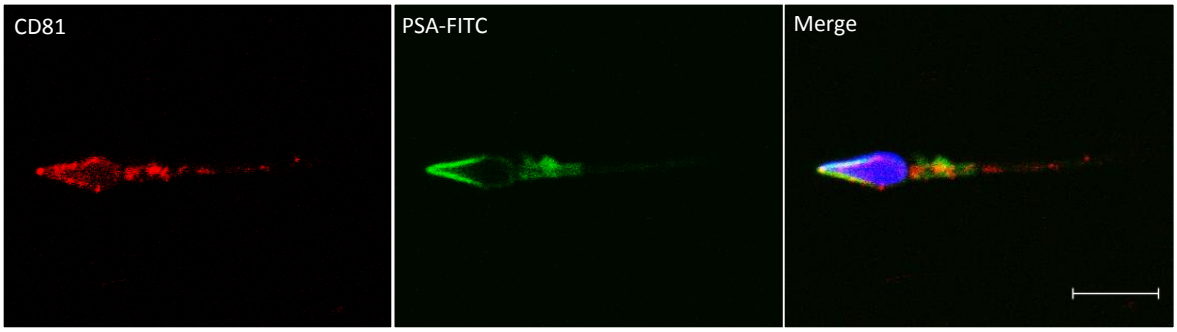

Figure 26. Subcellular localization of CD81 in acrosome-intact sperm cell. Capacitated sperm cells were stained with the anti-CD81 M38 antibody (red) and FITC - labbeled *Pisum sativum* agglutinin (PSA-FITC) (green).

By analysing Figure 26, it is possible to verify that some of the CD81 cellular pool co-localizes with PSA-FITC, indicating that CD81 is also located in the acrosome membrane. These sperm cells labelled PSA-FITC have an intact acrosome, since they did not undergo acrosome reaction. The side view represented in this figure allow us to better understand that CD81 is localized in the midpiece and in the sperm head, more specifically concentrated in the acrosome membrane.

4.4 Unravel the association between CD81 and APP

As previously described, CD81 was identified by us as an APP putative interaction partner in a YTH screen using APP as a bait and a testis cDNA library. Once a protein-protein interaction is identified, it is necessary to validate the interaction and establish the physiological function of the given interaction in a biological system. A combination of methods can be used to confirm the physical interaction and unveil the physiological significance of an interaction[100].

4.4.1 Study of APP/CD81 physical interaction

Co-immunoprecipitation is an *in vitro* protein-protein interaction detection method that allows to confirm interactions using whole cell extracts. Since CD81 is expressed on the oocytes surface, and due to its role in sperm-oocyte interaction, CHO cells were first used to study the physical interaction between CD81 and APP. However, tetraspanins are present in a detergent-resistant membrane environment called TEM, and so the choice of the lysis detergent to be used, in which these interactions can be retained, is a critical step of cell lysis. Taking this into account, different detergents were used along the co-immunoprecipitation procedures.

In the first experimental design, non-transfected and mApple-CD81 transfected CHO cells were used. After 24h of transfection in 100 mm cell culture plates, cells were harvested, lysated with 1% NP-40, and a CD81 co-immunoprecipitation was performed (Figure 27).

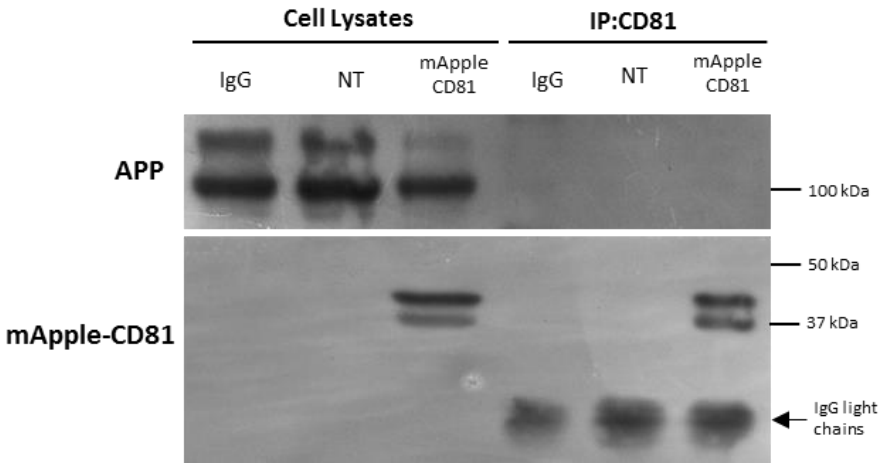

Figure 27. Co-immunoprecipitation of CD81 proteins in CHO cells, upon using 1% NP-40 as the lysis detergent. Co-immunoprecipitation of CD81 was performed using the anti-CD81 1D6 antibody, and CD81 immunoblotted with the anti-RFP antibody to ensure that mApple CD81 was successfully immunoprecipitated. The anti-APP 22C11 antibody was used to test if APP co-precipitated with CD81. IgG, Immunoglobulins used as immunoprecipitation control; NT, Non transfected.

Figure 27 shows that mApple-CD81 could be detected in cell lysates of cells transfected with mApple-CD81, and that it was efficiently immunoprecipitated by the 1D6 antibody. Unfortunately, APP was not co-immunoprecipitated with mApple-CD81 in these experimental conditions, although it could be readily detected with the 22C11 antibody.

To further clarify if CD81 and APP physically interact, we have decided to perform RFP- and GFP-Trap® Pull down assays. This fast and efficient method enables the purification of GFP- and RFP-fusion proteins, and of their binding partners, with the advantage that the bound fraction does not contain any immunoglobulin chain. In this procedure, we have chosen a different detergent as lysis buffer, and used 1% Triton-X to test if the CD81-APP complex could be retained in this new condition. RFP- and GFP-Trap pull down assays were carried out using cellular extracts (lysed with 1% Triton-X) of CHO cells under different co-transfections conditions. In order to immunoprecipitate mApple-CD81, RFP-Trap was performed in CHO cells expressing both mApple-CD81 and APP-GFP; as controls we have used cell co-transfected with the mApple empty vector and either the pEGFP-N1 empty vector, or APP-GFP. For the APP-GFP pull-down, a GFP-Trap was performed in CHO cells expressing both mApple-CD81 and APP-GFP; controls used were cells co-transfected with pEGFP-N1 and mApple-CD81. Cells were plated in 32 mm plates, harvested 24 h after transfection, and subject to the pull-down assay. The immunoblot was probed with anti-APP 22C11 and anti-RFP antibodies (Figure 28).

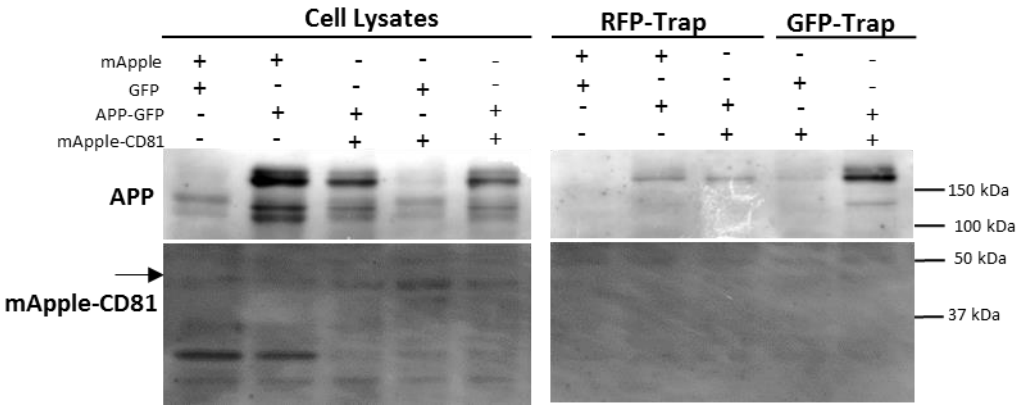

Figure 28. Immunoblot analysis of CHO cells subject to RFP- and GFP-Trap® pull down assays. CHO cells grown in 32 mm cell culture plates and were co-transfected with: mApple:GFP vectors; mApple vector:APP-GFP; GFP vector:mApple-CD81 and APP-GFP:mApple-CD81. Cell lysis was performed with 1% Triton-X, and mApple- and GFP-fused proteins precipitated with RFP- and GFP-Trap beads, respectively (right blot). Immunoblot analysis was performed with the anti-APP 22C11 and anti-RFP antibodies to detect APP and mApple-CD81. Arrow indicates mApple-CD81. A strong band of a lower molecular weight, corresponding to mApple vector alone, can be observed in mApple vector expressing cells.

The results first show that CHO cells were successfully co-transfected with APP-GFP and mApple-CD81. The immunoblotting with anti-APP 22C11 antibody detected endogenous APP and APP-GFP in cell lysates, and in some conditions of the pull-down assays. Regarding the GFP-Trap, APP-GFP was successfully pulled-down as we can see by the presence of this protein in the precipitates of cells co-transfected with APP-GFP and mApple-CD81. Unfortunately, we can not infer if mApple-CD81 was immunoprecipitated with APP-GFP as the anti-RFP antibody had a bad signal-to-noise ratio that difficult bands perception in the GFP-Trap precipitates. Also due to this, we also can not ensure that the RFP-Trap pulled down the mApple-CD81 proteins, since we could only detect mApple-CD81 in the cell lysates. Further, since APP-GFP was pulled-down by mApple-CD81 but also by the mApple tag alone (please see RFP-Trap lanes), this make it impossible to draw definitive conclusions on a potential APP-CD81 interaction.

Various problems could have occurred. Since CHO cells were somewhat resistant to the lysis buffer used (Triton-X) and the RFP- and GFP-Trap procedure were performed in 32 mm plates, the total amount of protein used in these pull-down assays could be not enough to detect CD81 in the pulled-down samples. The fact that both proteins were tagged may have interfered with their interaction. In an attempt to overcome this, another CD81 and APP co-immunoprecipitation was performed in SH-SY5Y cells transfected with untagged APP and CD81 cDNAs. Cell lysis was performed with the mild detergent CHAPS. Unfortunately, it was again not clear if CD81 was successfully immunoprecipitated and co-immunoprecipitated, since the intense signal from the immunoglobulin light chains overlapped the CD81 band signal.

4.4.2 Influence of CD81 overexpression in APP levels

In the co-immunoprecipitation procedures, different cell lines and lysis buffers were used. Although we were not able to confirm the physical interaction between CD81 and APP, an apparent functional interaction between these two proteins appeared from our experiments. To further evaluate if CD81 overexpression had an effect in endogenous APP levels, SH-SY5Y and CHO cells were transient transfected with increasing amounts of CD81 (0.5, 1.0, 1.5 and 2.0 μg of pCDM8 hCD81 cDNA; this last amount was only performed in CHO cells). APP levels was detected by immunoblot procedures, its levels quantified and expressed as fold-increase over basal levels in pCDM8 transfected SH-SY5Y cells, or in non-transfected CHO cells. The analysis of total sAPP in SH-SY5Y cells medium was also performed. Ponceau S staining of total proteins bands was performed

for all assays, and used as a loading control in the quantification analysis. Results are presented in Figure 29.

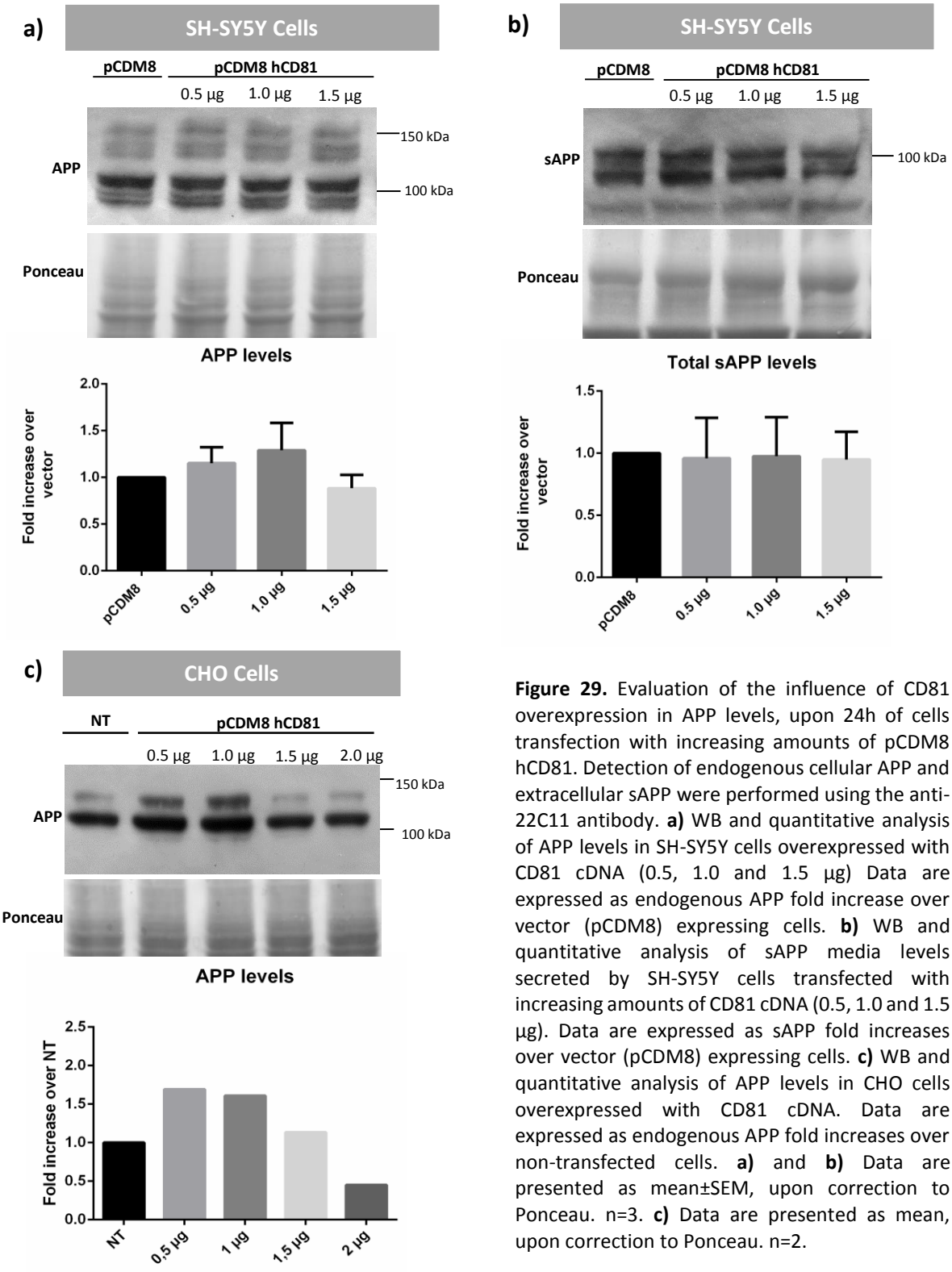

Figure 29. Evaluation of the influence of CD81 overexpression in APP levels, upon 24h of cells transfection with increasing amounts of pCDM8 hCD81. Detection of endogenous cellular APP and extracellular sAPP were performed using the anti-22C11 antibody. **a)** WB and quantitative analysis of APP levels in SH-SY5Y cells overexpressed with CD81 cDNA (0.5, 1.0 and 1.5 µg) Data are expressed as endogenous APP fold increase over vector (pCDM8) expressing cells. **b)** WB and quantitative analysis of sAPP media levels secreted by SH-SY5Y cells transfected with increasing amounts of CD81 cDNA (0.5, 1.0 and 1.5 µg). Data are expressed as sAPP fold increases over vector (pCDM8) expressing cells. **c)** WB and quantitative analysis of APP levels in CHO cells overexpressed with CD81 cDNA. Data are expressed as endogenous APP fold increases over non-transfected cells. **a)** and **b)** Data are presented as mean±SEM, upon correction to Ponceau. n=3. **c)** Data are presented as mean, upon correction to Ponceau. n=2.

Regarding the influence of CD81 overexpression in the APP levels of SH-SY5Y cells (Figure 29a), we can observe that the cellular transfection with 0.5 and 1.0 µg of pCDM8 hCD81 induced a slight increase in the levels of APP. This tendency was abolished when cells were transfected with 1.5 µg of pCDM8 hCD81, and APP levels were again similar to vector transfected samples. This decrease could be due to the cellular toxicity of the higher CD81 overexpression condition. Since CD81 transfection led to a slight increase in APP levels, it was relevant to investigate if this increase could be due to a decrease in APP cleavage into sAPP. Cell media were collected for each condition and analysed by WB using the anti-22C11 antibody (Figure 29b). After total sAPP quantification, evidences showed that CD81 overexpression did not affect sAPP production.

CHO cells seem to respond slight differently to CD81 overexpression than SH-SY5Y cells, probably due to its different tissue nature. To understand the effect of CD81 overexpression in CHO cells, a similar approach was used and APP levels were evaluated in CHO cells transfected with 0.5, 1.0, 1.5 and 2.0 µg of pCDM8 hCD81 (Figure 30c).The results obtained with CHO cells also indicate that CD81 overexpression increases APP levels. However, it seems that this CD81 effects is more prominent in CHO cells than in SH-SY5Y cells. Since the sAPP levels in CHO cells medium were not evaluated, we can not infer about the mechanism(s) underlying the increase in APP levels. The hypotheses that CD81 promotes APP´s half-life or induces *APP* gene expression will also be further addressed in the future.

4.4.3 APP/CD81 subcellular co-localization

Co-localization experiments in cultured cells can give information about the spatial dynamics of protein-protein interactions. Although we were not able to prove the physical interaction between APP and CD81, we further analysed potential subcellular regions of CD81 and APP *in vivo* co-localization trough immunocytochemistry. This procedure was carried out in sperm cells, and in SH-SY5Y cells non-transfected and co-transfected with mApple-CD81 and APP-GFP cDNAs. APP was stained with the anti-APP CT695 (labelled with red Alexa Fluor 594 in sperm cells, and with green Alexa Fluor 488 in SH-SY5Y cells), and endogenous CD81 was stained with anti-CD81 M38 (green Alexa Fluor 488 in sperm cells, and red Alexa Fluor 594, red in SH-SY5Y cells). Fluorescence microphotographs were taken at the cellular membrane plane by using a confocal microscope (Figure 30 and 31). All images retrieved from the endogenous CD81 and APP co-localization assays in SH-SY5Y cells were analysed using the Fiji software.

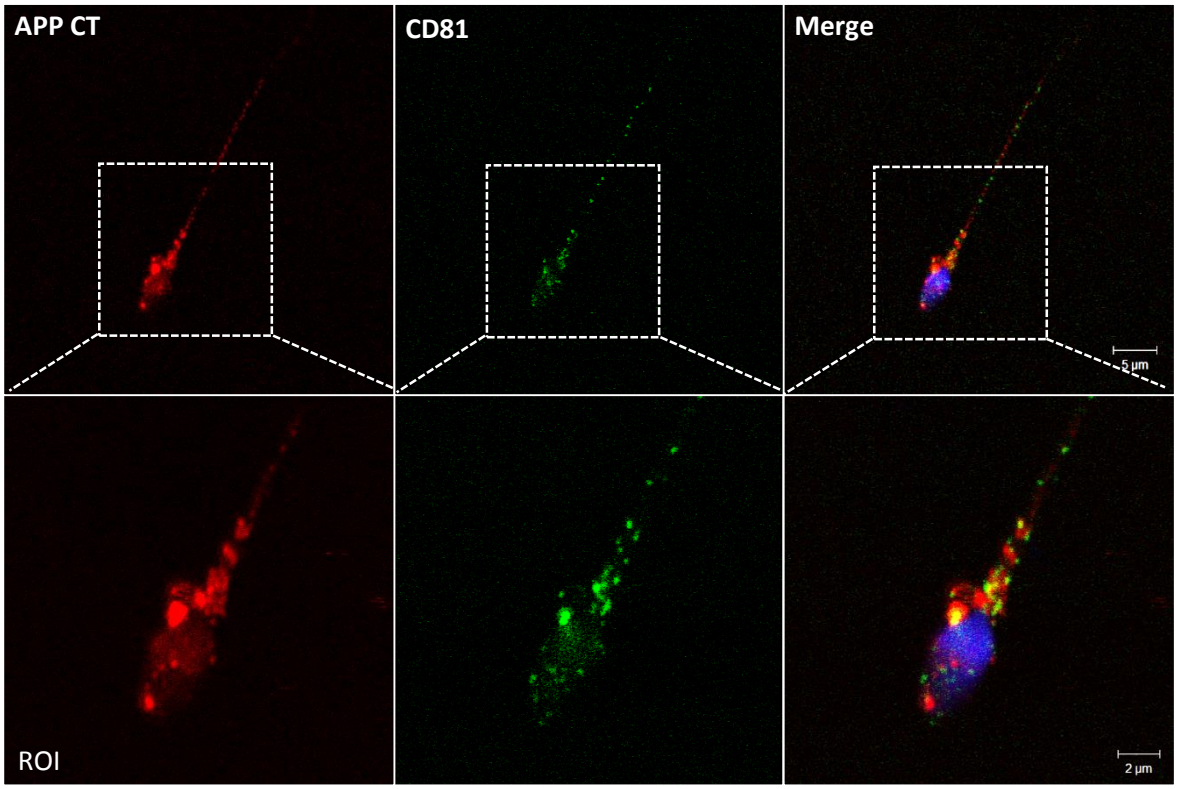

Figure 30. APP and CD81 subcellular co-localization in human capacitated sperm cells. APP protein was stained with anti-APP CT695 antibody (Alexa Fluor 594, red) and CD81 protein was stained with anti-CD81 M38 antibody (Alexa Fluor 488, green). ROI, region of interest.

By analysing the Figure 30 it is possible to observe that the anti-APP CT695 antibody immunoreacts with the entire sperm cell, although it is highly concentrated in the midpiece, where the signal was more intense. It is also possible to observe that the sperm head is positively stained. Confocal fluorescence microscopy showed that the anti-APP CT695 staining presented some degree of co-localization with the CD81 staining. As showed in the magnified ROI (region of interest of Figure 30), this co-localization seems to be in the midpiece region and in some fluorescent spots in the sperm head, at least in the post-acrosome region. No real co-localization was observed along the tail.

The co-localization of CD81 and APP in SH-SY5Y cells was also analyzed using again the anti-APP CT695 to detect APP (green) and anti-CD81 M38 to detect CD81 (red) (Figure 31).

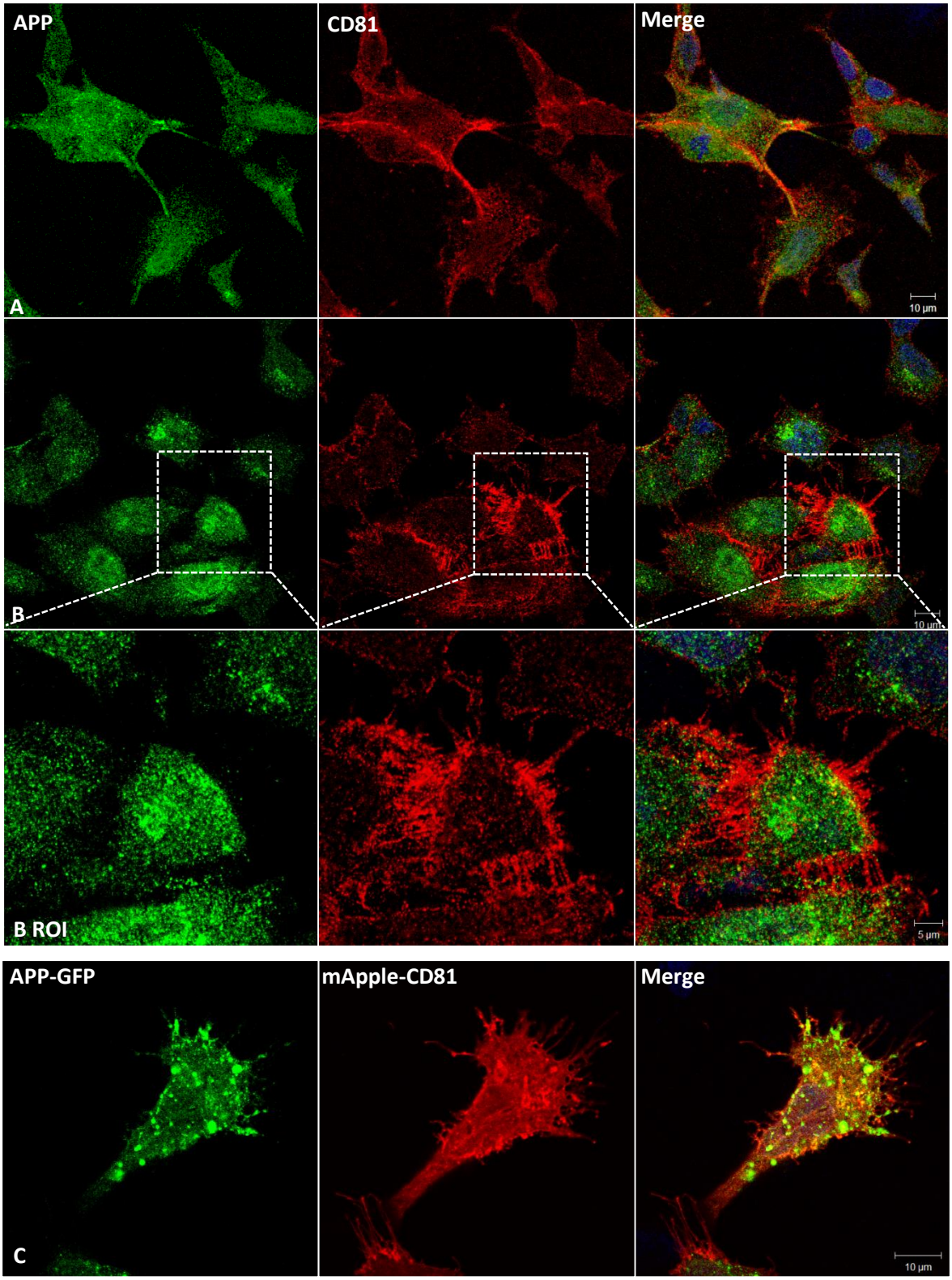

Figure 31. CD81 and APP subcellular co-localization in SH-SY5Y cells**. a)** and **b)** Endogenous CD81 and endogenous APP subcellular co-localization in non-transfected SH-SY5Y cells. APP proteins were labelled with the anti-APP CT695 antibody (Alexa Fluor 488; green fluorescence) and CD81 proteins were labelled with the anti-CD81 M38 antibody (Alexa-Fluor 594; red fluorescence). **c)** CD81 and APP subcellular co-localization in SH-SY5Y cells upon 24 h of co-transfection with APP-GFP and mApple-CD81 cDNAs.

Regarding the distribution of each of the proteins alone, APP CT695 antibody revealed that APP is mainly present in the Golgi apparatus and nearby regions, with a small fraction of APP being present in the plasma membrane. Regarding CD81 it is mainly localized at the plasma membrane, being more especially abundant in membrane extensions such as filopodia.

Regarding APP/CD81 co-localization, confocal fluorescence microphotographs showed that endogenous CD81 and APP present some degree of co-localization, particularly at the plasma membrane, including cellular processes (Figure 31a). 20 microphotographs were analysed with the ImageJ Fiji software, and approximately 33% of the CD81 cellular pool was found to co-localize with APP. Figure 31b and its ROI show that CD81 is enriched in the cellular membrane, mainly in cell-to-cell and cell-to-subtract communication filopodia ('finger'-like extruding structures). CD81 and APP co-localized in these filopodia and in some plasma membrane regions. A small pool of endogenous CD81 and APP were also observed to co-localize throughout the entire cytoplasm.

When SH-SY5Y cells were co-transfected with APP-GFP (green) and mApple-CD81 (red), cells attained a motile phenotype and a high degree of APP/CD81 co-localization was observed. This co-localization mainly occurs at the plasma membrane and in various large cytoplasmic spots. Of note, various APP-GFP-positive small vesicles do not co-localize with mApple-CD81. The nature of the subcellular regions of co-localization in the cytoplasm will have to be further analysed by using specific organelle markers.

Combining the overall data, we were not able to confirm that CD81 and APP physically interact but data from CD81 overexpression experiments suggest that CD81 has an effect on APP levels and CD81 and APP subcellular co-localization analyses show that probably these two proteins physically interact *in vivo* and are involved in a common biological process.

4.5 CD81 and other interacting proteins

Since CD81 seems to be involved in signalling pathways related with cytoskeleton remodelling and cell motility, an evaluation of its co-localization with AKT, and the influence of its overexpression in cytoskeleton proteins levels, namely in actin and tubulin, was performed.

4.5.1 CD81 and AKT1

As depicted in section 4.1, AKT (also known as Protein Kinase B) is a CD81 interacting protein. When activated, AKT phosphorylates a number of substrates involved in cytoskeleton remodelling, cell growth and cell survival in neurons, and also in sperm cells. To better understand the CD81 and AKT subcellular distribution, a co-localization assay was performed in sperm cells and in SH-SY5Y cells (Figures 32 and 33, respectively). This experiment was performed using an anti-AKT1 antibody to detect AKT isoform 1, and anti-CD81 M38.

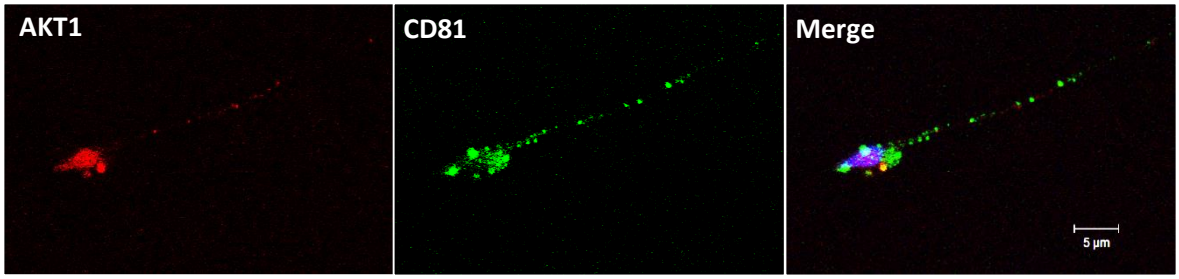

Figure 32. CD81 and AKT1 subcellular co-localization in human capacitated sperm cells. AKT1 protein was stained with the anti-AKT1 antibody (labelled with Alexa Fluor 594, red) and the CD81 protein was stained with the anti-CD81 M38 antibody (labelled with Alexa Fluor 488, green).

Figure 32 shows that AKT1 is present in human capacitated sperm cells, as expected, and although weaker, the immunostaining with the anti-AKT1 antibody indicated that AKT1 is mainly expressed in the sperm head, although a small protein pool is also present along the entire tail. Regarding its co-localization with CD81, few co-localization was observed. This could be due to the weak AKT immunostaining and so more experiments have to be done to better understand their subcellular co-localization in sperm cells.

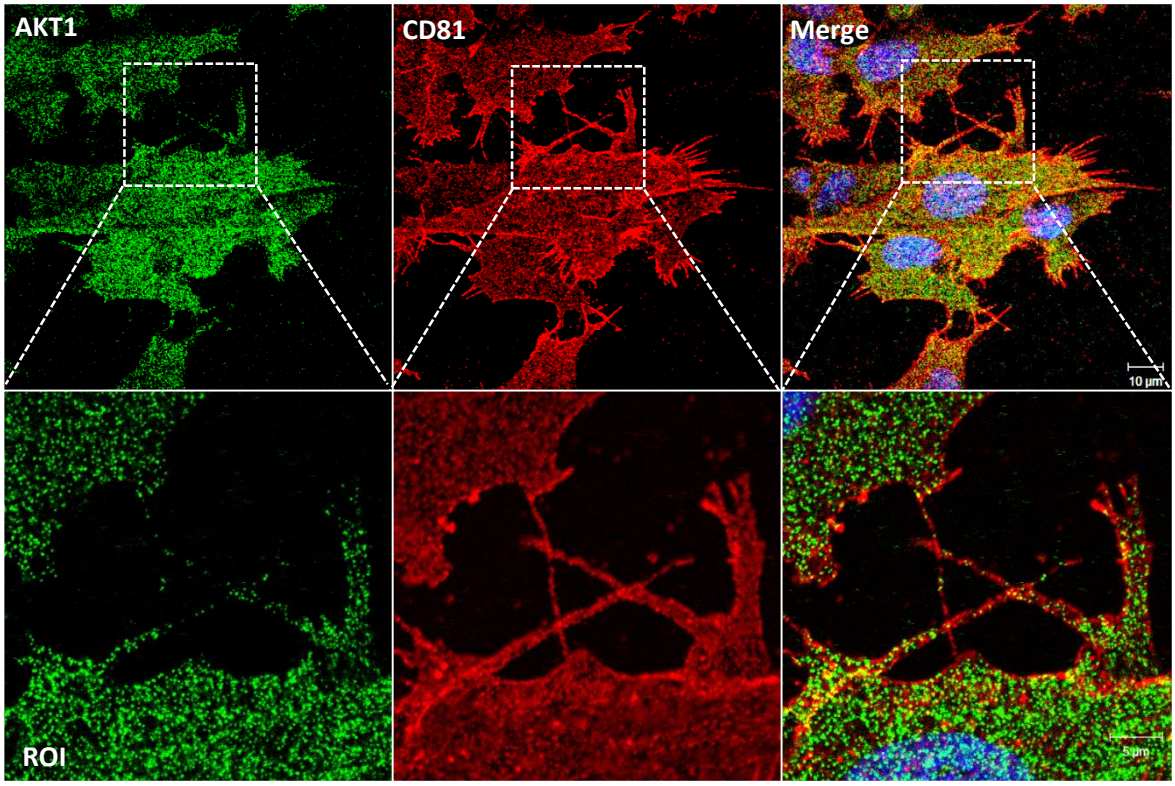

Figure 33. CD81 and AKT1 subcellular co-localization in non-transfected SH-SY5Y cells**.** AKT1 protein was stained with the anti-AKT1 antibody (labelled with Alexa Fluor 488, green) and CD81 was stained with anti-CD81 M38 antibody (labelled with Alexa-Fluor 594, red). ROI, region of interest

Regarding AKT1 distribution in SH-SY5Y cells (Figure 33), microphotographs showed that AKT1 is localized throughout the cytoplasm, which is in agreement with previous reports[101]. Although CD81 is mainly localized at the plasma membrane, Figure 33 shows also some cytoplasm localization and some degree of CD81 co-localization with AKT1. Surprisingly, this co-localization is predominantly at the inner leaflet of the plasma membrane and at the cell projections (Figure 33, ROI). Few localization between these proteins was observe in the cytoplasm. Overall, our data demonstrated that in SH-SY5Y cells these proteins co-localized in specific cellular compartments, supporting their physical interaction *in vivo.*

4.5.2 CD81 and cytoskeleton-related proteins

In order to better understand the influence of CD81 in cytoskeleton remodelling, we aimed to perform a co-localization procedure with CD81-binding cytoskeleton-related proteins. Unfortunately, our anti-actin and anti-tubulin antibodies are both raised in mouse, what did not allow to perform the co-localization between these proteins and CD81. To overcome this problem of lack of an anti-actin antibody, Alexa Fluor 568 Phalloidin, a drug that binds to F-actin and is red fluorescing, was used to stain the polymerized filamentous actin (F-actin), and determine its co-localization with CD81 (stained with anti-CD81 M38,in green). The results for sperm cells are presented in Figure 34.

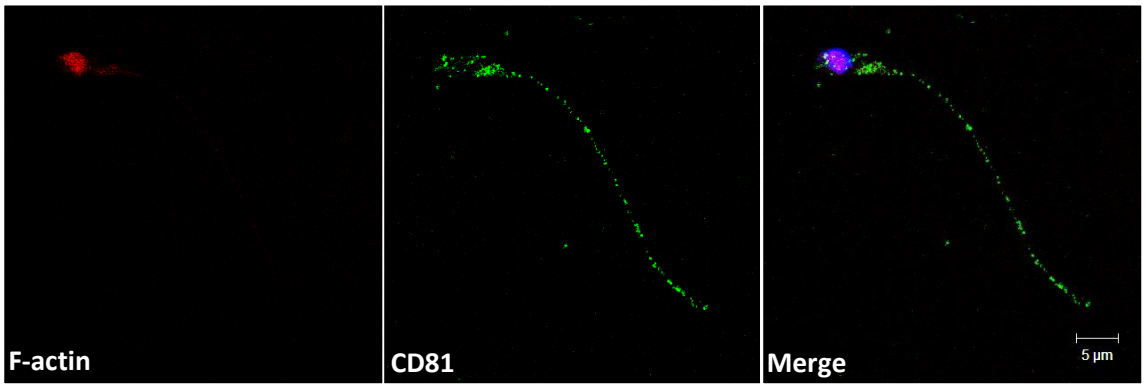

Figure 34. CD81 and filamentous actin (F-actin) o-localization in human capacitated sperm cells. CD81 protein was stained with the anti-CD81 M38 antibody (labelled with Alexa Fluor 488, green), and F-actin with Alexa Fluor 568 phalloidin (red). DAPI (blue nuclear staining) was used as a counterstaining.

A weak F-actin staining can be observed in the sperm head, and no or few staining in the tail. Regarding the sperm head, is seems that F-actin is enriched in the post-acrosomal region, and this would be the zone where it could co-localize with CD81, but F-actin staining was too weak to draw definitive conclusions. Further, since during capacitation and acrosome reaction, the relocation of the cytoskeleton proteins is likely to be important for subsequent events of fertilization, more experiments have to be done to access the subcellular localization between CD81 and cytoskeleton-related proteins.

In our previous experiments we observed that CD81 overexpression seemed to induce morphological changes in SH-SY5Y cells. This most probably comprised alterations in the levels or polymerization state of cytoskeleton proteins, namely actin and tubulin. The effects of overexpressing increasing amounts of CD81 in SH-SY5Y cells in β-actin and Acetylated α-tubulin

levels were evaluated by immunoblot analysis. Ponceau staining of total proteins in the membrane is shown as a loading control (Figure 35).

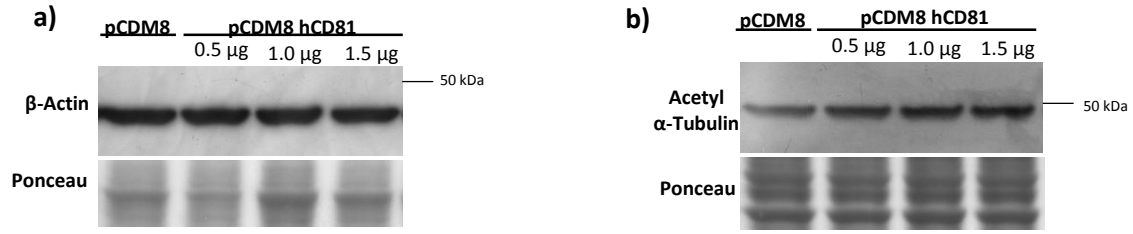

Figure 35. Western blot analyse of β-actin **(a)** and Acetyl α-tubulin **(b)** expression with conditions of CD81 overexpression in SH-SY5Y transfected cells. SH-SY5Y cells were transfected with 0.5, 1.0 and 1.5 µg of pCDM8 hCD81 for 24 h.

Results indicate that β-actin levels seem to decrease when cells were transfected with 1.0 and 1.5 µg of pCDM8 hCD81, when compared to empty vector-transfected cells (Figure 35a). Acetylated α-tubulin is a post-translational modification that is found microtubules that are relatively stable. Figure 35b shows that the levels of acetylated tubulin are also affected by CD81 transfection. In this case however, acetylated tubulin seems to mainly increase with the transfection of increasing amounts of CD81. More experiments will be performed to confirm and quantify these effects.

In a second approach, an ICC was performed in SH-SY5Y cells transfected with 1.0 µg of pCDM8 hCD81 for 24 h, in order to access the subcellular co-localization between F-actin (marked with Alexa Fluor 568 Phalloidin) and the CD81 protein (Figure 36). Results show that SH-SY5Y cells that were transfected with 1.0 µg of pCDM8 hCD81 acquired a migratory phenotype, as we can see by their more 'triangular' shape. Indeed, transfected cells presented a polarized and asymmetric morphology, and active membrane processes, including F-actin containing filopodia at the cell leading edge. Regarding transfected CD81, we can observe that this protein is enriched in the plasma membrane and along the cytoplasm. Of note, when z-stacks of cells were taken using confocal fluorescence microscopy, big spots with CD81 accumulation were visible in the cytoplasm, and some of them crossed the entire cytoplasm (data not shown). The microphotographs further showed a high degree of co-localization between transfected CD81 and F-actin. This co-localization was mainly visible along the F-actin stress fibres that crossed the cell, in potential focal adhesion

spots, and also in the filopodia. These results suggest a role for CD81 in promoting cellular mechanisms that underlie the acquisition of a clear migratory phenotype.

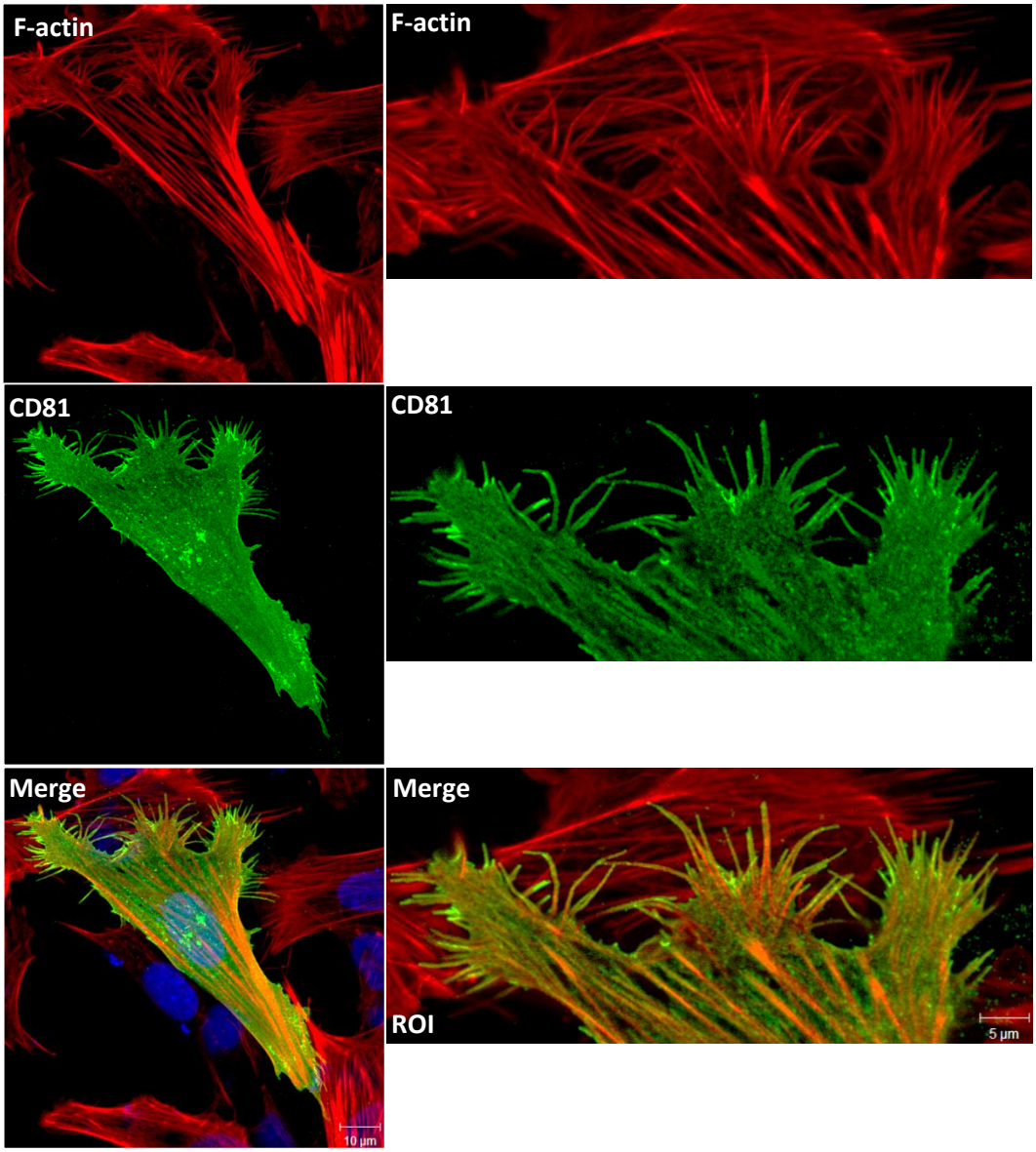

Figure 36. CD81 and F-actin subcellular co-localization in SH-SY5Y cells transfected with 1.0 µg of pCDM8 hCD81**.** CD81 protein was stained with anti-CD81 M38 antibody (green) and F-actin was probed with Alexa Fluor 568 Phalloidin (red). ROI, region of interest.

5. Discussion and conclusion

CD81 is a tetraspanin protein that has been mainly studied in the immune system. Few functions have been attributed to it, but it is known to be involved in processes such as cell adhesion and migration. Its expression levels, subcellular distribution and role in other cells, such as neuronal and germinal cells, are still barely known. A powerful approach for inquiring the biological functions of a protein of interest is to analyse its protein-protein interactions (PPIs). In the present work we aimed to characterize CD81 and some of its protein interactors in various cell lines and in human sperm cells. We mainly focused in its binding to APP, since an APP-CD81 interaction was originally identified in our lab in a YTH screen of human testis cDNA library when APP was used as a bait[46].

CD81 expression and subcellular distribution

Before studying the CD81 interactors, we have characterized CD81 expression and subcellular localization in different cells lines and in human sperm cells. CD81, as expected due its known large tissue distribution, was expressed in CHO, GC-1 and SH-SY5Y cell lines. In all cell lines tested (and in sperm cells), the molecular weight of the more intense CD81 band was ~24 kDa, as expected; a second fainter upper band appeared in all cell lines tested, and a fainter lower band appeared in GC-1 cell line, probably due a CD81 cleavage. CD81 does not suffer glycosylation, but undergoes palmitoylation and phosphorylation. This shift could hence correspond to two added phosphate groups, but this need to be further investigated.

Regarding CD81 subcellular distribution in SH-SY5Y cells, it is mainly expressed at the plasma membrane, but it can also be found in some accumulations in the cytoplasm. The small cytoplasmic spots could be exosomes, since CD81 is enriched in exosomes-like vesicles[36]. CD81 expression in this nervous system-related cell line is not surprising. Although the major role of CD81 is described in the immune system, CD81 has been implicated in the nervous system. Dijkstra *et al.* (2000) show that CD81 is dramatically up-regulated after spinal cord injury. CD81 is found concentrated at regions of cell-cell contact in cultured astrocytes and may play a central role in the process of CNS scar formation that involves various cellular populations: microglia, invading monocytes, and reactive astrocytes[102]. CD81 is required for the normal development of the brain. Geisert *et al.* (2002) performed a study in order to examine the effects of the CD81 -/- mutation on the CNS of mice and showed that these mice have extremely large brains. This was as a result of an increased number of astrocytes and microglia, whereas the number of neurons and oligodendrocytes appeared to be normal[103]. Hence, CD81 controls astrocytes and microglia cell

number, now known to occur by suppressing cell proliferation in a cell-cell contact-dependent manner[104].

Regarding the expression of CD81 in germinal cells, it has been reported that CD81 is located on the surface of oocytes and in cumulus cells[43]. Ohnami *et al.* (2012)[44] showed that CD81 is localized at the inner portion of ZP and hypothesized that it may be involved in any step of the fusion-related events that occur prior to sperm-oocyte membranes fusion. These authors also showed that CD81 is expressed in mouse sperm cells and, taking this into account, we further investigated if it was also expressed in human sperm cells. The present study provides the first evidence of the presence of CD81 in human sperm cells (Figure 25). The same pattern of CD81 expression was visible, with two CD81 bands appearing at the expected MW. Subsequent ICC evaluations revealed that CD81 immunoreactivity was predominantly detected in the sperm head including the acrosome membrane, and in the midpiece, being also present at lower abundance along the entire tail (Figure 26). The pattern of immunostaining seems to be altered during sperm capacitation, with CD81 being apparently less present in the sperm tail, but this needs to be further confirmed. Further, its localization after the acrosome reaction was not evaluated yet. These results lead us to speculate on the following points: 1) CD81 in the head and midpiece membranes may serve as an organizer for other proteins, forming tetraspanin webs necessary for signalling events related to acrosomal reaction and sperm motility; and 2) CD81 may play a role in the sperm-oocyte fusion event. This last hypothesis is of particular interest if we consider that egg proteins released from the oocyte surface could attach to the sperm surface. Indeed, before sperm-oocyte fusion, CD9 (a tetraspanin partner of CD81 located in oocyte surface) is transferred to the sperm membrane[44]. The authors hypothesized that CD81 is to be transferred first from the oocyte to the sperm membrane to support the subsequent transfer of CD9 through the formation of a complex between these two proteins. Hence, since CD81 can form dimers and bind CD9, sperm CD81 may bind to oocyte-transferred CD81 and CD9, forming a tetraspanin-tetraspanin binding complex between the sperm and oocyte surface, to facilitate the subsequent membranes fusion. More studies need thus to be performed to confirm the exact surface location of this protein in human sperm, and to prove this hypothesis.

CD81 and cytoskeleton remodelling

To better understand the CD81 physiological role, we first performed a bioinformatics analysis of its interacting proteins. A CD81 PPI network was constructed, and GO terms enrichments of these interactors were performed. A majority of CD81 interacting proteins are located in the

cytoplasm and nucleus, and are involved in the determination of DNA and RNA fates, or in cell metabolism, as revealed by GO enrichments in biological processes and functions. The bioinformatics pathways analysis showed that CD81 is linked to intracellular signalling components involved in cytoskeletal regulation by Rho GTPase family members, in the integrins signalling pathway and, surprisingly, in pathways related to the proteolytic cleavage of APP. From the proteins that were classified as involved in the CD81 signalling pathways, AKT1, RAC and cytoskeleton-related proteins as tubulin and actin are key players in CD81 signalling pathways.

AKT1, an AKT isoform, is a kinase involved in a variety of signalling pathways related to motility, cell survival and cytoskeleton remodelling in cells. In the present work, we performed an ICC in sperm cells and in SH-SY5Y cells to access the subcellular localization of CD81 and AKT1. A weak but visible immunostaining was obtained when using the anti-AKT1 antibody in sperm cells. Regarding its subcellular localization, our results are particularly distinct from the published data, since we observed an immunostaining in the head and Sagare-Patil *et al*. (2013) described that total AKT is only present in the midpiece and tail[105]. When AKT is activated by phosphorylation in the cytoplasm, it is targeted to the inner leaflet of the plasma membrane and phosphorylates a number of subtracts[106]. In sperm cells, AKT pathway can be activated by progesterone and is required for motility and sperm cell survival. Unfortunately, our co-localization results did not allow to take any conclusion. An optimization of the ICC in human sperm with this antibody needs to be done to better understand the subcellular AKT1 localization and AKT1/CD81 co-localization. However, in SH-SY5Y cells, AKT1 presented the expected subcellular localization along the entire cytoplasm. Interestingly, the co-localization of CD81 and AKT1 seems to be prominent at the inner leaflet of the plasma membrane. This result indicates that CD81 co-localizes with the active AKT1, and may indicate that CD81 participates in the PI3K/AKT pathway. Interestingly, Milosch, *et al*. (2014)[107] shows that in neuronal cells APP serves as a receptor for the sAPPα, to trigger G-protein-dependent activation of PI3K. This activation leads to the recruitment and downstream activation of the pro-survival kinase AKT, mediating sAPPα-induced neuroprotection. Our findings suggest that in SH-SY5Y cells, the CD81-AKT complex may be involved in cell survival and proliferation. Co-localization studies using antibody for the phosphorylated AKT should thus be performed to unveil the role of this complex in neural cells.

Rac is a member of the Rho-family of proteins (as Rho and cdc42), molecules that bind actin and regulate the actin cytoskeleton remodelling[108]. CD81 seems to be intimately involved in cytoskeleton remodelling, as Brazzoli *et al.* (2008)[109] showed that it increases the levels of activated Rac1, RhoA and Cdc42 in Huh-7 cells. Hence, CD81 engagement (via antibody binding) induces Rho

family GTPase-dependent actin rearrangements that are involved in e.g. hepatitis C virus (HCV) infection. Actin remodelling is also involved in cell-cell adhesion, cell ECM adhesion, cytoskeletal protrusion/contraction, proteolytic ECM remodelling, and cell migration. Indeed, tetraspanins play important roles in the migration of many different cell types, including cancer cells, endothelial cells, keratinocytes, fibroblasts, and leukocytes[110]. A direct association between CD81 and Rac in TEM seems to be involved in cell migration, as reported by Tejera *et at.* (2013)[111]. According to these findings, CD81 regulates Rac1 dynamics and localization at the cell membrane during membrane protrusion, and formation of adhesion complexes and establishes a mechanism through which CD81 regulates cell migration. CD81-Rac complexes were most prominent at the cell leading edge, in which Rac promotes actin polymerization into F-actin and the formation of dendritic actin branches, favouring the initial steps in adhesion formation. Moreover, actin itself is a CD81 interacting protein, as described by Perez-Hernandez *et al.* (2013)[112] (Appendix 1-Table 1 and Figure 14). In agreement with these findings, we observed that CD81 staining perfectly matches with F-actin staining in stress fibres and filopodia of the leading edge of migrating SH-SY5Y cells (Figure 36). Further, we have also observed that CD81 is highly abundant in cellular spots that transverse the cell cytoplasm and appear to be focal adhesions (data not shown). These observations reinforce a role of CD81 in cell migration, and it will be very interesting to future characterize the role of CD81 specifically in neuronal migration and in other processes that involve Rho-family-dependent actin rearrangements such as neuritogenesis. In fact, in SH-SY5Y cells transient transfected with 1.0 and 1.5 μg of pCDM8 hCD81, the levels of the cytoskeleton-related proteins β-actin and Acetylated α-Tubulin seem to be altered. While β-actin levels seem to decrease with increasing amounts of CD81, the levels of acetylated tubulin appear to increase (Figure 35). These kind of alterations are in accordance with a remodelling of the actin and microtubules cytoskeleton related with neuritogenic events. Indeed, we have reported that with the onset of neuritogenesis, the actin levels tend to first decrease, while with the elongation of cellular projections the levels of acetylated tubulin increase[113]. According to this, when we transfected SH-SY5Y cells with non-toxic amounts (as 1.0 μg) of mApple-tagged CD81, the number of cellular projections highly increased (data not shown). In the future, this will be scored and related to the levels of CD81, and to the levels of beta-actin, total tubulin, and acetylated tubulin (in triplicates).

Regarding sperm cells, our results showed no or few immunostaining of F-actin by Alexa Fluor 568 Phalloidin in sperm cells (Figure 34). Cytoskeleton proteins such as actin and tubulin (α-, β- and γ-tubulin) are implicated in key events such as capacitation and the acrosome reaction (AR), and these proteins are altered after the AR. F-actin polymerization occurs during capacitation and

is important for the translocation of phospholipase C from the cytosol to the sperm plasma membrane during this proccess[114]. Unfortunately, we cannot infer about the distribution of F-actin and its co-localization between CD81 since we have only tested this in one sample, and the staining was very weak. This has to be further repeated, but if CD81 is involved in sperm cells motility it will probably be via a different mechanism than SH-SY5Y cells migration, since sperm cells migrate through their flagellum.

CD81 and APP

Since CD81 was one of the APP potential interactors in human testis with one of the highest number of positive clones, we aimed to confirm and further characterize the CD81-APP interaction. Our first approach was to attempt to demonstrate the formation of a complex between CD81 and APP in two different cell lines. CHO and SH-SY5Y cells were single transfected or co-transfected with CD81 and APP cDNAs and then subjected to co-IP and pull-down assays, using different lysis buffers: 1% NP-40, 1% TRITON and 4% CHAPS. From the co-IP and pull-down assays it remained unclear whether CD81 and APP physically interact under the conditions tested. Three different levels of interactions have been proposed to occur in the tetraspanin web, based on the use of different detergents in the co-IP assays used to pull-down tetraspanins' interactors[40]. In the present work we performed cell lysis with harsh detergents (1% NP-40 and 1% Triton-X-100) and a mild detergent (4% CHAPS). At an advance state of our study we discovered that, in and until then elusive work whose main aim was not APP-CD81 interaction but classified their level of interaction. Sosa *et al*. (2013)[94] demonstrated by co-IP that APP forms Brij98-resistante complexes with CD81 in rat neuronal growth cones. We now aim to demonstrate that APP and CD81 form protein complexes in CHO, SH-SY5Y and human sperm cells through the use of a Brji98-containing buffer to lyse cells before the co-IP. We thus hypothesise that CD81 and APP physically interact by indirect associations, clustering with cholesterol in the TEM, as described for the Brji98-resistant tertiary interactions[37]. We hypothesize that CD81 bridges APP to these TEM membrane domains and helps to regulate its surface availability for cell adhesion or cleavage, and signalling via its sAPP and AICD fragments. Indeed, our bioinformatics analysis unravelled CD81 interacting enzymes that are involved in the cleavage of APP into these fragments: ADAM10 and presinilin 1 and 2 (Appendix 1-Table 1 and Figure 14). The role of CD81 in the APP proteolytic pathway was studied in two independent works. By the physical interaction with the α-secretase ADAM10, CD81 was observed to promote the ADAM10 activity and to consequently decrease Aβ formation[92]. In another work, CD81 was seen to interact with PS1 and PS2 (proteolytic subunits of the γ-secretase complex), and

also to modulate their activity. This study showed that the absence of CD81 led to an accumulation of the AICD-precursor βCTFs, indicating a partial disruption of either the γ-secretase activity or the interaction between γ-secretase and its CTF substrate in CD81-lacking condition[52]. It thus seems that CD81 can participate in the amyloidogenic pathway and in the non-amyloidogenic pathway. Contrary to the first report, our results suggests that CD81 does not significantly affect the cleavage of APP into sAPP, at least in SH-SY5Y cells (Figure 29), but it probably interferes with the APP half-life or increases the rate of APP mRNA translation. CD81 overexpression in SH-SY5Y and CHO cells can result in slightly higher APP levels until 1.0 μg of transfected pCDM8 hCD81 cDNA. This occurred in both cell lines, although the effect was more prominent in CHO cells (Figure 29). The increased APP translation hypothesis is supported by our bioinformatics findings that most of CD81 interactors are involved in biological processes related to translation (Table 6).

We next evaluated the potential cellular regions of CD81-APP interaction by monitoring their subcellular co-localization sites in sperm cells and SH-SY5Y cells. In our lab, we have previously characterized the distribution of members of the APP superfamily in sperm cells. Although their presence in the head (particularly at the equatorial region) suggests their possible involvement in sperm-oocyte interaction, no binding partner was attributed to APP/APLPs. The anti-APP C695 antibody here used detects the C-terminal of APP and also of APLP1 and APLP2 proteins. Results showed that CD81 mainly co-localizes with members of the APP superfamily in the midpiece and in some spots of the post-acrosomal region. Our previous studies showed that the midpiece mainly expressed APLP2, whereas APP is present in the surface of the entire head[77], suggesting that the co-localization in the midpiece is between APLP2 and CD81 and in the post-acrosomal region is between APP and CD81. Since these are specialized zones of the sperm cell, we hypothesize that their co-localization at the midpiece is involved in signalling pathways related to sperm motility, and that CD81 and APP co-localize at the sperm head for maintaining APP at the surface and mediate e.g. sperm-oocyte membrane-membrane adhesion.

The ICC studies in SH-SY5Y cells showed co-localization with endogenous CD81 and APP in very specific subcellular sites. The co-localization was present in cellular projections in non-differentiated cells. APP is preferentially enriched in the growing neurites and in neuritic growth cones, and stabilizes the neurites[113]. CD81 interacts with α3β1 integrin and this complex co-distributes on neurites and growth cones of human NT2N cells. This association is functionally relevant, as CD81 strongly and positively contributes toward neurite number, length, and rate of outgrowth in this model[115]. Taken together with the fact that APP also binds integrins and that we have observed CD81 increasing the number of cellular projections, the co-localization of CD81 and

APP suggests that this complex may have a role in neuritogenesis and in adhesion. The ICC analysis showed that CD81 and APP co-localized in filopodia, which are F-actin enriched membrane protrusions involved in neuritogenesis, cell migration, and cell-cell communication. APP has been described to mediate neuronal cell-cell adhesion and CD81 is also involved in cell adhesion in the immune system[33].

In synthesis, the bioinformatics analysis and our WB/ICC results indicate that CD81 and its interactors such as AKT1, APP and cytoskeleton-related proteins are involved in a variety of signalling pathways that comprise cytoskeleton remodelling and are related to processes such as sperm motility and cell migration, cell survival, and neuritogenesis. Several of these data still need to be confirmed and further explored, but we believe that this work will help to further advance the knowledge on the functions of CD81 and its interactors, particularly in sperm and neuronal cells.

6. References

1. Klinovska, K., Sebkova, N. & Dvorakova-Hortova, K. Sperm-egg fusion: a molecular enigma of mammalian reproduction. *Int. J. Mol. Sci.* **15,** 10652–68 (2014).

2. Evans, J. P. Sperm-egg interaction. *Annu. Rev. Physiol.* **74,** 477–502 (2012).

3. Evans, J. P. & Florman, H. M. The state of the union: the cell biology of fertilization. *Nat. Cell Biol.* **4 Suppl,** s57–s63 (2002).

4. Okabe, M. The cell biology of mammalian fertilization. *Development* **140,** 4471–9 (2013).

5. Amaral, A. *et al.* Human sperm tail proteome suggests new endogenous metabolic pathways. *Mol. Cell. Proteomics* **12,** 330–42 (2013).

6. Saladin, K. *Anatomy & Physiology: The Unity of Form and Function*. (McGraw Hill, 2007).

7. Gadella, B. M. & Luna, C. Cell biology and functional dynamics of the mammalian sperm surface. *Theriogenology* **81,** 74–84 (2014).

8. Miller, M. R., Mansell, S. A., Meyers, S. A. & Lishko, P. V. Flagellar ion channels of sperm: similarities and differences between species. *Cell Calcium* (2014). doi:10.1016/j.ceca.2014.10.009

9. Rahman, M. S., Kwon, W. S. & Pang, M. G. Calcium influx and male fertility in the context of the sperm proteome: An update. *BioMed Research International* **2014,** (2014).

10. Ramalho-Santos, J. *et al.* in *Modern Research and Educational Topics in Microscopy* (ed. Díaz, A. M.-V. and J.) 394–402 (Formatex, 2007).

11. Lishko, P. V. *et al.* The Control of Male Fertility by Spermatozoan Ion Channels. *Annual Review of Physiology* **74,** 453–475 (2012).

12. Gur, Y. & Breitbart, H. Mammalian sperm translate nuclear-encoded proteins by mitochondrial-type ribosomes. *Genes Dev.* **20,** 411–6 (2006).

13. Flesch, F. M. & Gadella, B. M. Dynamics of the mammalian sperm plasma membrane in the process of fertilization. *Biochim. Biophys. Acta* **1469,** 197–235 (2000).

14. Singh, A. & Rajender, S. CatSper channel, sperm function and male infertility. *Reprod. Biomed. Online* (2014). doi:10.1016/j.rbmo.2014.09.014

15. Moseley, F. L. C. *et al.* Protein tyrosine phosphorylation, hyperactivation and progesterone-induced acrosome reaction are enhanced in IVF media: An effect that is not associated with an increase in protein kinase A activation. *Mol. Hum. Reprod.* **11,** 523–529 (2005).

16. Liu, D. Y., Liu, M. L., Clarke, G. N. & Baker, H. W. G. Hyperactivation of capacitated human sperm correlates with the zona pellucida-induced acrosome reaction of zona pellucida-bound sperm. *Hum. Reprod.* **22,** 2632–2638 (2007).

17. Ickowicz, D., Finkelstein, M. & Breitbart, H. Mechanism of sperm capacitation and the acrosome reaction: role of protein kinases. *Asian Journal of Andrology* (2012). doi:10.1038/aja.2012.81

18. Salicioni, A. M. *et al.* Signalling pathways involved in sperm capacitation. *Soc. Reprod. Fertil. Suppl.* **65,** 245–259 (2007).

19. Visconti, P. E. Understanding the molecular basis of sperm capacitation through kinase design. *Proc. Natl. Acad. Sci. U. S. A.* **106,** 667–8 (2009).

20. Gadella, B. M. & Evans, J. P. Membrane fusions during mammalian fertilization. *Adv. Exp. Med. Biol.* **713,** 65–80 (2011).

21. Kate A. Redgrove, R. J. A. and B. N. in *Binding Protein* (ed. Abdelmohsen, K.) (InTech, 2012). doi:10.5772/2897

22. Nishigaki, T. *et al.* Intracellular pH in sperm physiology. *Biochemical and Biophysical Research Communications* **450,** 1149–1158 (2014).

23. Gupta, S. K. & Bhandari, B. Acrosome reaction: relevance of zona pellucida glycoproteins. *Asian J. Androl.* **13,** 97–105 (2011).

24. Ikawa, M., Inoue, N., Benham, A. M. & Okabe, M. Fertilization: A sperm's journey to and interaction with the oocyte. *Journal of Clinical Investigation* **120,** 984–994 (2010).

25. Inoue, N., Ikawa, M. & Okabe, M. The mechanism of sperm-egg interaction and the involvement of IZUMO1 in fusion. *Asian J. Androl.* **13,** 81–87 (2011).

26. Rubinstein, E., Ziyyat, A., Wolf, J. P., Le Naour, F. & Boucheix, C. The molecular players of sperm-egg fusion in mammals. *Seminars in Cell and Developmental Biology* **17,** 254–263 (2006).

27. Chalbi, M. *et al.* Binding of sperm protein Izumo1 and its egg receptor Juno drives Cd9 accumulation in the intercellular contact area prior to fusion during mammalian fertilization. *Development* **141,** 3732–9 (2014).

28. Bianchi, E., Doe, B., Goulding, D. & Wright, G. J. Juno is the egg Izumo receptor and is essential for mammalian fertilization. *Nature* **508,** 483–7 (2014).

29. Fujihara, Y. *et al.* Sperm equatorial segment protein 1, SPESP1, is required for fully fertile sperm in mouse. *J. Cell Sci.* **123,** 1531–6 (2010).

30. Hemler, M. E. Tetraspanin functions and associated microdomains. *Nat. Rev. Mol. Cell Biol.* **6,** 801–11 (2005).

31. Shoham, T., Rajapaksa, R., Kuo, C.-C., Haimovich, J. & Levy, S. Building of the tetraspanin web: distinct structural domains of CD81 function in different cellular compartments. *Mol. Cell. Biol.* **26,** 1373–85 (2006).

32. Levy, S. & Shoham, T. The tetraspanin web modulates immune-signalling complexes. *Nat. Rev. Immunol.* **5,** 136–48 (2005).

33. Levy, S., Todd, S. C. & Maecker, H. T. CD81 (TAPA-1): a molecule involved in signal transduction and cell adhesion in the immune system. *Annu. Rev. Immunol.* **16,** 89–109 (1998).

34. Andria, M. L., Hsieh, C. L., Oren, R., Francke, U. & Levy, S. Genomic organization and chromosomal localization of the TAPA-1 gene. *J. Immunol.* **147,** 1030–6 (1991).

35. Seigneuret, M. Complete predicted three-dimensional structure of the facilitator transmembrane protein and hepatitis C virus receptor CD81: conserved and variable structural domains in the tetraspanin superfamily. *Biophys. J.* **90,** 212–27 (2006).

36. Andreu, Z. & Yáñez-Mó, M. Tetraspanins in extracellular vesicle formation and function. *Front. Immunol.* **5,** 442 (2014).

37. Levy, S. Protein-Protein Interactions in the Tetraspanin Web. *Physiology* **20,** 218–224 (2005).

38. Levy, S. & Shoham, T. The tetraspanin web modulates immune-signalling complexes. *Nat. Rev. Immunol.* **5,** 136–48 (2005).

39. Levy, S. Protein-Protein Interactions in the Tetraspanin Web. *Physiology* **20,** 218–224 (2005).

40. Boucheix, C. & Rubinstein, E. Tetraspanins. *Cell. Mol. Life Sci.* **58,** 1189–205 (2001).

41. Rubinstein, E. *et al.* Reduced fertility of female mice lacking CD81. *Dev. Biol.* **290,** 351–358 (2006).

42. Takahashi, Y., Bigler, D., Ito, Y. & White, J. M. Sequence-specific interaction between the disintegrin domain of mouse ADAM 3 and murine eggs: role of beta1 integrin-associated proteins CD9, CD81, and CD98. *Mol. Biol. Cell* **12,** 809–820 (2001).

43. Tanigawa, M. *et al.* Possible involvement of CD81 in acrosome reaction of sperm in mice. *Mol. Reprod. Dev.* **75,** 150–5 (2008).

44. Ohnami, N. *et al.* CD81 and CD9 work independently as extracellular components upon fusion of sperm and oocyte. *Biology Open* **1,** 640–647 (2012).

45. Barraud-Lange, V., Naud-Barriant, N., Bomsel, M., Wolf, J.-P. & Ziyyat, A. Transfer of oocyte membrane fragments to fertilizing spermatozoa. *FASEB J.* **21,** 3446–3449 (2007).

46. Silva, J. V. *et al.* Amyloid precursor protein interaction network in human testis: sentinel proteins for male reproduction. *BMC Bioinformatics* **16,** 12 (2015).

47. Goldgaber, D., Lerman, M. I., McBride, W. O., Saffiotti, U. & Gajdusek, D. C. Isolation, characterization, and chromosomal localization of human brain cDNA clones coding for the precursor of the amyloid of brain in Alzheimer's disease, Down's syndrome and aging. *J. Neural Transm. Suppl.* **24,** 23–8 (1987).

48. Kang, J. *et al.* The precursor of Alzheimer's disease amyloid A4 protein resembles a cell-surface receptor. *Nature* **325,** 733–6

49. Robakis, N. K., Ramakrishna, N., Wolfe, G. & Wisniewski, H. M. Molecular cloning and characterization of a cDNA encoding the cerebrovascular and the neuritic plaque amyloid peptides. *Proc. Natl. Acad. Sci. U. S. A.* **84,** 4190–4 (1987).

50. Tanzi, R. E. *et al.* Amyloid beta protein gene: cDNA, mRNA distribution, and genetic linkage near the Alzheimer locus. *Science* **235,** 880–4 (1987).

51. Glenner, G. G., Wong, C. W., Quaranta, V. & Eanes, E. D. The amyloid deposits in Alzheimer's disease: their nature and pathogenesis. *Appl. Pathol.* **2,** 357–69 (1984).

52. Shariati, S. A. M. & De Strooper, B. Redundancy and divergence in the amyloid precursor protein family. *FEBS Lett.* **587,** 2036–45 (2013).

53. Walsh, D. M. *et al.* The APP family of proteins: similarities and differences. *Biochem. Soc. Trans.* **35,** 416–420 (2007).

54. WASCO, W., PEPPERCORN, J. & TANZI, R. E. Search for the Genes Responsible for Familial Alzheimer's Disease. *Ann. N. Y. Acad. Sci.* **695,** 203–208 (1993).

55. Yan, Y. C., Bai, Y., Wang, L. F., Miao, S. Y. & Koide, S. S. Characterization of cDNA encoding a human sperm membrane protein related to A4 amyloid protein. *Proc. Natl. Acad. Sci. U. S. A.* **87,** 2405–8 (1990).

56. Daigle, I. & Li, C. apl-1, a Caenorhabditis elegans gene encoding a protein related to the human beta-amyloid protein precursor. *Proc. Natl. Acad. Sci. U. S. A.* **90,** 12045–9 (1993).

57. Luo, L. Q., Martin-Morris, L. E. & White, K. Identification, secretion, and neural expression of APPL, a Drosophila protein similar to human amyloid protein precursor. *J. Neurosci.* **10,** 3849–61 (1990).

58. Müller, U. C. & Zheng, H. Physiological functions of APP family proteins. *Cold Spring Harb. Perspect. Med.* **2,** (2013).

59. Jacobsen, K. T. & Iverfeldt, K. Amyloid precursor protein and its homologues: A family of proteolysis-dependent receptors. *Cellular and Molecular Life Sciences* **66,** 2299–2318 (2009).

60. Sandbrink, R., Masters, C. L. & Beyreuther, K. APP gene family. Alternative splicing generates functionally related isoforms. *Ann. N. Y. Acad. Sci.* **777,** 281–7 (1996).

61. Kitaguchi, N., Takahashi, Y., Tokushima, Y., Shiojiri, S. & Ito, H. Novel precursor of Alzheimer's disease amyloid protein shows protease inhibitory activity. *Nature* **331,** 530–2 (1988).

62. Ling, Y., Morgan, K. & Kalsheker, N. Amyloid precursor protein (APP) and the biology of proteolytic processing: relevance to Alzheimer's disease. *Int. J. Biochem. Cell Biol.* **35,** 1505–1535 (2003).

63. Sandbrink, R., Masters, C. L. & Beyreuther, K. Similar alternative splicing of a non-homologous domain in βA4-amyloid protein precursor-like proteins. *J. Biol. Chem.* **269,** 14227–14234 (1994).

64. Lorent, K. *et al.* Expression in mouse embryos and in adult mouse brain of three members of the amyloid precursor protein family, of the alpha-2-macroglobulin receptor/low density lipoprotein receptor-related protein and of its ligands apolipoprotein E, lipoprotein lipase, . *Neuroscience* **65,** 1009–25 (1995).

65. Zhang, Y., Thompson, R., Zhang, H. & Xu, H. APP processing in Alzheimer's disease. *Mol. Brain* **4,** 3 (2011).

66. Haass, C., Kaether, C., Thinakaran, G. & Sisodia, S. Trafficking and proteolytic processing of APP. *Cold Spring Harb. Perspect. Med.* **2,** (2012).

67. Koo, E. H. *et al.* Precursor of amyloid protein in Alzheimer disease undergoes fast anterograde axonal transport. *Proc. Natl. Acad. Sci. U. S. A.* **87,** 1561–1565 (1990).

68. O'Brien, R. J. & Wong, P. C. Amyloid precursor protein processing and Alzheimer's disease. *Annu. Rev. Neurosci.* **34,** 185–204 (2011).

69. Wiltfang, J. Elevation of beta -Amyloid Peptide 2-42 in Sporadic and Familial Alzheimer's Disease and Its Generation in PS1 Knockout Cells. *J. Biol. Chem.* **276,** 42645–42657 (2001).

70. Zheng, H. & Koo, E. H. Biology and pathophysiology of the amyloid precursor protein. *Mol. Neurodegener.* **6,** 27 (2011).

71. Puig, K. L. & Combs, C. K. Expression and function of APP and its metabolites outside the central nervous system. *Experimental Gerontology* **48,** 608–611 (2013).

72. Von Koch, C. S. *et al.* Generation of APLP2 KO mice and early postnatal lethality in APLP2/APP double KO mice. *Neurobiol. Aging* **18,** 661–669 (1997).

73. Shoji, M. *et al.* Alzheimer amyloid beta-protein precursor in sperm development. *Am. J. Pathol.* **137,** 1027–1032 (1990).

74. Huang, P. *et al.* Expression and characterization of the human YWK-II gene, encoding a sperm membrane protein related to the alzheimer betaA4-amyloid precursorprotein. *Mol. Hum. Reprod.* **6,** 1069–78 (2000).

75. Zhuang, D. *et al.* Delineation of the functional domains of the extracellular region of YWK-II Protein/APLP2 of sperm membrane. *Front. Biosci.* **11,** 2371–80 (2006).

76. Zhuang, D. *et al.* YWK-II protein/APLP2 in mouse gametes: potential role in fertilization. *Mol. Reprod. Dev.* **73,** 61–7 (2006).

77. Fardilha, M. *et al.* Differential distribution of Alzheimer's amyloid precursor protein family variants in human sperm. *Ann. N. Y. Acad. Sci.* **1096,** 196–206 (2007).

78. Stark, C. *et al.* BioGRID: a general repository for interaction datasets. *Nucleic Acids Res.* **34,** D535–9 (2006).

79. Warde-Farley, D. *et al.* The GeneMANIA prediction server: biological network integration for gene prioritization and predicting gene function. *Nucleic Acids Res.* **38,** W214–20 (2010).

80. Thomas, P. D. *et al.* PANTHER: a library of protein families and subfamilies indexed by function. *Genome Res.* **13,** 2129–41 (2003).

81. Organization, W. H. *WHO laboratory manual for the examination and processing of human semen*. (WHO Press, 2010). at <http://www.who.int/reproductivehealth/publications/infertility/9789241547789/en/>

82. Thermo Fisher Scientific Inc. Pierce™ BCA Protein Assay Kit. (2015). at <https://www.thermofisher.com/order/catalog/product/23225>

83. Thermo Fisher Scientific Inc. Immunoprecipitation with Dynabeads® Protein G. at <http://www.thermofisher.com/pt/en/home/references/protocols/proteins-expression-isolation-and-analysis/protein-purification-protocol/immunoprecipitation-with-dynabeads-protein-g.html#prot1>

84. Mahmood, T. & Yang, P.-C. Western blot: technique, theory, and trouble shooting. *N. Am. J. Med. Sci.* **4,** 429–34 (2012).

85. Romero-Calvo, I. *et al.* Reversible Ponceau staining as a loading control alternative to actin in Western blots. *Anal. Biochem.* **401,** 318–20 (2010).

86. Burry, R. W. *Immunocytochemistry, A Practical Guide for Biomedical Research*. (Springer-Verlag New York, 2010).

87. Schindelin, J. *et al.* Fiji: an open-source platform for biological-image analysis. *Nat. Methods* **9,** 676–682 (2012).

88. Bolte, S. & Cordelières, F. P. A guided tour into subcellular colocalization analysis in light microscopy. *J. Microsc.* **224,** 213–32 (2006).

89. Zuidscherwoude, M. *et al.* The tetraspanin web revisited by super-resolution microscopy. *Sci. Rep.* **5,** 12201 (2015).

90. Charrin, S. *et al.* Lateral organization of membrane proteins: tetraspanins spin their web. *Biochem. J.* **420,** 133–54 (2009).

91. Schmidt, A., Forne, I. & Imhof, A. Bioinformatic analysis of proteomics data. *BMC Syst. Biol.* **8 Suppl 2,** S3 (2014).

92. Xu, D., Sharma, C. & Hemler, M. E. Tetraspanin12 regulates ADAM10-dependent cleavage of amyloid precursor protein. *FASEB J.* **23,** 3674–3681 (2009).

93. Wakabayashi, T. *et al.* Analysis of the gamma-secretase interactome and validation of its association with tetraspanin-enriched microdomains. *Nat. Cell Biol.* **11,** 1340–6 (2009).

94. Sosa, L. J. *et al.* Amyloid precursor protein is an autonomous growth cone adhesion molecule engaged in contact guidance. *PLoS One* **8,** e64521 (2013).

95. ATCC® Animal Cell Culture Guide: Tips and techniques for continuous cell lines. (2015). at <http://www.lgcstandards-atcc.org/Guides/Guides.aspx?geo_country=pt>

96. Assanga, I. Cell growth curves for different cell lines and their relationship with biological activities. *Int. J. Biotechnol. Mol. Biol. Res.* **4,** 60–70 (2013).

97. Czekanska, E. in *Mammalian Cell Viability: Methods and Protocols* (Humana Press, 2011).

98. ATCC®. ATCC® Animal Cell Culture: tips and techniques for continuous cell lines. at <https://www.atcc.org/~/media/PDFs/Culture Guides/AnimCellCulture_Guide.ashx>

99. Ohnami, N. *et al.* CD81 and CD9 work independently as extracellular components upon fusion of sperm and oocyte. *Biol. Open* **1,** 640–647 (2012).

100. Brückner, A., Polge, C., Lentze, N., Auerbach, D. & Schlattner, U. Yeast two-hybrid, a powerful tool for systems biology. *Int. J. Mol. Sci.* **10,** 2763–88 (2009).

101. Santi, S. A. & Lee, H. The Akt isoforms are present at distinct subcellular locations. *Am. J. Physiol. Cell Physiol.* **298,** C580–91 (2010).

102. Dijkstra, S., Geisert EE, J. R., Gispen, W. H., Bär, P. R. & Joosten, E. A. Up-regulation of CD81 (target of the antiproliferative antibody; TAPA) by reactive microglia and astrocytes after spinal cord injury in the rat. *J. Comp. Neurol.* **428,** 266–77 (2000).

103. Geisert, E. E. *et al.* Increased brain size and glial cell number in CD81-null mice. *J. Comp. Neurol.* **453,** 22–32 (2002).

104. Kelić, S., Levy, S., Suarez, C. & Weinstein, D. E. CD81 regulates neuron-induced astrocyte cell-cycle exit. *Mol. Cell. Neurosci.* **17,** 551–560 (2001).

105. Sagare-Patil, V., Vernekar, M., Galvankar, M. & Modi, D. Progesterone utilizes the PI3K-AKT pathway in human spermatozoa to regulate motility and hyperactivation but not acrosome reaction. *Mol. Cell. Endocrinol.* **374,** 82–91 (2013).

106. Xue, G. & Hemmings, B. A. PKB/Akt-dependent regulation of cell motility. *J. Natl. Cancer Inst.* **105,** 393–404 (2013).

107. Milosch, N. *et al.* Holo-APP and G-protein-mediated signaling are required for sAPPα-induced activation of the Akt survival pathway. *Cell Death Dis.* **5,** e1391 (2014).

108. Symons, M. Rho family GTPases: the cytoskeleton and beyond. *Trends Biochem. Sci.* **21,** 178–181 (1996).

109. Brazzoli, M. *et al.* CD81 is a central regulator of cellular events required for hepatitis C virus infection of human hepatocytes. *J. Virol.* **82,** 8316–29 (2008).

110. Wang, J. *et al.* Toward an understanding of the protein interaction network of the human liver. *Mol. Syst. Biol.* **7,** 536 (2011).

111. Tejera, E. *et al.* CD81 regulates cell migration through its association with Rac GTPase. *Mol. Biol. Cell* **24,** 261–73 (2013).

112. Perez-Hernandez, D. *et al.* The intracellular interactome of tetraspanin-enriched microdomains reveals their function as sorting machineries toward exosomes. *J. Biol. Chem.* **288,** 11649–61 (2013).

113. Da Rocha, J. F., da Cruz e Silva, O. A. B. & Vieira, S. I. Analysis of the amyloid precursor protein role in neuritogenesis reveals a biphasic SH-SY5Y neuronal cell differentiation model. *J. Neurochem.* **134,** 288–301 (2015).

114. Breitbart, H., Cohen, G. & Rubinstein, S. Role of actin cytoskeleton in mammalian sperm capacitation and the acrosome reaction. *Reproduction* **129,** 263–8 (2005).

115. Stipp, C. S. & Hemler, M. E. Transmembrane-4-superfamily proteins CD151 and CD81 associate with alpha 3 beta 1 integrin, and selectively contribute to alpha 3 beta 1-dependent neurite outgrowth. *J. Cell Sci.* **113 (Pt 1,** 1871–1882 (2000).

116. Little, K. D., Hemler, M. E. & Stipp, C. S. Dynamic regulation of a GPCR-tetraspanin-G protein complex on intact cells: central role of CD81 in facilitating GPR56-Galpha q/11 association. *Mol. Biol. Cell* **15,** 2375–87 (2004).

117. Kittanakom, S. *et al.* CHIP-MYTH: a novel interactive proteomics method for the assessment of agonist-dependent interactions of the human β_2-adrenergic receptor. *Biochem. Biophys. Res. Commun.* **445,** 746–56 (2014).

118. Cherukuri, A. *et al.* The Tetraspanin CD81 Is Necessary for Partitioning of Coligated CD19/CD21-B Cell Antigen Receptor Complexes into Signaling-Active Lipid Rafts. *J. Immunol.* **172,** 370–380 (2003).

119. Wolf, Z., Orsó, E., Werner, T., Boettcher, A. & Schmitz, G. A flow cytometric screening test for detergent-resistant surface antigens in monocytes. *Cytometry. A* **69,** 192–5 (2006).

120. Bradbury, L. E., Kansas, G. S., Levy, S., Evans, R. L. & Tedder, T. F. The CD19/CD21 signal transducing complex of human B lymphocytes includes the target of antiproliferative antibody-1 and Leu-13 molecules. *J. Immunol.* **149,** 2841–50 (1992).

121. Imai, T., Kakizaki, M., Nishimura, M. & Yoshie, O. Molecular analyses of the association of CD4 with two members of the transmembrane 4 superfamily, CD81 and CD82. *J. Immunol.* **155,** 1229–39 (1995).

122. Horváth, G. *et al.* CD19 is linked to the integrin-associated tetraspans CD9, CD81, and CD82. *J. Biol. Chem.* **273,** 30537–43 (1998).

123. Lozahic, S. *et al.* CD46 (membrane cofactor protein) associates with multiple beta1 integrins and tetraspans. *Eur. J. Immunol.* **30,** 900–7 (2000).

124. Nichols, T. C. *et al.* Gamma-glutamyl transpeptidase, an ecto-enzyme regulator of intracellular redox potential, is a component of TM4 signal transduction complexes. *Eur. J. Immunol.* **28,** 4123–9 (1998).

125. Booth, A. M. *et al.* Exosomes and HIV Gag bud from endosome-like domains of the T cell plasma membrane. *J. Cell Biol.* **172,** 923–35 (2006).

126. Rubinstein, E. *et al.* CD9, CD63, CD81, and CD82 are components of a surface tetraspan network connected to HLA-DR and VLA integrins. *Eur. J. Immunol.* **26,** 2657–65 (1996).

127. Kitadokoro, K. *et al.* Subunit association and conformational flexibility in the head subdomain of human CD81 large extracellular loop. *Biol. Chem.* **383,** 1447–52 (2002).

128. Radford, K. J., Thorne, R. F. & Hersey, P. CD63 associates with transmembrane 4 superfamily members, CD9 and CD81, and with beta 1 integrins in human melanoma. *Biochem. Biophys. Res. Commun.* **222,** 13–8 (1996).

129. Fénéant, L., Levy, S. & Cocquerel, L. CD81 and hepatitis C virus (HCV) infection. *Viruses* **6,** 535–72 (2014).

130. Havugimana, P. C. *et al.* A census of human soluble protein complexes. *Cell* **150,** 1068–81 (2012).

131. Stelzl, U. *et al.* A human protein-protein interaction network: a resource for annotating the proteome. *Cell* **122,** 957–68 (2005).

132. Coffey, G. P. *et al.* Engagement of CD81 induces ezrin tyrosine phosphorylation and its cellular redistribution with filamentous actin. *J. Cell Sci.* **122,** 3137–44 (2009).

133. Huang, X. *et al.* The identification of novel proteins that interact with the GLP-1 receptor and restrain its activity. *Mol. Endocrinol.* **27,** 1550–63 (2013).

134. Bhave, V. S. *et al.* Regulation of liver growth by glypican 3, CD81, hedgehog, and Hhex. *Am. J. Pathol.* **183,** 153–9 (2013).

135. Ewing, R. M. *et al.* Large-scale mapping of human protein-protein interactions by mass spectrometry. *Mol. Syst. Biol.* **3,** 89 (2007).

136. Lehner, B. & Sanderson, C. M. A protein interaction framework for human mRNA degradation. *Genome Res.* **14,** 1315–23 (2004).

137. Zona, L. *et al.* HRas signal transduction promotes hepatitis C virus cell entry by triggering assembly of the host tetraspanin receptor complex. *Cell Host Microbe* **13,** 302–13 (2013).

138. Rocha-Perugini, V. *et al.* CD81 controls sustained T cell activation signaling and defines the maturation stages of cognate immunological synapses. *Mol. Cell. Biol.* **33,** 3644–58 (2013).

139. Takahashi, S., Doss, C., Levy, S. & Levy, R. TAPA-1, the target of an antiproliferative antibody, is associated on the cell surface with the Leu-13 antigen. *J. Immunol.* **145,** 2207–13 (1990).

140. Clark, K. L., Zeng, Z., Langford, A. L., Bowen, S. M. & Todd, S. C. PGRL is a major CD81-associated protein on lymphocytes and distinguishes a new family of cell surface proteins. *J. Immunol.* **167,** 5115–21 (2001).

141. Serru, V. *et al.* Selective tetraspan-integrin complexes (CD81/alpha4beta1, CD151/alpha3beta1, CD151/alpha6beta1) under conditions disrupting tetraspan interactions. *Biochem. J.* **340 (Pt 1,** 103–11 (1999).

142. Mazzocca, A. *et al.* Expression of transmembrane 4 superfamily (TM4SF) proteins and their role in hepatic stellate cell motility and wound healing migration. *J. Hepatol.* **37,** 322–30 (2002).

143. Anzai, N. *et al.* C-kit associated with the transmembrane 4 superfamily proteins constitutes a functionally distinct subunit in human hematopoietic progenitors. *Blood* **99,** 4413–21 (2002).

144. Le, Q.-T., Blanchet, M., Seidah, N. G. & Labonté, P. Plasma Membrane Tetraspanin CD81 Complexes with Proprotein Convertase Subtilisin/Kexin Type 9 (PCSK9) and Low Density Lipoprotein Receptor (LDLR), and Its Levels Are Reduced by PCSK9. *J. Biol. Chem.* **290,** 23385–400 (2015).

145. Mazurov, D., Barbashova, L. & Filatov, A. Tetraspanin protein CD9 interacts with metalloprotease CD10 and enhances its release via exosomes. *FEBS J.* **280,** 1200–13 (2013).

146. Fautsch, M. P., Vrabel, A. M. & Johnson, D. H. The identification of myocilin-associated proteins in the human trabecular meshwork. *Exp. Eye Res.* **82,** 1046–52 (2006).

147. Yauch, R. L. & Hemler, M. E. Specific interactions among transmembrane 4 superfamily (TM4SF) proteins and phosphoinositide 4-kinase. *Biochem. J.* **351 Pt 3,** 629–37 (2000).

148. Charrin, S. *et al.* The major CD9 and CD81 molecular partner. Identification and characterization of the complexes. *J. Biol. Chem.* **276,** 14329–37 (2001).

149. Chibi, M. *et al.* RBBP6 interacts with multifunctional protein YB-1 through its RING finger domain, leading to ubiquitination and proteosomal degradation of YB-1. *J. Mol. Biol.* **384,** 908–16 (2008).

150. Carloni, V., Mazzocca, A. & Ravichandran, K. S. Tetraspanin CD81 is linked to ERK/MAPKinase signaling by Shc in liver tumor cells. *Oncogene* **23,** 1566–74 (2004).

151. Bhatnagar, S. *et al.* Phosphorylation and degradation of tomosyn-2 de-represses insulin secretion. *J. Biol. Chem.* **289,** 25276–86 (2014).

152. Chen, J. & Enns, C. A. CD81 promotes both the degradation of transferrin receptor 2 (TfR2) and the Tfr2-mediated maintenance of hepcidin expression. *J. Biol. Chem.* **290,** 7841–50 (2015).

153. Tachibana, I., Bodorova, J., Berditchevski, F., Zutter, M. M. & Hemler, M. E. NAG-2, a novel transmembrane-4 superfamily (TM4SF) protein that complexes with integrins and other TM4SF proteins. *J. Biol. Chem.* **272,** 29181–9 (1997).

154. Schaafhausen, A., Rost, S., Oldenburg, J. & Müller, C. R. Identification of VKORC1 interaction partners by split-ubiquitin system and coimmunoprecipitation. *Thromb. Haemost.* **105,** 285–94 (2011).

Appendix 1

Table 1. CD81 interactors obtained from BioGrid (in black) database and PubMed publications (in grey) after manual curation of respective publication.

Gene	Protein	UniProt ID	Ref.
ACTB	Actin, beta	P60709	112
ACTN1	actinin, alpha 1	P12814	112
ACTN4	Actinin, alpha 4	O43707	112
ADAM10	Desintegrin and metalloproteinase domain-containing protein 10	O14672	92
ADGRG1	Adhesion G Protein-Coupled Receptor G1	Q9Y653	116
ADRB2	Adrenoreceptor beta 2, surface	P07550	117
AKT1	RAC-alpha serine/threonine-protein kinase	P31749	112
ALYREF	Aly/REF export factor	Q86V81	112
ANP32B	Acid (leucine-rich) nuclear phosphoprotein 32 family, member B	Q92688	112
APP	Amyloid Beta (A4) Precursor Protein	P05067	94
ATP5A1	ATP synthase, H+ transporting, mitochondria F1 complex, alpha subunit	P25705	112
ATP5O	ATP synthase, H+ transporting, mitochondria F1 complex, O subunit	P48047	112
BCR	Breakpoint Cluster Region	P11274	118
CCT3	Chaperonin containing TCP1, subunit 3 (gamma)	P49368	112
CCT4	Chaperonin containing TCP1, subunit 4 (delta)	P50991	112
CD14	CD14 Molecule	P08571	119
CD19	CD19 molecule	P15391	120–122
CD4	CD4 molecule	P01730	121
CD46	CD46 molecule, complement regulatory protein	P15529	123
CD53	CD53 molecule	P19397	124
CD63	CD63 molecule	P08962	125
CD74	HLA-DR Antigens-Associated Invariant Chain	P04233	126
CD81	CD81 molecule	P60033	127
CD82	CD82 molecule	P27701	124
CD9	CD1 molecule	P21926	122,128
CFL1	Cofilin 1 (non-muscle)	P23528	112
CFL2	Cofilin 2 (muscle)	Q9Y281	112
CLDN1	Claudin 1	O95832	129
CNN2	Calponin 2	Q99439	112
CPSF6	cleavage and polyadenylation specific factor 6, 68kDa	Q16630	112
CR2	Complement component (3d/Epstein Barr virus) receptor 2	P20023	120
CRIP1	Cystein-rich protein 1 (intestinal)	P50238	112
CSNK2B	Casein kinase 2, beta polypeptide	P67870	110
CTSC	Cathepsin C	P53634	130
DDX17	DEAD (Asp-Glu-Ala-Asp) box helicase 17	Q92841	112

Gene	Protein	UniProt ID	Ref.
DDX3X	DEAD (Asp-Glu-Ala-Asp) box helicase 3, X-linked	O00571	[112]
DDX3Y	DEAD (Asp-Glu-Ala-Asp) box helicase 3, Y-linked	O00571	[112]
DDX5	DEAD (Asp-Glu-Ala-Asp) box helicase 5	O00571	[112]
DHX15	DEAH (asp-Glu-Ala-His) box helicase 15	O43143	[112]
DLG5	Discs, large homolog 5	Q8TDM6	[131]
EEF1A1	Eukaryotic translation elongation factor 1 alpha 1	P68104	[112]
EEF1A2	Eukaryotic translation elongation factor 1 alpha 2	Q05639	[112]
EEF1D	Eukaryotic translation elongation factor 1 delta	P29692	[112]
EIF3A	Eukaryotic translation initiation factor 3, subunit A	Q14152	[112]
EIF3B	Eukaryotic translation initiation factor 3, subunit B	P55884	[112]
EIF3C	Eukaryotic translation initiation factor 3, subunit C	Q99613	[112]
EIF3CL	Eukaryotic translation initiation factor 3, subunit C-like	Q13347	[112]
EIF3E	Eukaryotic translation initiation factor 3, subunit E	P60228	[112]
EIF3F	Eukaryotic translation initiation factor 3, subunit F	O00303	[112]
EIF3G	Eukaryotic translation initiation factor 3, subunit G	O75821	[112]
EIF3H	Eukaryotic translation initiation factor 3, subunit H	O15372	[112]
EIF3I	Eukaryotic translation initiation factor 3, subunit I	Q13347	[112]
EIF3K	Eukaryotic translation initiation factor 3, subunit K	Q9UBQ5	[112]
EIF3L	Eukaryotic translation initiation factor 3, subunit L	Q9Y2862	[112]
EIF4A1	Eukaryotic translation initiation factor 4A1	P60842	[112]
EIF4A2	Eukaryotic translation initiation factor 4A2	Q14240	[112]
EWSR1	EWS RNA-binding protein 1	Q01844	[112]
EZR	Ezrin	P15311	[132]
FAM98B	Family with sequence similarity 98, member B	Q52LJ0	[112]
FAU	Finkel-Biskis-Reilly murine sarcoma virus (FBR-MuSV) ubiquitously expressed	P62861	[112]
FLNA	filamin A, alpha	P21333	[112]
FUBP1	Far upstream element (FUSE) binding protein 1	Q96AE4	[112]
GAPDH	Glyceraldehyde-3-phophate dehydrogenase	P04406	[112]
GGT1	Gamma-glutamyltransferase 1	P19440	[124]
GLP1R	Glucagon-like peptide 1 receptor	P43220	[133]
GNA11	Guanine nucleotide binding protein (G protein), beta polypeptide 2-like 1	P29992	[116]
GNAQ	Guanine nucleotide binding protein (G protein), Q Polypeptide	P50148	[116]
GNB2L1	Guanine nucleotide binding protein (G protein), beta polypeptide 2-like 1	P63244	[112]
GPC3	Glypican 3	P51654	[134]
H3F3B	H3 histone, family 3B	P84243	[112]
HHEX	Hematopietically Expressed Homeobox	Q03014	[134]
HIST1H1A	Histone cluster 1, H1a	Q02539	[112]
HIST1H1C	Histone cluster 1, H1c	P16403	[112]
HIST1H1D	Histone cluster 1, H1d	P16402	[112]

Gene	Protein	UniProt ID	Ref.
HIST1H1E	Histone cluster 1, H1e	P10412	[112]
HIST1H2BA	Histone cluster 1, H2ba	Q96A08	[112]
HIST1H2BB	Histone Cluster 1, H2bb	P33778	[112]
HIST1H2BD	Histone cluster 1, H2bd	P58876	[112]
HIST1H2BE	Histone cluster 1, H2be	P62807	[112]
HIST1H2BH	Histone cluster 1, H2bh	Q93079	[112]
HIST1H2BJ	Histone cluster 1, H2bj	P06899	[112]
HIST1H2BK	Histone cluster 1, H2bK	O60814	[112]
HIST1H2BL	Histone cluster 1, H2bl	Q99880	[112]
HIST1H2BM	Histone cluster 1, H2bm	Q99879	[112]
HIST1H2BN	Histone cluster 1, H2bn	Q99877	[112]
HIST1H2BO	Histone cluster 1, H2bo	P23527	[112]
HIST1H3E	Histone cluster 1, H3e	P68431	[112]
HIST2H2BF	Histone cluster 2, H2bF	Q5QNW6	[112]
HIST2H3C	Histone cluster 2, H3c	Q71DI3	[112]
HIST3H3	Histone cluster 3, H3	Q16695	[112]
HLA-B	HLA class I histocompatibility antigen, B-42 alpha chain	P30480	[135]
HNRNPA1	Heterogeneous nuclear ribonucleoprotein A1	P09651	[112]
HNRNPA2B1	Heterogeneous nuclear ribonucleoprotein A2/B1	P22626	[112]
HNRNPA3	Heterogeneous nuclear ribonucleoprotein A3	P51991	[112]
HNRNPD	Heterogeneous nuclear ribonucleoprotein	Q14103	[112; 136]
HNRNPH1	Heterogeneous nuclear ribonucleoprotein H1 (H)	P31943	[112]
HNRNPK	Heterogeneous nuclear ribonucleoprotein K	P61978	[112]
HNRNPM	Heterogeneous nuclear ribonucleoprotein M	P52272	[112]
HNRNPU	Heterogeneous nuclear ribonucleoprotein U	Q00839	[112]
HRAS	Harvey Rat Sarcome Viral Oncogene Homolog	P01112	[137]
IBTK	Inhibitor of Bruton agammaglobulinemia tyrosine kinase	Q9P2D0	[112]
ICAM1	Intercellular adhesion molecule 1	P05362	[138]
IFITM1	Interferon induced transmembrane protein 1	P13164	[139]
IGSF8	Immunoglobulin superfamily, member 8	Q969P0	[140]
IMMT	Inner membrane protein, mitochondria	Q16891	[112]
INO80B	INO80 complex subunit B	Q9C086	[131]
INPP4A	Inositol polyphosphate-4-phosphatase, type I	Q96PE3	[112]
ITGA4	Integrin, alpha 4	P13612	[141]
ITGB1	Integrin, beta 1	P05556	[141,142]
JAK3	Janus kinase 3	P52333	[110]
KHDRBS1	KH domain containing, RNA binding, signal transduction associated 1	Q07666	[112]
KHSRP	KH-type splicing regulatory protein	Q92945	[112]
KIT	v-Kit Hardy-Zuckerman 4 feline sarcoma viral oncogene homolog	P10721	[143]
LASP1	LIM and SH3 protein 1	Q14847	[112]

Gene	Protein	UniProt ID	Ref.
LDLR	Low Density Lipoprotein Receptor	P01130	144
LRRC47	Leucine rich repeat containing 47	Q8N1G4	112
LUC7L2	LUC7-like 2 (*S.cerevisiae*)	Q9Y383	112
MCM5	Minichrosome maintenance complex component 5	P33992	112
MME	Membrane Metallo-Endopeptidase (CD10)	P08473	145
MSN	Moesin	P26038	112
MTHFD1	Methylenetetrahydrofolate dehydrogenase	P11586	112
MYOC	Myocilin, trabecular meshwork insucible glucocorticoid response	Q99972	146
NAMPT	Nicotinamide phosphoribosyltransferase	P43490	112
NCL	Nucleolin	P19338	112
NONO	Non-POU domain containing, octame-binding	Q15233	112
NPM1	Nucleophosmin (nucleolar phosphoprotein B23, Numatrin)	P06748	112
NUDT21	Nudix (nucleoside diphosphate linked moiety X)-type motif 21	O43809	112
PABPC1	poly(A) binding protein, cytoplasmic 1	P11940	112
PCBP1	Poly(rC) binding protein 1	Q15365	112
PCBP2	Poly(rC) binding protein 2	Q15366	112
PCSK9	Proprotein Convertase Subtilisin/Kexin Type 9	Q8NBP7	144
PDCD4	Programmed cell death 4 (neoplastic transformation inhibitor)	Q653EL6	112
PDIA6	Protein dissulfide isomerase family A, member 6	Q15084	112
PFKP	Phosphofrutokinase, platelet	Q01813	112
PI4K2A	Phosphatidylinositosol 4-Kinase Type 2 alpha	Q9BTU6	147
PKM	Pyruvate kinase, muscle	P14618	112
PKN1	Protein kinase N1	Q16512	112
PSEN1	Presenilin 1	P49768	93
PSEN2	Presenilin 2	P49810	93
PTGFRN	Prostaglandin F2 receptor inhibitor	P68104	115,148
RAC1	Ras-related C3 botulinum toxin substrate 1	P63000	111
RAC2	Ras-related C3 botulinum toxin substrate 1	P15153	112
RBBP4	Retinoblastoma binding protein 4	Q09028	112
RBBP6	Retinoblastoma binding protein 6	Q7Z6E9	149
RGPD6	RANBP2-like and GRID domain containing 5/6	Q99666	112
RPL11	Ribosomal proteil L11	P62913	112
RPL12	Ribosomal protein L12	P30050	112
RPL13	Ribosomal protein L13	P26373	112
RPL17	Ribosomal protein L17	P18621	112
RPL22	Ribosomal protein L22	P35268	112
RPL23A	Ribosomal protein L23a	P62750	112
RPL24	Ribosomal protein L24	P83731	112
RPL27	Ribosomal protein L27	P61353	112
RPL27A	Ribosomal protein L27a	P46776	112

Gene	Protein	UniProt ID	Ref.
RPL31	Ribosomal protein L31	P62899	112
RPL35	Ribosomal protein L35	P42766	112
RPL4	Ribosomal protein L4	P36578	112
RPL5	Ribosomal protein L5	P46777	112
RPL6	Ribosomal protein L6	Q02878	112
RPLP0	Ribosomal protein, large, P0	P05388	112
RPLP2	60S acidic ribosomal protein P2	P05387	112
RPS13	Ribosomal protein S13	P26373	112
RPS14	Ribosomal protein S14	P62263	112
RPS15	Ribosomal protein S15	P62841	112
RPS16	Ribosomal protein S16	P62249	112
RPS18	Ribosomal protein S18	P62269	112
RPS19	Ribosomal protein S19	P39019	112
RPS2	Ribosomal protein S2	P15880	112
RPS23	Ribosomal protein S23	P62266	112
RPS25	Ribosomal protein S8	P62851	112
RPS28	Ribosomal protein S28	P62857	112
RPS3	ribosomal protein S3	P23396	112
RPS3A	Ribosomal protein S3A	P61247	112
RPS4X	Ribosomal protei S4, X-linked	P62701	112
RPS4Y1	Ribosomal protein S4, Y-linked 1	P22090	112
RPS6	Ribosomal protei S6	P62753	112
RPS8	Ribosomal protein S26	P62241	112
RPS9	Ribosomal protein S9	P46781	112
RTF1	Rtf1, Paf1/RNA polymerase II complex component, homolog (S. cerevisiae)	Q92541	112
SAMHD1	SAM domain and HD domain	Q9Y3Z3	112
SERBP1	Plasminogen activator inhibitor 1 RNA-binding protein	Q8NC51	112
SERPINB9	Serpin peptidase inhibitor, clade B, member 9	P50453	112
SET	SET nulear proto-oncogene	Q01105	112
SF3B3	splicing factor 3b, subunit 3	Q15393	112
SFPQ	Splicing factor proline/glutamine-rich	P23246	112
SHC1	SHC-Transforming protein 1	P29353	150
SNRPB	small nuclear ribonucleoprotein polypeptide B and B1	P14678	112
SNRPC	small nuclear ribonucleoprotein polypeptide C	P09234	112
SNRPD1	Small nuclear ribonucleoprotein D1 polypeptide 16kDa	P62314	112
SNRPD3	Small nuclear ribonucleoprotein D3 polypeptide	P62318	112
SRSF3	serine/arginine-rich splicing factor 3	P84103	112
SRSF8	serine/arginine-rich splicing factor 8	Q9BRL6	112
STK10	Serine/threonine kinase 10	O94804	112
STXBP5L	Syntaxin Binding Protein 5-like	Q9Y2K9	151

Gene	Protein	UniProt ID	Ref.
SUPT16H	Suppressor of Ty 16 homolog (S. Cerevisae)	Q9Y5B9	[112]
SYNCRIP	Synaptotagmin binding, cytoplasmic RNA interacting protein	O60506	[112]
TFR2	Transferrin Receptor 2	Q9UP52	[152]
TMPO	Lamina-associated polypeptide 2, isoform alpha	P42166	[112]
TRAF6	TNF Receptor-associated Factor 6	Q9Y4K3	[135]
TSPAN4	Tetraspanin 4	O14817	[153]
TUBA1A	Tubulin, alpha 1a	Q71U36	[112]
TUBA1B	Tubulin, alpha 1b	P68363	[112]
TUBA1C	Tubulin, alpha 1c	Q9BQE3	[112]
TUBA3C	Tubulin, alpha 3c	Q13768	[112]
TUBA3D	Tubulin, alpha 3d	Q13768	[112]
TUBA3E	Tubulin, alpha 3e	Q6PEY2	[112]
TUBA4A	Tubulin, alpha 4a	P68366	[112]
TUBA8	Tubulin, alpha 8	Q9NY65	[112]
TUBB	Tubulin, beta class I	P07437	[112]
TUBB2A	Tubulin, beta 2A class IIa	Q13885	[112]
TUBB2B	Tubulin, beta 2A class Iib	Q9BVA1	[112]
TUBB3	Tubulin, beta 3 class III	Q13509	[112]
TUBB4A	Tubulin, beta 4B class IVa	P04350	[112]
TUBB4B	Tubulin, beta 4B class Ivb	P68371	[112]
TUBB6	Tubulin, beta 6 class V	Q9BUF5	[112]
TUBB7P	Tubulin, beta 7, pseudogene	I0CMK4	[112]
TUBE1	Tubulin, epsilon 1	Q9UJTO	[112]
TUFM	Tu translation elongation factor, mitochondrial	P49411	[112]
UBXN1	UBX domain protein 1	Q04323	[112]
VKORC1	vitamin K epoxide reductase complex, subunit 1	Q9BQB6	[154]
WARS	Tryptophanyl-Trna synthetase	P23381	[112]
ZBTB16	Zinc finger and BTB domain containing 16	Q05516	[131]

Table 2. Full list of proteins with the associated score extracted from the network using GeneMania.

Gene Symbol	Score	Gene Symbol	Score	Gene Symbol	Score
STK10	100.00	CD14	97.34	RTF1	94.89
TUBE1	100.00	RBBP6	97.28	ALYREF	94.75
STXBP5L	99.87	PSEN2	97.22	CCT4	94.73
TUBA3D	99.87	EIF3I	97.22	RPS3A	94.71
RPS4Y1	99.86	ADAM10	97.17	NONO	94.70
RGPD6	99.82	HNRNPA3	97.03	TUFM	94.69
HIST1H2BE	99.76	RPS23	96.99	HLA-B	94.63
H3F3B	99.63	TUBB3	96.99	GNAQ	94.60
INPP4A	99.61	RPLP2	96.98	MCM5	94.42
GGT1	99.60	BCR	96.90	TUBB4B	94.40
CD81	99.60	PDCD4	96.86	RPS3	94.38
PTGFRN	99.57	RPL5	96.86	SNRPD1	94.22
HIST1H2BH	99.53	ITGA4	96.82	KHSRP	94.19
HIST2H2BF	99.50	GNA11	96.77	DDX3X	94.16
HIST1H2BM	99.50	JAK3	96.75	CFL1	94.13
IGSF8	99.50	PFKP	96.70	PABPC1	94.11
CD53	99.49	SNRPC	96.69	PKM	94.11
TUBA8	99.46	TUBB2A	96.66	EEF1D	94.05
CRIP1	99.43	RPL27A	96.64	CCT3	94.03
PI4K2A	99.30	RPS25	96.63	SF3B3	93.97
HIST1H2BN	99.30	KIT	96.62	EIF4A1	93.96
IFITM1	99.27	EIF3E	96.57	EWSR1	93.80
TSPAN4	99.23	EIF3H	96.57	ACTN1	93.78
EIF3CL	99.15	RPL27	96.56	SNRPB	93.74
PCSK9	99.13	ZBTB16	96.55	PCBP1	93.71
HIST1H3E	99.13	RPL35	96.55	HRAS	93.60
IBTK	99.08	RPL17	96.54	TUBB	93.51
HIST1H1D	99.06	RPS14	96.52	PSEN1	93.40
HHEX	99.00	TUBA1B	96.46	DDX17	93.32
SERPINB9	98.96	EIF4A2	96.43	KHDRBS1	93.07
GPC3	98.96	MTHFD1	96.36	SYNCRIP	93.04
DDX3Y	98.94	RPL4	96.34	SET	93.01
FAM98B	98.88	EIF3B	96.26	DHX15	92.89
TFR2	98.86	RPL22	96.26	HNRNPM	92.88
DLG5	98.85	IMMT	96.23	RBBP4	92.84
HIST1H2BD	98.85	PKN1	96.22	SNRPD3	92.73
HIST1H2BA	98.67	RPL12	96.21	HNRNPA2B1	92.71
INO80B	98.60	RPL13	96.21	EZR	92.63
CD19	98.59	RPS13	96.19	GAPDH	92.44
CD46	98.59	LUC7L2	96.19	AKT1	92.38

Gene Symbol	Score	Gene Symbol	Score	Gene Symbol	Score
CTSC	98.55	HIST1H1C	96.14	GNB2L1	92.37
CD82	98.49	RAC2	96.10	EEF1A1	92.35
TUBA3C	98.46	CD4	96.09	HNRNPD	92.33
HIST1H2BO	98.43	RPS9	96.06	NCL	92.28
ANP32B	98.40	WARS	96.03	DDX5	91.57
HIST1H2BK	98.37	RPS16	96.02	RAC1	91.54
CD63	98.33	GLP1R	95.98	ADRB2	91.51
TUBA3E	98.29	UBXN1	95.93	FLNA	91.43
ATP5O	98.18	TMPO	95.83	ACTB	91.41
EIF3G	98.16	NUDT21	95.82	ITGB1	91.35
HIST1H2BJ	98.14	RPS18	95.74	CSNK2B	91.27
LASP1	98.12	FUBP1	95.74	HNRNPK	91.12
ICAM1	98.08	MME	95.71	HNRNPH1	90.93
NAMPT	98.07	RPL6	95.70	HNRNPU	90.86
RPS28	98.04	CPSF6	95.69	SHC1	89.79
TUBB2B	98.02	TUBA4A	95.68	TRAF6	89.08
CNN2	98.01	ATP5A1	95.64	NPM1	88.34
HIST1H1A	97.95	RPL24	95.63	HNRNPA1	88.10
EIF3K	97.92	RPL11	95.63	APP	82.15
HIST1H2BB	97.92	SERBP1	95.62	UBC	8.72
LRRC47	97.87	EEF1A2	95.59	MAGOH	6.20
CD74	97.86	ACTN4	95.57	EIF4A3	5.73
CR2	97.80	RPL23A	95.54	CDK2	4.56
SAMHD1	97.80	EIF3C	95.53	PAN2	4.09
TUBB6	97.76	VKORC1	95.52	TARDBP	3.33
PDIA6	97.63	RPS4X	95.49	UBL4A	3.11
RPL31	97.57	RPS6	95.41	EIF3M	3.07
CLDN1	97.57	PCBP2	95.41	SF3A2	3.04
HIST2H3C	97.57	MSN	95.38	SRRM2	3.01
RPS15	97.54	RPS19	95.36	EIF3D	2.99
FAU	97.53	HIST3H3	95.35	RPA2	2.54
CFL2	97.53	TUBA1A	95.34	RPA1	2.50
TUBA1C	97.50	EIF3F	95.33	RPA3	2.44
LDLR	97.49	RPS8	95.31	YWHAZ	2.41
CD9	97.49	RPS2	95.22	CSNK2A2	2.33
EIF3L	97.41	EIF3A	95.17	SRRM1	2.27
HIST1H2BL	97.40	SUPT16H	95.16	IPO11	1.69
HIST1H1E	97.36	SFPQ	95.04	EIF3J	1.58
TUBB4A	97.36	SRSF3	95.01	HADHA	1.50
MYOC	97.34	RPLP0	94.98		

Appendix 2

Culture media and Solutions

I. Bacterial Media

- **LB (Luria-Bertani) Medium**

To 950 ml of deonizated H_20 add:

LB	25 g
Agar	15 g (for plates only)
Antibiotic	

Shake until the solutes have dissolved. Adjust the volume of the solution to 1 l with deonizated H_20. Sterilize by autoclaving. Add antibiotic to a final concentration of: 30 µg/ml kanamycin or 50 µg/ml ampicillin.

II. Cell culture Solutions

- **PBS (1x)**

For a final volume of 500 ml, dissolve one pack of BupH Modified Dulbecco's Phosphate Buffered Saline Pack (Pierce) in deionised H_2O. Final composition:

- 8 mM Sodium Phosphate
- 2 mM Potassium Phosphate
- 140 mM Sodium Chloride
- 10 mM Potassium Chloride

Sterilize by filtering through a 0.2 µm filter and store at 4°C.

- **10% FBS MEM:F12 (1:1)**
  - 4.805 g MEM
  - 5.315 g F12
  - 1.5 g NaHCO3
  - 0.055 g Sodium Pyruvate
  - 10 ml Streptomycin/Penicillin/Amphotericin solution

- 100 ml 10% FBS
- 2.5 ml L-glutamine (200 mM stock solution)

Dissolve in deionised H_2O. Adjust the pH to 7.2-7.3. Adjust the volume to 1000 ml with deionised H_2O.

- **10% FBS F12 Nutrient Mixture + L-Glutamine**

  -10.6 g F12

  -1.5 g $NaHCO_3$

  -0,146 g (1mM) L-Glutamine

  - 10 ml Streptomycin/Penicillin/Amphotericin solution (AAs)

  - 100 ml 10% FBS

  Dissolve in deionised H_2O. Adjust the pH to 7.2-7.3. Adjust the volume to 1000 ml with deionised H_2O.

- **10% FBS DMEM**

  -13.4 g DMEM

  -3.7 g $NaHCO_3$

  - 10 ml Streptomycin/Penicillin/Amphotericin solution (AAs)

  - 100 ml 10% FBS

  Dissolve in deionised H_2O. Adjust the pH to 7.2-7.3. Adjust the volume to 1000 ml with deionised H_2O.

- **Earl's balance solution (Sebss)**

  - 1.8 mM $CaCl_2$

  - 5.4 mM KCl 1.8 mM $CaCl_2$

  -5.4 mM KCl, 0.81 mM $MgSO_4$,

  -25.0 mM $NaHCO_3$,

  - 1.0 mM NaH_2PO_4, 116.4 mM NaCl,

  -5.5 mM D-glucose, 2.5 mM Na–pyruvate,

  -41.8 mM Na–lactate and

  -0.3% BSA

III. Western Blot Solutions

- **LGB (lower gel buffer) (4x)**

  To 900 ml of deionised H_2O add:

  - 181.65 g of Tris
  - 4 g of SDS

  Mix until the solutes have dissolved. Adjust pH to 8.9 and adjust the volume to 1 L with deionised H_2O.

- **UGB (Upper gel buffer) (4x)**

  To 900 ml of deionised H_2O add:

  - 75.69 g of Tris

  Mix until the solute has dissolved. Adjust the pH to 6.8 and adjust the volume to 1 L with deionised H_2O.

- **10% APS (ammonium persulfate)**

  In 10 ml of deionised H_2O dissolve 1 g of APS. Note: prepare fresh before use.

- **10% SDS (sodium dodecilsulfate)**

  In 10 ml of deionised H_2O dissolve 1 g of SDS.

- **Loading Gel Buffer (4x)**

  - 2.5 ml 1M Tris solution (pH 6.8) 2.5 ml (250 mM)
  - 0.8 g SDS (8%)
  - 4 ml Glicerol (40%)
  - 2 ml β-mercaptoethanol (2%)
  - 1 mg Bromofenol blue (0.01%)

  Adjust the volume to 10 ml with deionised H_2O. Store in darkness at room temperature.

- **1 M Tris (pH 6.8) solution**

  To 150 ml of deionised H_2O add:

  - 30.3 g Tris base

  Adjust the pH to 6.8 and adjust the final volume to 250 ml with deionised H_2O.

- **10x Running Buffer**
  - 30.3 g Tris (250 mM)
  - 144.2 g Glycine (2.5 M)
  - 10 g SDS (1%)

  Dissolve in deionised H_2O, adjust the pH to 8.3 and adjust the volume to 1l.

- **Stacking and resolving gel**

Type of Gel	Stacking	Resolving	
Polyacrylamide percentage	3.5 %	5 %	20 %
H_2O	13.2 ml	17.4 ml	2.2 ml
Acrylamide stock mixture	2.4 ml	5 ml	20 ml
UGB (5x)	4 ml	n/a	n/a
LGB (4x)	n/a	7.5 ml	7.5 ml
10% SDS	200 µL	n/a	n/a
10% APS	200 µL	150 µL	150 µL
TEMED	20 µL	15 µL	15 µL

- **Transfer Buffer (1x)**
  - 3.03 g Tris (25 mM)
  - 14.41 g Glycine (192 mM)

Mix until solutes dissolution. Adjust the pH to 8.3 with HCl and adjust the volume to 800 ml with deionised H_2O. Just prior to use add 200 ml of methanol (20%).

- **10x TBS (Tris buffered saline)**
  - 12.11 g Tris (10 mM)
  - 87.66 g NaCl (150 mM)

  Adjust the pH to 8.0 with HCl and adjust the volume to 1 l with deionised H_2O.

- **10x TBST (TBS+Tween)**
  - 12.11 g Tris (10 mM)
  - 87.66 g NaCl (150 mM)
  - 10 ml Tween-20 (0.01%)

  Adjust the pH to 8.0 with HCl and adjust the volume to 1 L with deionised H_2O.

IV. Immunofluorescence Solutions

- **4% Paraformaldehyde**

For a final volume of 100 ml, add 4 g of paraformaldehyde to 25 ml deionised H_2O. Dissolve by heating the mixture at 58°C while stirring. Add 1-2 drops of 1 M NaOH to clarify the solution and filter through a 0.2 µM filter. Add 50 ml of PBS 2x and adjust the volume to 100 ml with deionised H_2O.